

THESIS FOR THE DEGREE OF DOCTOR OF PHILOSOPHY

Biofabrication, Biomechanics and Biocompatibility of Nanocellulose-based Scaffolds for Auricular Cartilage Regeneration

HÉCTOR D. MARTÍNEZ ÁVILA



CHALMERS

Biopolymer Technology
Department of Chemistry and Chemical Engineering
CHALMERS UNIVERSITY OF TECHNOLOGY
Göteborg, Sweden 2015

Biofabrication, Biomechanics and Biocompatibility of Nanocellulose-based Scaffolds for Auricular Cartilage Regeneration

© HÉCTOR D. MARTÍNEZ ÁVILA

Göteborg, Sweden 2015

ISBN 978-91-7597-161-2

Doktorsavhandlingar vid Chalmers tekniska högskola
Ny serie Nr 3842
ISSN 0346-718X

Biopolymer Technology
Department of Chemistry and Chemical Engineering
Chalmers University of Technology
SE-41296 Göteborg
Sweden
Telephone +46 (0)31 772 1000

Cover:

Redifferentiated chondrocytes in patient-specific, auricular bacterial nanocellulose scaffold with bilayer architecture. Elastica van Gieson staining.

Photographer: Jan-Olof Yxell.

Cover Designer: J. Carlos Martínez Ávila.

Chalmers Reproservice

**Biofabrication, Biomechanics and Biocompatibility of Nanocellulose-based Scaffolds for
Auricular Cartilage Regeneration**
HÉCTOR D. MARTÍNEZ ÁVILA
ABSTRACT

In about 2:10,000 births the external part of the ear, the auricle, is severely malformed or absent. Furthermore, tumors and trauma can cause defects to the auricle. For patients with dysplasia of the auricle, and especially for children, an inconspicuous outer appearance with life-like auricles is important for their psychological and emotional well being as well as their psycho-social development. Auricular reconstruction remains a great challenge due to the complexity of surgical reconstruction using rib cartilage. Despite the advances in stem cell technology and biomaterials, auricular cartilage tissue engineering (TE) is still in an early stage of development due to critical requirements demanding appropriate mechanical properties and shape stability of the tissue-engineered construct. This thesis has focused on developing patient-specific tissue-engineered auricles for one-step surgery using a novel biomaterial, bacterial nanocellulose (BNC), seeded with human nasoseptal chondrocytes (hNC) and bone marrow mononuclear cells (MNC).

Biomechanical properties of human auricle cartilage were measured and used as a benchmark for tuning BNC properties. In order to meet the biomechanical requirements, a scaffold with bilayer architecture composed of a dense BNC support layer and a macroporous structure was designed. Firstly, the biocompatibility of the dense BNC layer was investigated, demonstrating a minimal foreign body response according to standards set forth in ISO 10993. Secondly, different methods to create macroporous BNC scaffolds were studied and the redifferentiation capacity of hNCs was evaluated *in vitro*; revealing that macroporous BNC scaffolds support cell ingrowth, proliferation and neocartilage formation. The bilayer BNC scaffold was biofabricated and tested for endotoxins and cytotoxicity before evaluating in long-term 3D culture, and subsequently *in vivo* for eight weeks—in an immunocompromised animal model. The results demonstrated that the non-pyrogenic and non-cytotoxic bilayer BNC scaffold offers a good mechanical stability and maintains a structural integrity, while providing a porous 3D environment that is suitable for hNCs and MNCs to produce neocartilage, *in vitro* and *in vivo*. Furthermore, patient-specific auricular BNC scaffolds with bilayer architecture were biofabricated and seeded with autologous rabbit auricular chondrocytes (rAC) for implantation in an immunocompetent rabbit model for six weeks. The results demonstrated the shape stability of the rAC-seeded scaffolds and neocartilage depositions in the immunocompetent autologous grafts. 3D bioprinting was also evaluated for biofabrication of patient-specific, chondrocyte-laden auricular constructs using a bioink composed of nanofibrillated cellulose and alginate. Bioprinted auricular constructs showed an excellent shape and size stability after *in vitro* culture. Moreover, this bioink supports redifferentiation of hNCs while offering excellent printability, making this a promising approach for auricular cartilage TE. Furthermore, the use of bioreactors is essential for the development of tissue-engineered cartilage *in vitro*. Thus, a compression bioreactor was utilized to apply dynamic mechanical stimulation to cell-seeded constructs as a means to enhance production of extracellular matrix *in vitro*.

In this work, a potential clinical therapy for auricular reconstruction using tissue-engineered auricles is demonstrated; where BNC is proposed as a promising non-degradable biomaterial with good chemical and mechanical stability for auricular cartilage TE. Although the primary focus of this thesis is on auricular reconstruction, the methods developed are also applicable in the regeneration of other cartilage tissues such as those found in the nose, trachea, spine and articular joints.

Keywords: Tissue Engineering; 3D Bioprinting; Auricular reconstruction; Auricular Cartilage; Neocartilage; Bacterial Nanocellulose; Nanofibrillated Cellulose; Nasoseptal Chondrocytes; Mononuclear Cells

LIST OF PUBLICATIONS

This thesis is based on the work of the following Papers, as well as some unpublished work. Articles are referred to in the text by roman numerals:

- I. Mechanical evaluation of bacterial nanocellulose as an implant material for ear cartilage replacement.**
Nimeskern L*, Martínez Ávila H*, Sundberg J, Gatenholm P, Müller R, Stok KS.
Journal of the Mechanical Behavior of Biomedical Materials. 2013;22:12–21.
*indicates that the authors contributed equally to the study and should be considered as first authors.
- II. Biocompatibility evaluation of densified bacterial nanocellulose hydrogel as an implant material for auricular cartilage regeneration.**
Martínez Ávila H, Schwarz S, Feldmann E-M, Mantas A, von Bomhard A, Gatenholm P, Rotter N.
Applied Microbiology and Biotechnology. 2014;98:7423–35.
- III. Novel bilayer bacterial nanocellulose scaffold supports neocartilage formation *in vitro* and *in vivo*.**
Martínez Ávila H, Feldmann E-M, Pleumeekers MM, Nimeskern L, Kuo W, de Jong WC, Schwarz S, Müller R, Hendriks J, Rotter N, van Osch GJVM, Stok KS, Gatenholm P.
Biomaterials. 2015;44:122–133.
- IV. 3D bioprinting of human chondrocyte-laden nanocellulose hydrogel for patient-specific auricular cartilage regeneration.**
Martínez Ávila H*, Schwarz S*, Rotter N, Gatenholm P.
Submitted to Biomaterials
*indicates that the authors contributed equally to the study and should be considered as first authors.
- V. Mechanical stimulation of fibroblasts in micro-channeled bacterial cellulose scaffolds enhances production of oriented collagen fibers.**
Martínez Ávila H, Brackmann C, Enejder A, Gatenholm P.
Journal of Biomedical Materials Research Part A. 2012;100:948–57.

Reprints were made with permission from the respective publishers.

CONTRIBUTION REPORT

- I. Shared main authorship. Conceived of the study design, performed equal amount of experimental work as LN and took active part in writing manuscript.
- II. Main author. Took active part in planning and coordination of study, performed part of the experimental work, i.e. synthesis, purification and characterization of material, took active part in analysis and interpretation of data and drafted the manuscript.
- III. Main author. Took active part in planning and coordination of study, performed part of the experimental work, i.e. fabrication and characterization of scaffold, took active part in analysis and interpretation of data, performed statistical analysis and drafted the manuscript.
- IV. Shared main authorship. Conceived of the study design, performed equal amount of experimental work as SS and drafted the manuscript.
- V. Main author. Conceived of the study design, performed most of the experimental work including acquisition, analysis and interpretation of data and drafted the manuscript.

ADDITIONAL PUBLICATIONS

Developing staining protocols for visualization of tissue-engineering scaffolds using micro computed tomography in native wet state.

Kuo W, Nimeskern L, Martínez Ávila H, Hofmann S, Freedman J, Grinstaff MW, Muller R, Stok KS.

Biomedical Engineering-Biomedizinische Technik. 2013;58.

3D bioprinting human chondrocytes with nanocellulose-alginate bioink for cartilage tissue engineering applications.

Markstedt K, Mantas A, Tournier I, Martínez Ávila H, Hägg D, Gatenholm P.

Submitted to Biomacromolecules

TABLE OF CONTENTS

| | |
|--|-----------|
| ABSTRACT | iii |
| LIST OF PUBLICATIONS..... | iv |
| CONTRIBUTION REPORT | v |
| CHAPTERS | |
| 1 INTRODUCTION | 1 |
| 1.1 Motivation..... | 1 |
| 1.2 Hypotheses..... | 3 |
| 2 BACKGROUND | 4 |
| 2.1 Clinical needs in auricular cartilage reconstruction | 4 |
| 2.2 State-of-the art in auricular cartilage reconstruction | 5 |
| 2.3 The ear | 6 |
| 2.4 Auricular cartilage tissue engineering..... | 7 |
| 2.5 Bacterial nanocellulose as a biomaterial..... | 9 |
| 2.6 3D Bioprinting of tissue analogues..... | 11 |
| 3 AIMS OF THE THESIS | 12 |
| 3.1 Specific aims..... | 12 |
| 4 MATERIALS AND METHODS | 13 |
| 4.1 Biosynthesis of bacterial nanocellulose | 13 |
| 4.2 Mechanical evaluation of bacterial nanocellulose as an implant material for auricular cartilage replacement..... | 13 |
| 4.3 Biofabrication of patient-specific auricular bacterial nanocellulose implants | 15 |
| 4.4 Biocompatibility evaluation of densified bacterial nanocellulose hydrogel | 15 |
| 4.5 Bacterial nanocellulose and alginate as scaffold materials for auricular cartilage regeneration | 18 |
| 4.6 Bilayer bacterial nanocellulose scaffold for auricular cartilage regeneration..... | 19 |
| 4.7 Patient-specific bacterial nanocellulose scaffold for auricular cartilage regeneration. | 19 |
| 4.8 3D bioprinting of human chondrocyte-laden nanocellulose hydrogel for patient-specific auricular cartilage regeneration..... | 20 |

| | |
|--|-----------|
| 4.9 Mechanical stimulation of cell-seeded BNC scaffolds to enhance neo-tissue development | 21 |
| 4.10 Cell culture | 21 |
| 4.11 Chondrogenic differentiation..... | 22 |
| 4.11.1 Chondrogenic differentiation in vitro | 22 |
| 4.11.2 Chondrogenic differentiation in vivo | 23 |
| 4.12 Evaluation methods for chondrogenic differentiation | 24 |
| 4.13 Statistics | 26 |
| 5 RESULTS AND DISCUSSION | 28 |
| 5.1 Evaluation of bacterial nanocellulose as an implant material for auricular cartilage replacement..... | 28 |
| 5.2 Biocompatibility evaluation of densified bacterial nanocellulose hydrogel | 31 |
| 5.3 Macroporous BNC-A composite scaffolds for auricular cartilage regeneration..... | 38 |
| 5.4 Bilayer bacterial nanocellulose scaffold for auricular cartilage regeneration..... | 42 |
| 5.5 <i>In vivo</i> evaluation of patient-specific BNC scaffold for auricular cartilage regeneration | 50 |
| 5.6 3D bioprinting of human chondrocyte-laden nanocellulose hydrogel for patient-specific auricular cartilage regeneration..... | 55 |
| 5.7 Mechanical stimulation of cell-seeded BNC scaffolds to enhance neo-tissue development | 62 |
| 6 CONCLUDING REMARKS | 67 |
| 6.1 SUGGESTIONS FOR FUTURE RESEARCH | 69 |
| ACKNOWLEDGMENTS | 71 |
| REFERENCES..... | 73 |

CHAPTER 1

INTRODUCTION

1.1 Motivation

Cartilage is a tissue with a limited capacity for self-repair due to its avascular nature and sparse distribution of highly differentiated cells, i.e. the chondrocytes. The cartilage found in the auricle (e.g. outer ear), can be malformed by congenital defects or damaged by trauma. Malformations of the auricle are collectively termed microtia.¹ The reported prevalence of microtia varies among regions, from 0.83 to 12.0 per 10,000 births, and the prevalence is considered to be higher in Native Americans, Andeans, Hispanics and Asians.² Although the diagnosis of microtia encompasses a spectrum of phenotypes, even minor deformities may bring psychological distress upon the affected individuals, due to actual or perceived defect and its effect on psychosocial development. For patients with microtia, especially children, an inconspicuous outer appearance with life-like auricles is important for their psychological and emotional well-being. Without reconstructive surgery many patients suffer from reduced self-confidence, which can lead to severe psychosocial problems.^{3,4} In addition, more than 90% of individuals diagnosed with microtia experience hearing loss on the affected side.^{1,5,6} For these reasons, successful auricle restoration is of utmost concern within the field of reconstructive surgery.

Today, auricular reconstruction uses multiple-step surgical techniques where autologous tissue, such as rib cartilage, is formed into the shape of the auricle and supported by skin.⁷ Due to the complexity of this multistep procedure, unsatisfactory cosmetic results might occur. Moreover, harvesting large pieces of rib cartilage causes donor-site morbidity with a risk for lung collapse or thorax deformities, especially in young patients.⁸ Alternatively, synthetic implants made of polyethylene can be implanted with a better cosmetic outcome but higher risk for infection and extrusion.^{9,10} Therefore, there is still a great need for competitive alternatives.

A new technology that is being developed for reconstruction of the auricle is tissue engineering.^{11,12} This technology uses various scaffold materials and structures to support the cells harvested from the patient, followed by implantation of the engineered-tissue into the damaged area. It is of great importance that the scaffold material used can be shaped into the desired form and allows the seeded cells to perform the function as in the native tissue. Furthermore, the engineered tissue should have long-term durability *in vivo*.^{13,14} The pioneering work by Vacanti et al. demonstrated that chondrocytes seeded onto synthetic, biodegradable scaffolds with a complex architecture, like a human ear, could produce neocartilage after transplantation in athymic mice.^{15,16} The engineering of autologous tissues and organs is a promising alternative therapy with potential for tissue replacement.^{13,14}

Although scientists have been investigating the possibility to engineer cartilage-like structures in the shape of a human auricle since the early 1990s,^{12,15} few successful outcomes have been reported.¹⁷⁻¹⁹ Most studies that have used biodegradable scaffold materials have resulted in poor structural integrity (i.e. shape and size stability) of the auricular scaffold after implantation;

caused by the short-lived chemical and mechanical stability.^{16,20-23} On the other hand, recent studies that have investigated the use of non-degradable biomaterials for auricular cartilage reconstruction have reported a better structural integrity of the implant;^{18,19,24} likely caused by the chemical stability of the support biomaterial, which translates into long-lasting mechanical properties even after implantation. Thus, there is evidence that problems that have arisen in auricular cartilage TE, particularly poor structural integrity of the implant, could be solved using non-degradable scaffold materials.

Besides maintaining a long-term structural integrity, the engineered auricular graft must have adequate mechanical properties and porosity, as these are key factors for successful auricular cartilage tissue engineering (TE). The scaffold must be mechanically stable while providing a porous architecture that supports cell ingrowth and neocartilage formation. Another important requirement for engineered-auricular grafts is to be able to control the external shape of the implant to obtain satisfying esthetic results. This outcome is often used as a measure of success for a potential biomaterial.^{18,19,22} However, most efforts in auricular cartilage TE have used standardized auricular shapes.^{18,19,22,24} The optimal esthetic outcome would be to produce scaffolds that mimic the shape of patient's own auricle. That is, the shape must be patient-specific. A number of technologies can be used to acquire the 3D shape of the intact contralateral auricle of a patient undergoing surgical auricular reconstruction. After processing the patient's medical images, a 3D model is available for the production of a patient-specific auricular scaffold for TE purposes.²⁵

To engineer the auricle, there is a need for a cell source that can be easily accessible and that has the ability to form cartilage of sufficient quality. Potential cell sources include auricular chondrocytes,²⁶ nasoseptal chondrocytes²⁷ and mesenchymal stem cells from bone marrow and adipose tissue.^{28,29} The use of autologous cells in cartilage repair is an attractive strategy as it may result in regeneration of the lost tissue. However, the clinical application of a cell-aided treatment does feature challenges – a limited supply of autologous chondrocytes with the proper phenotype being the most stringent one. Autologous cells could be isolated within the operating room and applied directly in order to avoid double surgery and cell culture. In addition, the combination of chondrocytes with a less limited source of autologous cells, such as bone marrow mononuclear cells (MNC), can overcome the challenge of having too few cells and may even increase the treatment's performance.^{30,31} The use of freshly isolated autologous cells, together with a non-degradable material, represents a novel strategy for delivering tissue-engineered auricles in a straightforward manner to the patients, using an undemanding one-step surgical method.

Most auricular cartilage TE strategies have revolved around biodegradable scaffolds, where the hypothetical optimum has been the scaffold's degradation orchestrated by the neo-tissue formation. It would be ideal if the scaffold could be degraded by the time the neocartilage has reached full mechanical strength. However, fine-tuning this intricate play has proven to be a challenge in TE. As opposed to the many biodegradable scaffolds previously evaluated for auricular cartilage TE, the long-term structural integrity of bacterial nanocellulose (BNC) scaffolds should not be compromised after implantation since humans do not produce enzymes capable of breaking down cellulose. This would allow the material to retain the shape of the auricle after implantation. We aim for a hybrid implant – BNC well integrated with the host and

neo-tissue. The non-degradable BNC will provide long-term structural integrity after implantation, and has previously shown remarkable integration with the host tissue in different animal models.³²⁻³⁴ The overall aim of this thesis is to design and biofabricate non-degradable, patient-specific BNC scaffolds for use with cells in auricular cartilage regeneration.

1.2 Hypotheses

- The biomechanical properties of BNC could be increased by densification of the BNC network (i.e. increase cellulose content) and potentially match the mechanical properties of cartilage tissues.
- Although native BNC (1% cellulose content, 99% water) is known for its biocompatibility, there are no studies that have investigated the host tissue response to densified BNC hydrogels. We hypothesized that the biocompatibility of BNC should not be affected after densification of the nanocellulose network, provided that endotoxin levels in the material are below the endotoxin limit set by the FDA for medical devices.
- Porous BNC-Alginate composite scaffolds will support neocartilage formation by human chondrocytes, as it has been shown that these biomaterials maintain a chondrogenic phenotype.
- The combination of a dense BNC layer with a porous BNC-Alginate layer will result in a scaffold architecture with high porosity for cell infiltration and neocartilage formation, while providing good structural integrity after implantation.
- The long-term structural integrity of auricular BNC scaffolds seeded with autologous chondrocytes should not be compromised after implantation in an immunocompetent animal model.
- 3D bioprinted cell-laden nanocellulose-alginate constructs should support neocartilage formation by human chondrocytes in chondrogenic differentiation medium conditions.
- Dynamic mechanical stimulation to cell-seeded BNC constructs will have a positive effect on the development of the neo-tissue.

CHAPTER 2

BACKGROUND

2.1 Clinical needs in auricular cartilage reconstruction

The cartilage found in the auricle, external part of the ear, can be malformed by congenital defects or damaged by traumatic injuries, cancer or acute auricular hematoma³⁵ (**Figure 1**). Malformations of the auricle are collectively termed microtia. Thus, the diagnosis of microtia encompasses a spectrum of congenital defects that range in severity from mild structural abnormalities to complete absence of the ear (anotia).¹

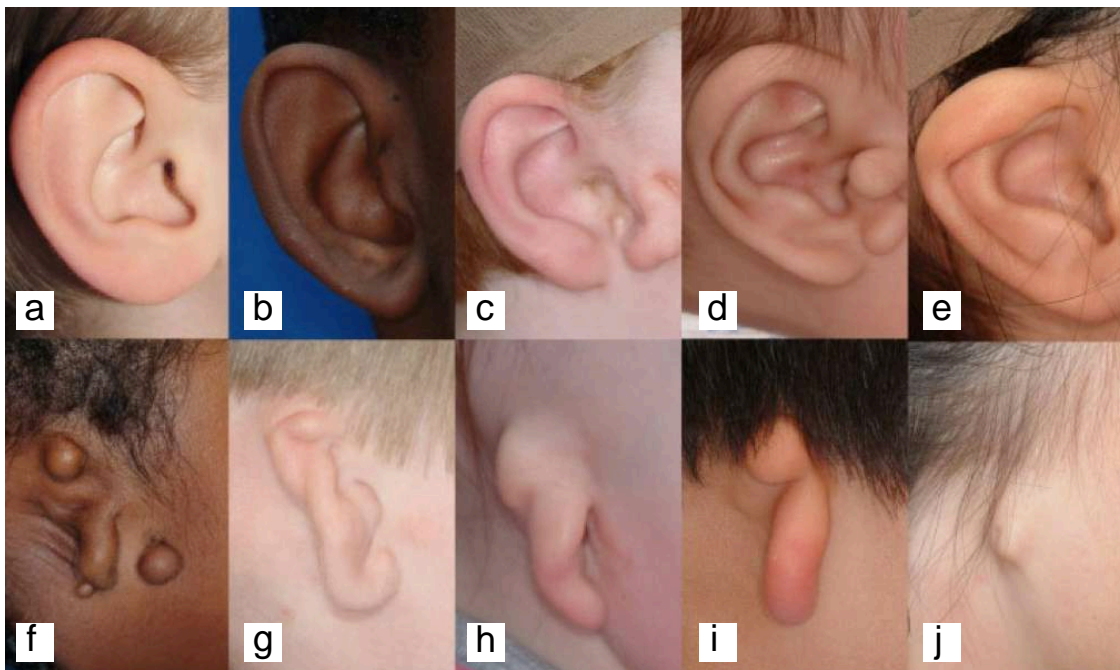


Figure 1 – Photographs of individuals with different types of microtia. (a) typical ear, (b-d) first degree dysplasia, (e) second degree dysplasia, (f-j) third degree dysplasia. Classification proposed by Hunter et al.³⁶ Reprinted from *Microtia: Epidemiology and genetics*, Daniela V. Luquetti, Carrie L. Heike, Anne V. Hing, Michael L. Cunningham and Timothy C. Cox, *Am J Med Genet Part A* 158A, Copyright © 2011 Wiley Periodicals, Inc., with permission from John Wiley and Sons.²

The reported prevalence of microtia varies among regions, from 0.83 to 12.0 per 10,000 births, and the prevalence is considered to be higher in Native Americans, Andeans, Hispanics and Asians.² Population-based studies on microtia prevalence conducted in France (0.83), Sweden (2.35), Finland (4.34), and United States (2.0-3.8) found prevalence rates ranging between 0.83 and 4.34 per 10,000 births. Microtia is more common among males, 20–40% higher compared to females, and the right ear is affected in approximately 60% of the cases. Microtia can also occur bilaterally in approximately 10–20% of the cases.^{6,37-40}

Although the diagnosis of microtia encompasses a spectrum of phenotypes, even minor deformities may bring psychological distress upon the affected individuals, due to actual or perceived defect and its effect on psychosocial development. For patients with microtia, especially children, an inconspicuous outer appearance with life-like auricles is important for their psychological and emotional well-being. Without reconstructive surgery many patients suffer from reduced self-confidence, which can lead to severe psychosocial problems.^{3,4,41} In addition, more than 90% of individuals diagnosed with microtia experience hearing loss on the affected side.^{1,5,6} For these reasons, successful auricle restoration is of utmost concern within the field of reconstructive surgery.

2.2 State-of-the art in auricular cartilage reconstruction

The first auricular reconstruction technique using autologous costal cartilage was developed by Tanzer in the late 1950s.⁴² Today, the most commonly used methods for auricular reconstruction are based on the work of Brent⁴³ and Nagata.⁴⁴ These procedures require multiple surgeries and the complexity of the operation depends on the size of the defect. The current gold standard for reconstruction of microtia and other auricular deformities uses multiple-step surgical techniques where autologous tissue, such as costal cartilage, is formed into the shape of the auricle and implanted under the periauricular skin. For total reconstruction, the sixth, seventh, and eighth costal ribs are harvested (**Figure 2**). The sixth and seventh ribs are used to form the auricular body framework, whereas the eighth rib is used to form the helical structure.⁷ Implantation is then performed in 4 stages⁴³ or 2 stages.⁴⁴ In step 1, the autologous framework is implanted subcutaneously. In steps 2 and 3, remnants of the auricle are used to complete the implanted framework and the tragus is reconstructed. In step 4, the framework is elevated from the head. Two-stage implantation techniques combine the first three steps into a single surgery. The main advantage of the 2-stage techniques is the reduction of time. However, these techniques also require more experienced surgeons since they are more challenging.⁴⁵ Thus, due to the complexity of multiple-step surgical techniques, unsatisfactory cosmetic results might occur. Moreover, harvesting large pieces of rib cartilage causes donor-site morbidity with a risk for lung collapse or thorax deformities, especially in young patients.⁸

An alternative approach to reconstruct the auricle has been to use alloplastic implants such as silicone^{46,47} or porous high-density polyethylene.^{48,49} Advantages of alloplastic implants include unlimited availability, consistent predetermined shape and shortened operation time. However, the use of alloplastic implants is associated with increased rates of infection, extrusion and uncertain long-term durability.^{9,10} Alloplastic auricular reconstruction using prostheses anchored with magnets on osseointegrated implants is considered in patients with poor local tissue resulting from radiation, cancer resection, absence of lower half of the auricle and failed autogenous reconstruction.^{7,50,51}

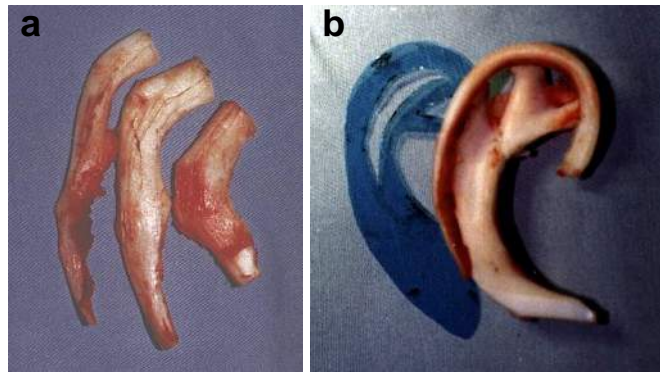


Figure 2 – For total auricular reconstruction, (a) the sixth, seventh, and eighth costal ribs are first harvested. (b) The sixth and seventh ribs are used to form the auricular body framework, whereas the eighth rib is used to form the helical structure. Reprinted from *J Plast Reconstr Aesthet Surg*, 61, B. Pan, H. Jiang, D. Guo, C. Huang, S. Hu, H. Zhuang, *Microtia: ear reconstruction using tissue expander and autogenous costal cartilage*, Pages S98–S103, Copyright © 2008, with permission from Elsevier.⁵²

A new technology that is being developed for reconstruction of the auricle is tissue engineering.^{11,12} This technique uses various scaffold materials to support the cells harvested from the patient, followed by implantation of the engineered-tissue into the damaged area. It is of great importance that the scaffold material used can be shaped into the desired form and allows the seeded cells to perform the function as in the native tissue. Furthermore, the engineered-tissue should have long-term durability *in vivo*. The pioneering work by Vacanti et al. demonstrated that chondrocytes seeded onto synthetic, biodegradable scaffold with a complex architecture like a human ear could produce neocartilage after transplantation in athymic mice.^{15,16} The engineering of autologous tissues and organs is a promising alternative therapy with potential for tissue replacement. This thesis contributes to the field of auricular cartilage tissue engineering.

2.3 The ear

The outer ear is responsible for receiving sound waves and transmitting those inwards. It is further divided into the auricle, the external auditory canal and the eardrum. The auricle is the visible part of the outer ear and consists of elastic cartilage, which is covered by skin.⁵³ Auricular cartilage is the main component of the external ear. It is surrounded by a thin layer of perichondrium, a connective tissue that connects it to the highly vascularized skin and provides the necessary nutrients.⁷ The first elevations that will later build the auricle, arise already at the sixth week of embryonic development.⁵⁴

2.3.1 Auricular cartilage and the extracellular matrix

Several types of cartilage are found in the body: fibrous, hyaline and elastic cartilage. Fibrocartilage is found in the menisci and intervertebral discs of the spine, hyaline cartilage can be found in the joints and elastic cartilage in the external ear.^{53,55} Cartilage consists of chondrocytes, extracellular matrix (ECM) and water. It is the composition of the ECM that determines the type of cartilage, where variation in composition among different types of

cartilage is due to site-specific mechanical loading.^{56,57} Cartilage has been suggested to have a hydrogel-like structure⁵⁸ as it is composed of a large amount of water (60-80%). Cartilage has a sparse distribution of highly differentiated cells, i.e. the chondrocytes, which are found in small empty spaces called lacunae and are surrounded by ECM.⁵⁹ Furthermore, cartilage is an avascular tissue with no nerve supply, which means that nutrients and waste can only be exchanged by diffusion and the self-repair capacity of the tissue is limited. This limited capacity is further reduced due to the low amount of chondrocytes in the tissue and limited supply of progenitor cells.^{57,59}

The ECM functions as a physical support for cells, but it also contains ligands for cell adhesion and migration, and provides biological factors to control cell function. It is produced and maintained by the local cells, where the matrix composition determines its biomechanical function. The ECM of elastic cartilage consists of fibrous proteins (elastin and type II and V collagen) and proteoglycans (aggrecan), where the most abundant matrix protein is type II collagen.^{56,60} Among the cartilage subtypes, elastin is almost exclusively found in elastic cartilage.^{56,61} The fibrous proteins in the ECM are responsible for the tissue's tensile strength, high resilience and large extensibility.⁵⁶ A proteoglycan typical for cartilage is aggrecan, which consists of glycosaminoglycans (GAG),^{62,63} such as chondroitin sulfate and keratan sulfate, attached to a core protein. Chondroitin sulfate is an important structural component of cartilage and provides much of its resistance to compression, which is due to the binding of water to GAGs. Hyaluronan is also an important component of cartilage. When aggrecan monomers bind to hyaluronan in the presence of link protein, large and highly negative-charged proteoglycan aggregates form. These aggregates bind water, growth factors and cytokines.^{62,63} Due to the limited self-renewal and self-repair capacity of cartilage, tissue engineering can provide unlimited possibilities in auricular reconstruction.^{11,12,64}

2.4 Auricular cartilage tissue engineering

Since the early 1990s scientists have investigated the possibility to engineer cartilage-like structures in the shape of a human auricle.¹⁵ In tissue engineering (TE) applications, scaffolds are used to create a mechanical and biochemical environment that is adequate for development of the tissue of interest. That is, the scaffold should promote cell adhesion, proliferation and differentiation. Additionally, the shape of the scaffolds should be retained until the neo-tissue matures and is able to maintain the shape of the construct, in this case an auricle shape.

2.4.1 Scaffold materials and outcomes

Most scaffold materials evaluated for auricular cartilage TE have been synthetic biodegradable polymers: polylactic acid (PLA),^{16,22,65} polyglycolic acid (PGA),^{16,22,65-67} polycaprolactone (PCL),²² poly-4-hydroxybutyrate (P4HB),²² and their copolymers.^{20,21,23,68,69} The combination of these different polymers allows tuning of the mechanical properties as well as the degradation rate of the scaffold. The longest *in vivo* studies reported were performed over a period of 10 and 3 months in immunocompromised²¹⁻²³ and immunocompetent²² animal models, respectively. All studies performed in immunocompromised mouse models reported cartilage formation and

adequate shape stability at 10 months post-implantation, based on a qualitative assessment of shape and size of the implant. However, in the immunocompetent rabbit model, Shieh et al. reported a severe foreign body reaction in all investigated polymeric scaffolds (PGA coated with PLA, PCL and P4HB) and a severe deformation and collapse of the implants at 3 months post-implantation (no images were shown). The foreign body reaction was attributed to the degradation products of the scaffolds, whereas the loss of shape stability was presumably caused by the inflammatory reaction and skin contraction force against the implants.²²

2.4.2 Requirements for tissue-engineered auricles

Although several groups have attempted to engineer auricular cartilage,^{11,12} few successful outcomes have been reported.¹⁷⁻¹⁹ Most studies that have used biodegradable scaffold materials have resulted in poor structural integrity (i.e. shape and size stability) of the auricular scaffold after implantation; caused by the short-lived chemical and mechanical stability.^{16,20-23} On the other hand, recent studies that have investigated the use of non-degradable biomaterials for auricular cartilage reconstruction have reported a better structural integrity of the implant,^{18,19,24} likely caused by the chemical stability of the support biomaterial, which translates into long-lasting mechanical properties even after implantation. Thus, there is evidence that common problems in auricular cartilage TE, particularly poor structural integrity of the implant, could be solved using a non-degradable scaffold material. As opposed to the many biodegradable scaffolds previously evaluated for auricular cartilage TE, the long-term structural integrity of bacterial nanocellulose (BNC) scaffolds should not be compromised after implantation since humans do not produce enzymes capable of breaking down cellulose.⁷⁰ This would allow the material to retain the shape of the auricle after implantation. Besides maintaining a long-term structural integrity, the engineered auricular graft must have adequate mechanical properties and porosity, as these are key factors for successful auricular cartilage TE. The scaffold must be mechanically stable while providing a porous architecture that supports cell ingrowth and neocartilage formation.

It is key in the field of auricular reconstructive surgery to control the external shape of the implant to obtain satisfying esthetic results. This outcome is often used as a measure of success for a potential biomaterial.^{18,19,22} However, most efforts in auricular cartilage TE have used standardized auricular shapes.^{18,19,22,24} The optimal esthetic outcome would be to produce scaffolds that mimic the shape of patient's own auricle. That is, the shape must be patient-specific. Furthermore, the scaffold should mimic the shape of the auricular cartilage, rather than the external ear. Consequently, in this thesis we aimed at producing patient-specific BNC scaffolds with the shape of auricular cartilage. A number of technologies can be used to acquire the 3D shape of the intact contralateral auricle of a patient undergoing surgical auricular reconstruction. Protocols that can be applied in daily clinical practice with existing infrastructure have also been developed. These methods offer high precision and accuracy to detect patient-specific variation in auricular cartilage geometry. After processing the patient's medical images a 3D model is available for the production of a patient-specific auricular scaffold for TE purposes.²⁵

To engineer the auricle, there is a need for a cell source that can be easily accessible and that has the ability to form cartilage of sufficient quality. Cells from auricular cartilage would be optimal since they have already been shown to produce elastic cartilage in a tissue engineering setting.²⁶ However, if the patient has no or very small auricles, a different source is needed. Nasal septal cartilage is an option,²⁷ although less optimal because it tends to form hyaline cartilage rather than elastic cartilage. Moreover, harvesting nasal cartilage will create a defect in the nasal septum that, albeit small, cannot be regenerated. Mesenchymal stem cells are available in bone marrow and adipose tissue and can be harvested easily in surgery in large quantities. Cells from these sources are known to have the capacity to differentiate into chondrocytes,^{28,29} although formation of stable, more specific elastic cartilage remains to be shown. The use of autologous cells in cartilage repair is an attractive strategy as it may result in regeneration of the lost tissue. However, the clinical application of a cell-aided treatment does feature challenges – a limited supply of autologous chondrocytes with the proper phenotype being the most stringent one. To cancel out cell culture, including the concomitant laboratory logistics and the double surgery, autologous cells should be isolated within the operating room and applied directly. In addition, the combination of chondrocytes with a less limited source of autologous cells, such as bone marrow mononuclear cells, can overcome the challenge of having too few cells and may even increase the treatment's performance.^{30,31} The use of freshly isolated autologous cells, together with a non-degradable material, represents a novel strategy for delivering tissue-engineered auricles in a straightforward manner to the patients, using an undemanding one-step surgical method.

2.5 Bacterial nanocellulose as a biomaterial

Cellulose is a polysaccharide consisting of chains of (1–4)-linked glucose monomers and is the most abundant polymer in nature. Although it is generally considered a plant material, some bacteria also produce cellulose. In nature, cellulose-producing bacteria are found in rotten fruits and vegetables. Bacterial nanocellulose (BNC) is the extracellular product of *Gluconacetobacter xylinus*. These gram-negative aerobic bacteria produce pure nanocellulose fibrils in the presence of sugar and oxygen,⁷¹ where the production of cellulose occurs mainly at the air-liquid interface. BNC can hold as much as 100 times its dry weight of water.⁷² Its high water content suggests that it can be seen as a hydrogel, although not by definition, as it is not a network of polymer chains that are water-soluble. Hydrogels are known for their favorable biocompatible properties due to little protein adsorption. BNC holds interesting properties for tissue engineering applications, as it is a biomaterial with excellent biocompatibility and remarkable tissue integration capability.^{32,34,73,74}

The past decade has seen a tremendous interest of scientists evaluating BNC for several tissue engineering applications with positive outcomes reported.^{34,75-82} The material-cell interaction and subsequent positive effects on cell fate processes could be attributed to the highly hydrated nanocellulose fibrils and their morphological similarity with extracellular matrix components such as collagen.⁷⁶ Several *in vitro* studies of BNC scaffolds seeded with bovine articular chondrocytes and human articular, auricular and nasoseptal chondrocytes have also exhibited

good cell adhesion, proliferation and, most importantly, have demonstrated the maintenance of chondrogenic phenotype—as confirmed by the synthesis of cartilage-specific ECM.^{75,78,81,83}

2.5.1 *Biomedical applications of bacterial nanocellulose*

BNC products, such as temporary skin, have been introduced into the wound care market. BNC films have found an application in the health care sector because of their unique absorption properties. Cellulose has been most commonly used in applications such as blood purification, anticoagulant and plasma expander in aqueous systems. More recently, medical devices made from BNC are used in the clinic as wound and burn dressings (e.g. Dermafill®, Bioprocess®, XCell® and Biofill®), surgical meshes (e.g. Xylos®, Macro-Porous Surgical Mesh and Securian®) and dura mater substitutes (SyntheCel® Dura Repair), which have been used successfully to repair dural defects in 62 patients.⁸⁴

2.5.2 *Biofabrication of macroporous bacterial nanocellulose scaffolds*

BNC is a novel biomaterial with potential use in several TE applications. However, its dense nanocellulose network prevents cells from penetrating the material. To circumvent this problem, several techniques have been developed to create pores and support cell ingrowth in BNC scaffolds by tuning pore size and pore interconnectivity during biosynthesis of BNC,⁷⁶ via laser ablation⁷⁵ and freeze-dry processing.⁸⁵ Such macroporous BNC scaffolds have been shown to provide an adequate environment that supports ingrowth and differentiation of bovine and human chondrocytes.^{75,78,81,83}

2.5.3 *Purification of bacterial nanocellulose*

The purification of BNC consists on removing all bacterial residues, chiefly lipopolysaccharides (LPS), from the BNC network; which results in a material that is composed of pure cellulose and water. LPS, also known as endotoxins, are found in the outer membrane of gram-negative bacteria. These molecules consist of an O-antigen glycan, a core oligosaccharide, and a lipid A—known as a toxic fatty acid.⁸⁶ LPS are considered to be the most potent microbial pyrogens responsible for triggering the immune system.⁸⁷ When endotoxins enter the blood stream, they bind to circulating LPS-binding proteins and subsequently to the Toll-like receptor 4 on many leukocytes, primarily macrophages and B cells. This binding initiates the secretion of pro-inflammatory cytokines to counterattack the microbial invasion. High levels of LPS in the bloodstream trigger the production of excessive amounts of cytokines (IL-1 β , IL-1 α , IL-6, IL-8, and TNF), causing severe infection and inflammation that can lead to fatal septic shock.^{88,89} Due to the high risks associated with endotoxin contamination in medical devices, the United States Food and Drug Administration (FDA) has set guidelines for endotoxin limits in medical devices, which are no more than 0.5 endotoxin units (EU)/ml or 20 EU/device.⁹⁰ Thus, it is of utmost importance to comply with these guidelines to guarantee the non-pyrogenicity of biomaterials.

The potential use of BNC as a scaffold material for auricular cartilage regeneration requires, first and foremost, the depyrogenation of the material. Previous studies have only reported purification methods for thin BNC scaffolds (i.e. 0.2 to 3 mm in thickness) and have not

systematically evaluated the removal of endotoxins from the BNC network.^{32,34,75-77,91,92} There are various depyrogenation methods ensuring endotoxin inactivation and removal.⁹³⁻⁹⁵ In this context, treatment of BNC with aqueous sodium hydroxide solution, followed by rinsing with deionized water is the most common depyrogenation method reported in literature. In large BNC scaffolds, such as an auricle, the purification process is challenged by the higher bioburden and slower transport of bacterial residues compared to the thin and highly porous BNC scaffolds previously evaluated for various tissue engineering applications. Thus, it is of utmost importance to develop and validate an effective depyrogenation process for large BNC scaffolds before any *in vivo* studies are conducted.

2.6 3D Bioprinting of tissue analogues

A major challenge in tissue engineering has been the limitation of the widely used production methods to generate cell-seeded scaffolds with structures that mimic the target tissue, both in anatomic geometry and intra-tissue architecture with controlled spatial cell distribution. The characteristic of a material to be shaped into anatomical, patient-specific structures with high shape fidelity is considered a significant quality for any potential biomaterial in auricular cartilage TE.^{18,19,22} Of equal importance is to control the inner micro- and macro-scale features of the engineered-tissue to obtain satisfying aesthetic and functional results. In response to this need, more than a decade ago, advances in additive manufacturing inspired scientists to employ this technology for organ bioprinting and tissue engineering strategies.⁹⁶⁻⁹⁸ Bioprinting, an additive manufacturing technology, has gained due attention for its ability to spatially control the placement of cells, biomaterials and biological molecules.^{99,100} Bioprinting 3D tissue analogues provides the possibility of combining living tissue-specific cells with appropriate materials—natural, synthetic or decellularized ECM hydrogels—in a defined and organized manner. Consequently, this technology offers endless possibilities to the future of tissue and organ regeneration, basic research and drug screening.¹⁰¹⁻¹⁰⁴ Moreover, this technology allows the biofabrication of biomimetic-shaped three-dimensional (3D) structures unique to the target tissue or organ, since it can be combined with CAD/CAM technology using patients' medical images.^{105,106} Despite the challenges encountered when bioprinting hydrogel materials of low viscosity,¹⁰⁷⁻¹⁰⁹ considerable advances have been made to bioprint complex cell-laden 3D tissue constructs.^{103,110-116} However, the biofabrication of biomimetic-shaped 3D structures with high resolution, mimicking the intricate inner architecture unique to the target tissue, still remains a challenge.^{101,102,104} The development of hydrogel bioinks with good printability and bioactive properties that guide cellular fate processes would contribute to translation of this promising technology into the clinic.

CHAPTER 3

AIMS OF THE THESIS

Most auricular cartilage TE strategies have revolved around biodegradable scaffolds, where the hypothetical optimum has been the scaffold's degradation orchestrated by the neo-tissue formation. It would be ideal if the scaffold could be degraded by the time the neocartilage has reached full mechanical strength. However, fine-tuning this intricate play has proven to be a challenge in TE. Problems concerning poor structural integrity of the implant could be solved using non-degradable biocompatible scaffold materials, such as bacterial nanocellulose, in order to retain the shape of the auricle after implantation. We aim for a hybrid implant—BNC well integrated with the host and neo-tissue—that supports cell ingrowth, neocartilage formation and long-term structural integrity after implantation. The overall aim of this thesis is to design and biofabricate non-degradable, biocompatible, patient-specific BNC scaffolds for use in auricular cartilage regeneration.

3.1 Specific aims

- Determine the biomechanical specifications for auricular cartilage replacement materials. Assess whether 1) BNC's properties can be tuned to reach mechanical properties of relevance for auricular cartilage replacement materials, and 2) BNC can be produced in patient-specific auricular shapes.
- Develop and validate a depyrogenation process for BNC scaffolds that complies with the guidelines set by the FDA for endotoxin limits in medical devices. Then, assess the *in vitro* and *in vivo* biocompatibility of purified and densified BNC hydrogels according to standards set forth in ISO 10993.
- Evaluate the redifferentiation capacity of human nasoseptal chondrocytes cultured in porous BNC-Alginate composite scaffolds.
- Design and fabricate a scaffold that integrates mechanical stability and high porosity to maintain a long-term structural integrity while providing a porous architecture that supports cell ingrowth and neocartilage formation. Develop methods to produce patient-specific auricular BNC scaffolds with bilayer architecture. Evaluate neocartilage formation and stability of the bilayer BNC scaffolds *in vitro* and *in vivo*—in immunocompromised and immunocompetent animal models.
- Evaluate 3D bioprinting as an automated biofabrication process of patient-specific, chondrocyte-laden auricular constructs using a bioink composed of nanofibrillated cellulose and alginate. Furthermore, evaluate the effect of this bioink on cellular response, proliferation, and neocartilage formation in chondrogenic conditions *in vitro*.
- Re-design a compression bioreactor and evaluate the effect of dynamic mechanical stimulation to cell-seeded BNC constructs on neo-tissue development *in vitro*.

CHAPTER 4

MATERIALS AND METHODS

Please refer to **Papers I-V** for a more detailed description of materials and methods used in this thesis.

4.1 Biosynthesis of bacterial nanocellulose

Cellulose-producing bacteria strain *Gluconacetobacter xylinus* (ATCC[®] 700178[™]) was used in **Papers I, II, III** and **V** and other unpublished work. The culture media used was fructose media with addition of corn steep liquor, as it has been shown in previous studies to be the most suitable.¹¹⁷ The culture media contains fructose (40 g/L), yeast extract (5 g/L), (NH₄)₂SO₄ (3.3 g/L), KH₂PO₄ (1 g/L), MgSO₄·7H₂O (0.25 g/L), corn steep liquor (20 mL/L), trace metal solution (10 mL/L) and vitamin solution (5 mL/L) in 1 liter of distilled water, pH 5.5. The trace metal solution consists of (mg): FeSO₄·7H₂O (3.60), CaCl₂·2H₂O (14.70), Na₂MoO₄·2H₂O (2.42), ZnSO₄·7H₂O (1.73), MnSO₄·5H₂O (1.39), CuSO₄·5H₂O (0.05) and EDTA (3) in 1 liter of distilled water, pH 5; and the vitamin solution (mg): inositol (2.0), nicotinic acid (0.4), pyridoxine hydrochloride (0.4), thiamine hydrochloride (0.4), D-pantothenic acid calcium (0.2), riboflavin (0.2), *p*-amino benzoic acid (0.2), folic acid (0.0002) and d-biotin (0.0002) in 1 liter of distilled water, pH 5. For pre-cultivation, 6 cellulose-forming colonies were cultured for 2 days at 30 °C in a tissue culture flask (75 cm², working volume of 50 ml). The bacteria were liberated from the cellulose network by vigorous shaking and inoculated into the culture media. The culture time was varied depending on the desired thickness of the BNC pellicle.

4.2 Mechanical evaluation of bacterial nanocellulose as an implant material for auricular cartilage replacement

In **Paper I** we investigated the potential use of BNC in auricular cartilage tissue engineering. Firstly, the mechanical properties of human auricular cartilage were measured in order to set a preliminary benchmark for auricular cartilage replacement materials. Secondly, the capacity of BNC to match these requirements was assessed. Finally, a novel biofabrication process to produce patient-specific auricular BNC implants was developed (**Figure 3**). Two distinct mechanisms are involved in the response of cartilage to loading: the intrinsic mechanical properties of the ECM and the resistance to interstitial fluid flow through the ECM,¹⁴³ which is governed by the permeability and swelling pressure (Donnan osmotic pressure) of the ECM.¹¹⁸ Creep and stress relaxation tests are commonly performed to characterize these properties, using confined or unconfined compression, as well as indentation testing.^{118,119} In **Papers I, III** and other unpublished work, stress-relaxation indentation testing was used to evaluate the mechanical properties of native cartilage, densified BNC hydrogels and tissue-engineered constructs. In an indentation test, a porous or non-porous indenter is used to indent the sample. The diameter of the indenter is chosen to allow fluid flow, while the sample is confined radially. Indentation can be performed at different locations of the same sample, so as to evaluate spatial variation in mechanical properties.¹²⁰

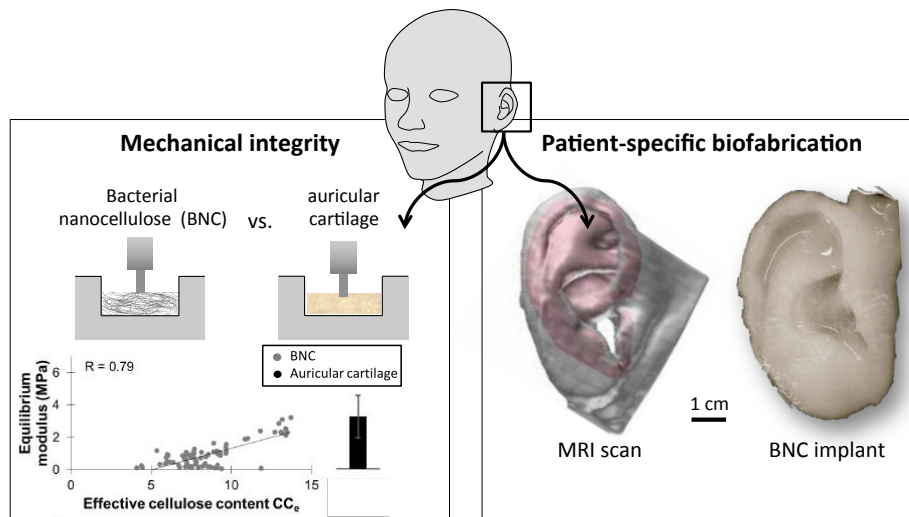


Figure 3 – Graphical abstract of Paper I. Firstly, the mechanical properties of human auricular cartilage were measured. Secondly, the capacity of BNC to match these requirements was assessed. Finally, a novel biofabrication process to produce patient-specific auricular BNC implants was developed.

4.2.1 Harvesting of human auricular cartilage

Human auricular cartilage samples were obtained according to the ethics regulations of the University Hospital Zurich (Zurich, Switzerland), the Ulm University Medical Center, (Ulm, Germany) and the Erasmus Medical Center, (Rotterdam, The Netherlands). Samples were either harvested from patients undergoing ear reconstructive surgery or from complete auricles obtained post mortem from human donors. Prior to testing, the perichondrium was removed to expose the cartilage surface.

4.2.2 Preparation of densified bacterial nanocellulose hydrogels

First, large BNC cylinders were biosynthesized in static culture for 30 days, until the bacteria had produced large cylindrical BNC structures with height of approximately 5 cm. The protocol used to remove the bacteria and its residues from the cellulose matrix was adapted from previous studies.^{32,80} In brief, the BNC cylinders were washed in 0.1 M NaOH for 21 days, changing the solution every day, and then rinsed with large amounts of deionized water to remove bacterial residues and neutralize the pH. BNC pellicles with varying nominal cellulose content of 2.5%, 5%, 7.5%, 10%, 12.5% and 15% were produced by compressing BNC cylinders with different initial heights down to a final height of 1 mm, as described in **Paper I**.

4.2.3 Mechanical testing

BNC samples ($n = 78$) with varying nominal cellulose content (2.5–15%) were compared using stress-relaxation indentation with human auricular cartilage ($n = 17$, from 4 males, aged 49–93 years old). Samples were placed in close-fitting stainless steel cylindrical wells. Mechanical testing was performed with a materials testing machine (Zwick Z005) equipped with a 10 N load cell, a built-in displacement control, and a cylindrical, plane ended, stainless steel indenter ($\varnothing 0.35$ mm). Measurements of maximum stress (σ_{\max}), equilibrium modulus (E_{eq}), and

instantaneous modulus (E_{in}) were determined for every sample, as described previously.¹²⁰ Additionally, a relaxation half-life time ($t_{1/2}$) and a characteristic relaxation time (τ) were computed to estimate the viscoelastic relaxation after the first strain application.

4.3 Biofabrication of patient-specific auricular bacterial nanocellulose implants

In **Paper I**, we also presented a novel biofabrication process to produce patient-specific BNC implants with complex 3D shapes. A bioprinter, consisting of a high precision micro-dispensing system, used to dispense controlled volumes of culture media, and a precision motion system, used to control the dispensing location, was developed in-house for the biofabrication of a patient-specific auricular BNC implant prototype. First, the auricle of a volunteer was segmented and reconstructed from magnetic resonance imaging (MRI) data and subsequently 3D rapid prototyped using selective laser sintering. A negative auricle mold, produced by casting silicone around the auricle model, was inoculated with bacteria suspension and positioned in the bioprinter to guide the bacteria to reproduce the large-scale features of the auricle. Meanwhile, the micro-dispensing valve was programmed to spray sterile culture media into the mold every 6 hours. The 3D biofabrication process continued for 18 days, until the cellulose layer filled the silicone mold. The auricular BNC implant prototype was removed from the mold and cleaned following the same protocol described for the BNC pellicles.

4.4 Biocompatibility evaluation of densified bacterial nanocellulose hydrogel

In **Paper II**, we investigated the biocompatibility of densified BNC hydrogel with cellulose content of 17%. First, cylindrical BNC structures ($\text{Ø}48 \times 20$ mm) were produced, purified in a built-in house perfusion system, and compressed to increase the cellulose content in the BNC hydrogels (densification of BNC described in **Paper I**). The reduction of endotoxicity of the material was quantified by bacterial endotoxin analysis throughout the purification process. Afterward, the biocompatibility of the purified dense BNC hydrogels was assessed *in vitro* and *in vivo*, according to standards set forth in ISO 10993. It was hypothesized that biocompatibility of BNC should not be affected after densification of the nanocellulose network, provided that endotoxin levels in the BNC network are below the endotoxin limit (0.5 EU/ml) set by the FDA for medical devices.⁹⁰

4.4.1 Depyrogenation process

The potential use of BNC as a scaffold material for auricular cartilage regeneration requires, first and foremost, the depyrogenation of large BNC structures before the compression and densification of the BNC network is done. Previous studies have only reported purification methods for thin BNC scaffolds (i.e. 0.2 to 3 mm in thickness) and have not systematically evaluated the removal of endotoxins from the BNC network.^{32,34,75-77,91,92} Thus, in **Paper II**, we developed and validated a depyrogenation process for large BNC structures. The depyrogenation of BNC consisted of two purification steps (see **Figure 4**). The first step involved washing the BNC cylinders with 0.5 M NaOH in a built-in house perfusion system to speed up the removal of

bacteria and endotoxins from the BNC network. The second step involved washing the densified BNC hydrogel disks in sterile and non-pyrogenic conditions using endotoxin-free water with an endotoxin specification of <math><0.005\text{ EU/ml}</math>.

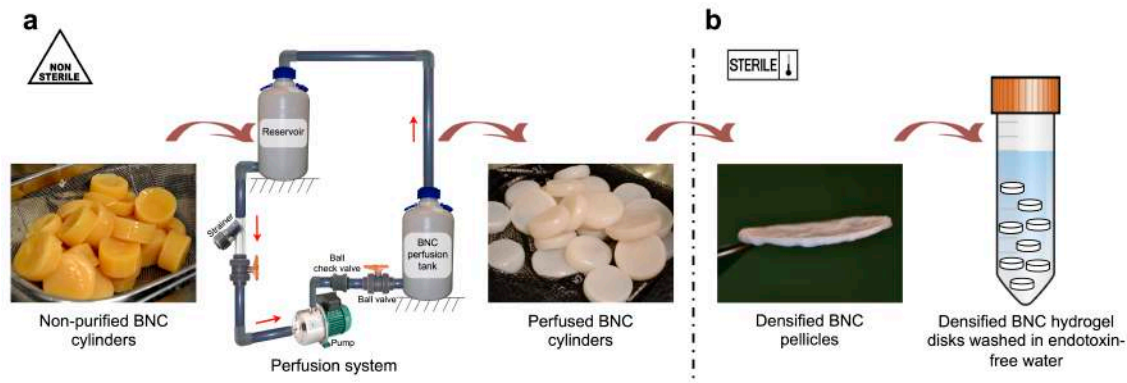


Figure 4 – Overview of depyrogenation of densified BNC before biocompatibility evaluation. (a) The first depyrogenation process consisted in washing large BNC cylinders with 0.5M NaOH in a built-in-house perfusion system (schematic) for 28 days in a non-sterile environment. The perfused BNC cylinders were then compressed to increase the cellulose content. (b) The second depyrogenation process consisted in washing the densified BNC disks with endotoxin-free water for 14 days in sterile conditions. (Paper II)

4.4.2 Validation of depyrogenation process

The reduction in endotoxicity and cytotoxicity of BNC was monitored throughout the purification process. Densified BNC hydrogels were analyzed for surface chemical composition, endotoxin content, crystallinity and *in vitro* cytotoxicity.

Electron spectroscopy for chemical analysis: In **Paper II**, surface chemical composition analyses were performed on BNC samples during the first purification process using a PHI Quantum 2000 scanning ESCA microprobe (Physical Electronics, MN, USA). The percent content of nitrogen, oxygen and carbon, as well as the signal peak for C–C bonds in the high resolution spectra were analyzed to monitor the 1) removal of bacterial and medium residues, shown by the reduction of nitrogen; 2) removal of LPS molecules, shown by the reduction of the signal peak for C–C bonds; and 3) purity of the material, indicated by the oxygen to carbon ratio of 0.83 which is found in pure cellulose.

Bacterial endotoxin testing: An endotoxin-mediated pyrogen test was performed on extracts of scaffolds studied in this thesis to evaluate the potential of the materials to induce a pyrogenic response (fever). This test can be performed *in vitro* using the bacterial endotoxin test, or *in vivo* using a rabbit model; the former method was selected in this work. Endotoxin extraction from the BNC scaffolds was done in accordance to the international standard ISO 10993-12:2009. Samples were incubated in endotoxin-free water, using the extraction ratio of 0.1 g of BNC/ml of extraction medium, for 72 ± 2 hours at 37 ± 1 °C under orbital motion. Endotoxicity of the extracted samples was determined by the PyroGene™ recombinant Factor C assay performed by Lonza Verviers (**Papers II, III** and other unpublished work). This assay has a minimum detection limit of 0.005 EU/ml.

X-ray diffraction: In **Paper II**, the crystallinity of the purified BNC was investigated with XRD to analyze any possible changes in the crystalline structure of BNC fibrils caused during the purification process. The crystallinity was analyzed with a Siemens D5000 X-ray diffractometer. The relative crystallinity index (CrI) was calculated by Segal's method,¹²¹ using the equation $CrI = (I_{200} - I_{am})/I_{200} \times 100$, where I_{200} is the peak intensity of the (200) plane at $2\theta = 22.6^\circ$ for cellulose I, and I_{am} is the peak intensity of the amorphous fraction at $2\theta = 18^\circ$ for cellulose I.

In vitro cytotoxicity testing: In **Papers II-IV**, the studied scaffold materials were tested according to the international standard ISO 10993-5:2009 (Biological evaluation of medical devices–Part 5: Tests for *in vitro* cytotoxicity) to determine the biological response of mammalian cells *in vitro*. This test is a common cytotoxicity assessment designed to assess the toxicity to cells of leachable components of the material. The material is extracted in cell culture media. Extracts are placed in contact with a monolayer of L929 mouse fibroblast cells. Cells are incubated in standard culture conditions for an additional period of time, after which they are examined for indications of cytotoxicity. CellTiter 96® aqueous one solution cell proliferation assay (Promega, WI, USA) was used to determine the number of viable cells. The cytotoxic potential of the tested samples was identified based on the percentage of cell viability; classified as toxic when cell viability was below 50%, slightly cytotoxic when it was between 51% and 70%, and non-cytotoxic when cell viability was above 71%.

4.4.3 *In vivo* biocompatibility evaluation

In **Paper II**, the *in vivo* biocompatibility of densified BNC hydrogels was assessed according to international standard ISO 10993-6:2009 (Biological evaluation of medical devices–Part 6: Tests for local effects after implantation). An *in vivo* intradermal reactivity test was performed to determine adverse biological reactions caused by the implanted BNC material. All experiments were carried out in accordance with European guidelines for the Care and Use of Laboratory Animals and performed with the approval of the Regional Ethical Board in Tübingen, Germany. The intradermal implantations were conducted on female Chinchilla Bastard rabbits (Charles River Laboratories). In this study, we established three experimental groups (**Table 1**). The first group was implanted with autologous auricular cartilage (control group), since it is the gold standard in auricular cartilage reconstruction. The second group was implanted with densified BNC hydrogel disks, whereas the third group was implanted with medical grade Gore-Tex matrices (Gore-Tex® Soft Tissue Patch, expanded polytetrafluoroethylene), since it is considered an inert biomaterial. After 1 week *in vivo* retention time, animals were terminated and samples were explanted for examination of macroscopic and microscopic tissue responses.

Table 1 - Experimental groups and number of implants per group.

| Group | Implant | Animals/group | Implants/animal |
|-------|--------------------------------|---------------|-----------------|
| 1 | Autologous auricular cartilage | 3 | 4 |
| 2 | Densified BNC hydrogel | 3 | 4 |
| 3 | Medical grade GoreTex® | 3 | 4 |

4.4.3.1 Histopathological evaluation of biocompatibility index

A semi-quantitative scoring system was used to analyze hematoxylin and eosin stained sections of explants for inflammatory and fibrotic reactions, according to the recommendations of ISO 10993-6 appendix E. Inflammatory reactions were evaluated according to the presence of neutrophil polymorphonuclear cells (PMNC), lymphocytes, plasma cells, macrophages, giant cells, and necrosis. The fibrotic reaction was evaluated according to the presence of neovascularization, fibrosis, and fatty infiltration. On the basis of tissue and cellular responses, we determined the biocompatibility index (B_i) of the densified BNC hydrogel and control groups. The B_i was defined as the sum of the scores from the inflammatory and fibrotic reactions. Based on the B_i of each implant group, an irritant ranking was determined for each implant group: non-irritant (0.0–2.9), slight irritant (3.0–8.9), moderate irritant (9.0–15.0), and severe irritant (>15.1).

4.5 Bacterial nanocellulose and alginate as scaffold materials for auricular cartilage regeneration

Native BNC hydrogels are impenetrable to cells due to the lack of macroporosity in the material. However, there are several methods available to create macroporous BNC scaffolds that support cell ingrowth.^{75,76,85} The redifferentiation capacity of culture-expanded human nasoseptal chondrocytes was studied in BNC-Alginate (BNC-A) composite scaffolds *in vitro*, where the effect of scaffold composition on neocartilage formation was evaluated. Two groups of BNC-A composite scaffolds, 50/50 and 90/10, with similar macro-architecture but different surface topographies were investigated.

4.5.1 Fabrication and characterization of BNC-Alginate composite scaffolds

Macroporous BNC-A composite scaffolds were fabricated by a freeze-drying process, as described in **Paper III**. First, thin BNC pellicles were produced and cleaned as described in **Paper V**. The BNC pellicles were then homogenized, until a pulp consistency was achieved, and steam sterilized. Different amounts of 1.1 % (w/w) sterile sodium-alginate solution were mixed with sterile BNC suspension to achieve two different ratios (BNC/Alginate: 50/50 and 90/10), expressed as percent dry weight of BNC and alginate compared to the total dry weight. Subsequently, the BNC-A mixtures were dispersed, frozen to $-80\text{ }^{\circ}\text{C}$ and lyophilized to sublimate the ice crystals and create a macroporous architecture. BNC-A composite scaffolds ($\text{Ø}5\text{ mm} \times 2\text{ mm}$) were cut and stabilized by crosslinking the alginate with 100 mM CaCl_2 solution. Prior to cell culture, BNC-A composite scaffolds (each $n = 87$) were sterilized in 70% ethanol for 30 minutes.

Endotoxin levels in the BNC-A composite scaffolds were measured using the Limulus amoebocyte lysate (LAL) test. The LAL test was performed in triplicate using the Endosafe[®]-PTS[™] assay (Charles River Laboratories). Endotoxin extraction was performed as described in section 4.4.2. Furthermore, *in vitro* cytotoxicity of BNC-A composite scaffolds was tested according to ISO

10993-5, as described in section 4.4.2. Finally, the micro- and macro-structure of BNC-A composite scaffolds was characterized using a Leo Ultra 55 field-emission gun SEM (Carl Zeiss).

4.6 Bilayer bacterial nanocellulose scaffold for auricular cartilage regeneration

In **Paper III** we investigated the *in vitro* and *in vivo* performance of a novel bilayer BNC scaffold, composed of a dense BNC layer (**Paper II**) joined with a macroporous composite layer of BNC and alginate, designed to be mechanically stable and maintain a long-term structural integrity while providing a porous architecture that supports cell ingrowth and neocartilage formation.

4.6.1 Fabrication and purification of bilayer BNC scaffold

Densified BNC hydrogel disks (i.e. dense layer) were produced and purified as described in **Papers I** and **II**, respectively. Whereas 90/10 BNC-A composite scaffolds (i.e. porous layer) were fabricated by a freeze-drying process, using non-pyrogenic BNC. In **Paper III** we used a novel cellulose solvent system, consisting of the ionic liquid EMIMAc (1-ethyl-3-methylimidazolium acetate), to achieve a strong interfacial molecular bonding between the dense and porous layers. Bilayer BNC scaffolds were crosslinked with 100 mM CaCl₂ solution and then washed in sterile and non-pyrogenic conditions to remove cytotoxic EMIMAc residues and endotoxins. Subsequently, the purified bilayer BNC scaffolds (Ø8 mm × 3 mm) were steam sterilized in endotoxin-free water.

4.6.2 Validation of purification process and characterization of scaffold

Removal of EMIMAc residues from the bilayer BNC scaffolds was evaluated by infrared spectroscopy analysis (ATR-FTIR). The peak at wavenumber 1566 cm⁻¹ was used to detect EMIMAc residues in the ATR spectra of bilayer BNC scaffolds. This peak is composed of two overlapped peaks that correspond to the carboxyl group of the acetate and an underlying ring mode of the cation, as shown by previous studies.^{122,123} Furthermore, the removal of cytotoxic EMIMAc residues and endotoxins from the bilayer BNC scaffolds was evaluated by *in vitro* cytotoxicity testing and by the PyroGene™ recombinant Factor C assay, respectively (see section 4.4.2). Moreover, the morphology of bilayer BNC scaffolds was characterized by SEM and micro-computed tomography (microCT). 3D morphometric parameters such as scaffold porosity and mean pore size were computed from microCT reconstructions of the porous BNC-A scaffold layer.

4.7 Patient-specific bacterial nanocellulose scaffold for auricular cartilage regeneration.

We continued the development of a patient-specific auricular BNC scaffold with a bilayer architecture that integrates mechanical stability and high porosity (**Paper III**). In this study we investigated the *in vivo* performance of auricular BNC scaffolds in an immunocompetent animal model.

4.7.1 Fabrication and purification of patient-specific auricular BNC scaffold

Patient-specific auricular BNC scaffolds ($n = 12$), composed of a dense and porous layer, were fabricated by combining the methods developed in **Papers I-III**. First, auricular cartilage of a volunteer was reconstructed from MRI data, scaled to 60% of original size and then the 3D model was rapid prototyped, as described in **Paper I**. A negative auricular mold, produced by casting silicone around the auricular cartilage model and which consists of a top and bottom part, was used to mold already compressed BNC pellicles into auricular cartilage-shaped structures (dense BNC layer). Meanwhile, 90/10 BNC-A composite scaffolds ($\text{Ø}52 \text{ mm} \times 2 \text{ mm}$) were fabricated by a freeze-drying process, then crosslinked with 100 mM CaCl_2 solution and rinsed with sterile water. The wet BNC-A porous layer was placed on the dense BNC layer and the top part of the mold was used for molding the porous layer. Both scaffold layers were frozen to -80 °C overnight while being supported by the mold, then detached from the mold and freeze-dried. The ionic liquid EMIMAc was used to achieve a strong interfacial molecular bonding between the dense and porous layers, as described in **Paper III**. Auricular BNC scaffolds were then purified in sterile and non-pyrogenic conditions, as described in **Paper III**, for up to 8 weeks. Subsequently, the purified auricular BNC scaffolds were steam sterilized. Removal of endotoxins and cytotoxic ionic liquid residues from the auricular BNC scaffolds was evaluated by the PyroGene™ recombinant Factor C assay and *in vitro* cytotoxicity testing, respectively (see section 4.4.2).

4.8 3D bioprinting of human chondrocyte-laden nanocellulose hydrogel for patient-specific auricular cartilage regeneration

In **Paper IV** we evaluated the biological functionality of a nanocellulose-based bioink for auricular cartilage TE. 3D bioprinted auricular constructs, laden with human chondrocytes, were cultured for up to 28 days to study the redifferentiation capacity of the chondrocytes.

4.8.1 Preparation and cytotoxicity evaluation of NFC-Alginate bioink

A highly viscous, shear-thinning dispersion of nanofibrillated cellulose (NFC) was provided by Innventia AB (Sweden) and produced as described by Pääkkö et al.¹²⁴ The NFC dispersion was concentrated to 3 % (w/w) and mannitol was dissolved at a concentration of 4.6 % (w/w). The mixture was loaded in syringes and sterilized by electron irradiation at a dose of 25 kGy. Sterile alginate (FMC BioPolymer AS, Norway) was dissolved in 4.6 % (w/w) sterile-filtered mannitol solution at a concentration of 30 mg/ml. The NFC dispersion and alginate solution were then combined at a volume ratio of 4:1 (NFC:Alginate) and mixed thoroughly with a spatula, under sterile conditions. *In vitro* cytotoxicity of the NFC-Alginate (NFC-A) bioink was tested according to ISO 10993-5.

4.8.2 Bioprinting of cell-laden NFC-Alginate bioink into auricular and gridded structures

A 3D model of a human auricle reconstructed from an MRI scan (described in **Paper I**) was used for the bioprinting experiment. Using a 3D Discovery® instrument (regenHU Ltd, Switzerland),

chondrocyte-laden NFC-A hydrogel constructs were bioprinted in the shape of a human auricle and gridded structures. After bioprinting, the cell-laden NFC-A constructs were immediately crosslinked with 100 mM aqueous CaCl₂ solution and cultured in standard culture conditions (see section 4.11.1)

4.9 Mechanical stimulation of cell-seeded BNC scaffolds to enhance neo-tissue development

In **Paper V**, cell-seeded macro-channeled BNC scaffolds were cultured under dynamic mechanical stimulation in a compression bioreactor to enhance collagen production by the cells. In this study, the mouse fibroblast 3T6 cell line was used as a model, as it is a robust collagen secreting line. The *in vitro* culture of cell-seeded scaffolds under mechanical stimulation consisted of two phases. The constructs were first cultured under static conditions for 14 days, followed by dynamic stimulation conditions in a built in-house compression bioreactor for 14 days. The constructs were subjected to a dynamic compression of 5% at a loading frequency of 0.1 Hz, during a 10-min period followed by a 15-min pause, for a total duration of 5 h/day. These loading conditions fall in the range of the physiological conditions relevant for native cartilage tissue (0.1–1 Hz, 5–10% strain).^{125,126} A static culture was used as control. The three-dimensional distributions of collagen fibers and fibroblasts in the cellulose scaffolds were studied under native, soft-matter conditions by combined second harmonic generation (SHG) and coherent anti-Stokes Raman scattering (CARS) microscopy. Collagen type I¹²⁷ and cellulose¹²⁸ fibers can be visualized by SHG microscopy. With CARS microscopy, visualization of cell arrangement can be done by probing a hydrogen-carbon vibration of CH₂ groups present in cell membranes and storage lipids.¹²⁹

4.10 Cell culture

4.10.1 Cell source

Human nasoseptal chondrocytes (hNC) were used in **Papers III** and **IV**. Nasoseptal cartilage biopsies were obtained during routine surgeries, like rhinoplasty or septorhinoplasty, at the Department of Otorhinolaryngology, Ulm University Medical Center (Ulm, Germany). Cartilage harvesting was approved by the University of Ulm ethics committee (No. 152/08), and all patients involved in this research responded to an informed consent. Donor age ranged from 22 to 54 years.

In **Paper III**, culture-expanded hNCs as well as a combination of freshly isolated (uncultured) hNCs and human bone marrow mononuclear cells (MNC) were used. Nasoseptal cartilage biopsies were obtained from male and female patients (mean age 31 years; age range 18–69 years) undergoing routine reconstructive septorhinoplasty at the Department of Otorhinolaryngology, Ulm University Medical Center, with approval of the local medical ethics committee (No. 152/08). The cartilage biopsies were divided in three pools prior to the isolation of hNCs. Additionally, bone marrow aspirate was collected from three donors (mean age 70 years, 2 males, 1 female) during total hip replacement surgery at the Department of Orthopaedics,

Erasmus Medical Center (Rotterdam, The Netherlands), after acquiring written patient consent and approval of the local medical ethics committee (MEC-2004-142). Biopsies were sent to CellCoTec (Bilthoven, The Netherlands) for rapid isolation of hNCs and MNCs.

Rabbit auricular chondrocytes (rAC) were used for the immunocompetent autologous graft. Auricular cartilage biopsies were harvested from the right auricle of New Zealand White (NZW) rabbits (Charles River Laboratories), after acquiring the approval of the Regional Ethical Board in Tübingen, Germany.

4.10.2 Cell isolation and expansion

Isolation of hNCs and rACs from the cartilage was done by enzymatic digestion of the tissue with 0.3% type II collagenase in culture medium (DMEM/Ham's F-12 supplemented with 10% FBS and 0.5% gentamycin) for 16-18 hours at 37 °C under agitation. Cells were separated by filtration through a 100-µm cell strainer and resuspended in culture medium. Total cell number and viability were determined using the trypan blue exclusion method. Subsequently, the hNCs and rACs were seeded for expansion in monolayer culture at a density of 5,000 cells/cm². When reaching 80%–90% confluence, hNCs were detached, counted, and cryopreserved to ensure an equal treatment for all cells harvested from different donors. rACs and hNCs were expanded one more week in monolayer culture to obtain a sufficient cell number, where medium was changed three times per week. When reaching 80%–90% confluence, cells were detached, counted and resuspended in culture medium at the desired cell concentration. All experiments were conducted using hNCs and rACs at passage 2.

In **Paper III** (*in vivo* study), a combination of freshly isolated (uncultured) hNCs and MNCs was used. The rapid isolations of hNCs and MNCs were performed by CellCoTec. Patented clinically applied protocols were used to isolate the cells within the hour.¹³⁰ In brief, cartilage pieces were digested enzymatically under mechanical stimulation. Upon rapid digestion, any remaining debris was filtered out with a cell strainer. For the collection of MNCs, the bone marrow aspirate was relieved of its erythrocyte content using lysis buffer. Standard cell buffer was used for washing steps. Cell numbers and viability were measured using the trypan blue exclusion method.

4.11 Chondrogenic differentiation

4.11.1 Chondrogenic differentiation *in vitro*

Prior to cell seeding, BNC-A composite scaffolds and bilayer BNC scaffolds (**Paper III**) were conditioned in culture medium and chondrogenic medium, respectively, for 24 h. All incubations were done in standard culture conditions (37 °C, 5% CO₂ and 95% relative humidity). Subsequently, hNCs were seeded in the scaffolds at a cell density (cells/apparent scaffold volume) of 25×10⁶ cells/cm³ (BNC-A composite scaffolds) and 10×10⁶ cells/cm³ (bilayer BNC scaffolds). In **Paper IV**, hNCs were encapsulated in NFC-A bioink at a concentration of 20×10⁶ cells/ml. After bioprinting and crosslinking, the hNC-laden NFC-A constructs were rinsed with culture medium. HNCs were cultured in defined chondrogenic medium (StemMACS

ChondroDiff media) containing recombinant analog of insulin-like growth factor-I (R3 IGF-1), transforming growth factor beta 1 (TGF- β 1), insulin, transferrin, L-glutamine and FBS. The addition of IGF-1 and TGF- β 1 enhances chondrogenic differentiation and stimulates the synthesis of cartilage-specific ECM. Furthermore, IGF-1 decreases matrix catabolism (destructive metabolism) and TGF- β 1 decreases catabolic activity of numerous catabolic cytokines, including interleukin 1 (IL-1) and matrix metalloproteinases (MMPs).¹³¹⁻¹³⁶ Chondrogenic differentiation in hNC-seeded/laden scaffolds was studied *in vitro* for six weeks (BNC-A composite scaffolds and **Paper III**) and four weeks (**Paper IV**) in standard culture conditions.

4.11.2 Chondrogenic differentiation in vivo

Chondrogenic differentiation in cell-seeded scaffolds was also studied *in vivo*. The first *in vivo* study was performed in an immunocompromised animal model for eight weeks (**Paper III**), and the second study was performed in an immunocompetent animal model for six weeks with patient-specific auricular BNC scaffolds.

4.11.2.1 Implantation of constructs in immunocompromised animal model

In **Paper III**, we explored the application of a clinically relevant strategy, seeding a low number of freshly isolated human chondrocytes in combination with freshly isolated human mononuclear cells, in order to test the translation of this auricular cartilage TE technology to the clinic. Cells were first encapsulated in alginate as a combination of 80% freshly isolated MNCs and 20% freshly isolated hNCs at a total cell concentration of 20×10^6 cells/ml and subsequently seeded in bilayer BNC scaffolds. To evaluate the stability of the bilayer BNC scaffolds and neocartilage formation in a more complex biological environment, MNC/hNC-seeded and cell-free bilayer BNC scaffolds were implanted subcutaneously on the dorsal side of 9-week-old nude female mice (NMRI nu/nu, Charles River Laboratories). At the time of implantation, mice were anesthetized with 2.5% Isoflurane. Eight weeks after subcutaneous implantation, animals were terminated and samples were explanted for immunohistochemical, biochemical and biomechanical analyses. Animal experiments were carried out with approval of the local Animal Experiments Committee of the Erasmus Medical Center, Rotterdam, The Netherlands (EMC 2429).

4.11.2.2 Implantation of constructs in immunocompetent autologous model

For the immunocompetent autologous tissue-engineered auricular graft, we used New Zealand White (NZW) rabbits (3 months old). Four weeks prior to implantation, rabbit auricular cartilage was harvested and isolated rACs were expanded in monolayer culture for 2 weeks. Prior to cell seeding, patient-specific auricular BNC scaffolds ($n = 6$) were conditioned in 3D-culture medium (high glucose DMEM supplemented with 50 μ g/ml L-ascorbic acid, 2.5 μ g/ml human insulin, 0.4 mM L-proline, 10% FBS and 0.5% gentamicin) for 24 h. RACs were seeded into auricular BNC scaffolds (50×10^6 cells/cm³) and cultured for 2 weeks *in vitro*. Before the implantation, rAC-seeded ($n=6$) and cell-free ($n=6$) scaffolds were rinsed with sterile saline solution to remove medium components, such as FBS, that could cause an unwanted inflammatory reaction.

Subsequently, the autologous grafts were implanted to the same rabbit donor. NZW rabbits ($n=6$) were anesthetized and the dorsum shaved. Through a 5 cm incision along the spine, each animal received subcutaneously a seeded (left side) and a cell-free (right side) auricular BNC scaffold. Animals received antibiotics and pain treatment for 3 days post-implantation. Six weeks after subcutaneous implantation, animals were terminated and samples were explanted for gross morphological, immunohistochemical and biomechanical analyses. All experiments were carried out at the Department of Otorhinolaryngology, Ulm University Medical Center, in accordance with European guidelines for the Care and Use of Laboratory Animals and approval of the Regional Ethical Board in Tübingen, Germany.

4.12 Evaluation methods for chondrogenic differentiation

4.12.1 Electron microscopy

In order to study the interaction between the scaffold material and chondrocytes, cell morphology and ECM neo-synthesis in the scaffolds, scanning electron microscopy (SEM; Leo Ultra 55 field-emission gun SEM) and transmission electron microscopy (TEM; Zeiss EM 10 and JEM-1400) analyses were performed.

4.12.2 Histological analysis

The cell-seeded scaffolds were fixed with 4% formaldehyde, embedded in paraffin and sectioned (5 μ m). Formaldehyde is used to fixate the tissue by crosslinking the proteins, particularly between the lysine residues. The stainings used in the thesis are listed in **Table 2**.

Table 2 – Short description of histological stainings used.

| Stain | ECM component analyzed | Comment |
|-----------------------------|--|--|
| Hematoxylin and Eosin (H&E) | Extracellular matrix in general Proteins are stained red or pink and nuclei is stained dark blue. | Hematoxylin binds to basophilic substances (e.g. DNA/RNA). Eosin binds to acidophilic substances (e.g. proteins). |
| Alcian blue (AB) | Sulfated glycosaminoglycans (s-GAG), proteoglycans Cartilage is stained blue and nuclei black. | Cationic dye that forms reversible electrostatic bonds with the negative sites of polysaccharides (s-GAG). |
| Safranin O and fast green | Proteoglycans Cartilage is stained orange to red, cytoplasm blue-green and nucleic black. | Cationic dye that binds to negative sites of chondroitin-6-sulfate or keratin sulfate-components of cartilage. |
| Verhoeff's stain | Elastin Elastic fibers and nuclei are stained black. | Verhoeff's stain forms a variety of cationic, anionic and non-ionic bonds with elastin. |

4.12.3 Immunohistochemical analysis

In **Papers III** and **IV** and other unpublished work, cell-seeded scaffolds were processed for immunohistochemical (IHC) staining to detect cartilage-specific proteins such as aggrecan, type II collagen, cartilage oligomeric protein (COMP) and matrilin-3, and the dedifferentiation marker type I collagen. Positive immunostains were confirmed with the use of native ear or nasoseptal cartilage. A monoclonal mouse IgG1 antibody was used as a negative control. Sections were deparaffinized and dehydrated. An enzymatic antigen retrieval step followed by quenching of endogenous peroxidase activity was performed before incubation with primary antibodies. For visualization of these markers the LSAB+System-HRP kit (Dako), which is based on the labeled streptavidin biotin method, was used according to the manufacturer's protocol. The color reaction was developed using DAB and AEC chromogens, resulting in a brown or red precipitate at the antigen site, respectively.

4.12.4 Gene expression analysis

In **Papers III** and **IV** and other unpublished work, the capacity of hNCs to synthesize cartilage-specific ECM components in the scaffolds was also investigated on the basis of the expression of the chondrogenic marker genes *ACAN* and *COL2A1*. The dedifferentiation markers, *VCAN* and *COL1A1*, were also investigated. Additionally, in **Paper IV** expression of chondrogenic markers such as SRY-box 9 (*SOX9*), cartilage oligomeric matrix protein (*COMP*) and matrilin-3 (*MATN3*), and osteoblastic marker runt-related transcription factor 2 (*RUNX2*) were investigated.

Isolation of RNA: Total RNA was extracted by disruption and homogenization of the hNC-seeded scaffolds in lysis buffer. The RNA was isolated and purified using the RNeasy Mini kit and DNase mix according to the manufacturer's instructions. The amount and quality of total RNA was quantified using a multimode microplate reader at 260 nm and 280 nm. The ratio of $\lambda_{260}/\lambda_{280}$ between 1.9 and 2.1 was considered an adequate marker for RNA purity.

Real-time two-step RT-PCR analysis: Total RNA was converted to cDNA using QuantiTect Reverse Transcription kit, according to manufacturer's protocol, in a thermocycler. Real-time PCR was performed using the LightCycler TaqMan Master kit and Universal Probe Library. The following genes were analyzed to study the redifferentiation of the chondrocytes: *ACAN*, *COL2A1*, *SOX9*, *COMP*, *MTN3*, *VCAN*, *COL1A1* and *RUNX2*. Glyceraldehyde 3-phosphate dehydrogenase (*GAPDH*) was used as housekeeping gene. Threshold cycle (C_T) values were determined using a LightCycler 2.0 instrument. Relative gene expression was calculated using the $2^{-\Delta CT}$ or $2^{-\Delta\Delta CT}$ methods as described elsewhere.^{137,138} Using the $2^{-\Delta CT}$ method, the data is presented as the fold change in gene expression normalized to *GAPDH* (**Paper III**). Using the $2^{-\Delta\Delta CT}$ method, the data is presented as the fold change in gene expression normalized to *GAPDH* and relative to human nasoseptal cartilage (**Paper IV**).

4.12.5 Biochemical analysis

Glycosaminoglycan content: The proteoglycan content in the neocartilage produced by the hNCs was quantified using the 1,9-dimethylmethylene blue (DMMB) dye-binding assay. DMMB is a cationic dye that binds to sulfated glycosaminoglycans (s-GAG) and thereby changes in the absorption spectrum occur. For this assay to be suitable for cell cultures containing alginate, the DMMB pH level must be decreased to pH 1.5, as described by Enobakhare et al.¹³⁹ In **Paper III**, the metachromatic reaction of the GAG-DMMB complex was measured spectrophotometrically at absorption ratios of 540 and 595 nm to determine the s-GAG content with chondroitin sulfate C as a standard.¹⁴⁰ In **Paper IV**, the s-GAG content was measured according to the protocol by Barbosa et al.,¹⁴¹ which is based on the isolation and subsequent dissociation of the GAG-DMMB complex to render DMMB soluble. The absorption of the decomplexed DMMB is proportional to the GAG amount complexed from the original sample. The absorbance was measured at 656 nm and the s-GAG content was calculated against a standard curve of chondroitin sulfate C.

DNA content: Quantitation of DNA in hNC-seeded BNC-A composite scaffolds was performed using Hoechst 33258. Hoechst is a bisbenzimidazole derivate that fluoresces when it binds to AT-rich regions of double stranded DNA. The DNA concentration was calculated against a standard curve of monolayer-cultured hNCs, as described elsewhere.¹⁴² In **Paper IV**, cell number per NFC-A hydrogel construct was measured using the QuantiFluor® dsDNA System (Promega). This system contains a fluorescent dsDNA-binding dye that enables sensitive quantitation of small amounts of double stranded DNA. Cell concentration was calculated against a standard curve of monolayer-cultured hNCs.

Gelatine Zymography: In **Paper IV**, the expression and activity of the matrix metalloproteases MMP-2 (gelatinase A) and MMP-9 (gelatinase B) were determined by gelatine zymography. These enzymes control the matrix degradation of denatured collagen. Media samples were loaded on zymography gels and proteins were separated by electrophoresis. For evaluation of the MMPs, the volume intensity of the bands was corrected for the mean cell number per scaffold as determined by the QuantiFluor® dsDNA assay.

4.12.6 Biomechanical analysis

Stress-relaxation indentation testing was used to evaluate the mechanical properties of tissue-engineered constructs (**Paper III** and auricular BNC scaffolds). Three samples were analyzed for each rAC-seeded and cell-free auricular BNC scaffold at 6 weeks post-implantation. Indentation was performed at two locations of the same sample, so as to evaluate spatial variation in mechanical properties.¹²⁰ See section 4.2.3 for more details on the mechanical testing setup.

4.13 Statistics

In this thesis statistical analyses were performed using parametric and non-parametric statistical tests, depending on whether the data was normally distributed and had similar variance. In **Paper I**, a univariate analysis of variance (ANOVA) was used to test significant differences in the

measured mechanical parameters between densified BNC hydrogels and human auricular cartilage. The relationships between cellulose content and the measured mechanical parameters were evaluated using Pearson's linear regression coefficient of correlation. In **Paper III** comparison of means for the cytotoxicity and biomechanical analyses were assessed by one-way ANOVA and Tukey's HSD test. When the data did not meet the requirements for a parametric test, the Kruskal-Wallis ANOVA on ranks was performed, followed by the Dunn's test for post hoc comparisons (**Papers II** and **IV**). For comparing two groups, a two-sample Kolmogorov-Smirnov test or Wilcoxon-Mann-Whitney test was performed (**Papers III** and **IV**). Values of $p < 0.05$ were considered statistically significant.

CHAPTER 5

RESULTS AND DISCUSSION

In this chapter the results from each paper and some unpublished work will be presented and discussed, starting with **Paper I** in section 5.1 and ending with **Paper V** in section 5.7.

5.1 Evaluation of bacterial nanocellulose as an implant material for auricular cartilage replacement

In **Paper I**¹⁴³ we investigated the potential use of BNC in auricular cartilage tissue engineering. Firstly, the mechanical properties of human auricular cartilage were measured in order to set a preliminary benchmark for auricular cartilage replacement materials. Secondly, the capacity of BNC to match these requirements was assessed. Finally, a novel biofabrication process to produce patient-specific BNC implants was developed.

5.1.1 *Tuning the mechanical properties of bacterial nanocellulose to match the mechanical requirements of human auricular cartilage*

In this study, the mechanical properties (E_{in} , E_{eq} , σ_{max} , $t_{1/2}$ and τ) of human auricular cartilage were measured using stress-relaxation indentation. The following mechanical properties were determined: 6.4 ± 3.2 MPa for E_{in} , 3.3 ± 1.3 MPa for E_{eq} , 1.6 ± 0.5 MPa for σ_{max} , 2.1 ± 1.3 s for $t_{1/2}$ and 6.0 ± 2.6 s for τ (**Figure 5**). Moderate standard deviations are observed. These variations are expected to result from factors such as donor age, gender and harvesting location within the auricle. Since a detailed investigation of these factors was out of the scope of **Paper I**, these values represent a preliminary benchmark for BNC and other scaffold materials aimed at auricular cartilage TE. The mechanical characteristics of hyaline cartilage (e.g. articular cartilage, nasoseptal cartilage)^{144,145} and fibrocartilage (e.g. meniscus)¹⁴⁶ are well documented, yet there is little data available for elastic cartilage (e.g. auricular cartilage).⁵⁶ In comparison to hyaline and fibrocartilage, elastic cartilage contains significantly more elastin,⁵⁶ which is known to be a highly resilient protein, and which plays a mechanically functional role in tissues like heart valves¹⁴⁷ and skin.¹⁴⁸ For this reason, a profile of the mechanical properties of auricular cartilage was required, since using published mechanical properties of hyaline cartilage or fibrocartilage may not be an appropriate substitute.

Densified BNC hydrogels with cellulose content ranging from 4.1% up to 13.7% were characterized. The compressive mechanical properties (E_{in} , E_{eq} , and σ_{max}) of densified BNC hydrogels were correlated to cellulose content with R values of 0.66, 0.79, and 0.78, respectively ($p < 0.05$ in all cases); demonstrating the tunability of the material (**Figure 5**). The computed correlation coefficients are moderate. Nonetheless, by varying cellulose content in BNC, an increase in E_{eq} from 0.06 to 3.2 MPa (at the highest cellulose content 13.7%) was observed; partly covering the range of values observed for auricular cartilage (3.3 ± 1.3 MPa). The same observation holds for E_{in} and σ_{max} . These parameters of tunability make BNC a promising candidate as a non-degradable implant material for auricular cartilage TE.

Despite observing a typical stress relaxation behavior in all BNC samples, the relaxation half-life, $t_{1/2}$, of BNC (0.4 ± 0.1 s) was significantly less than auricular cartilage (2.1 ± 1.3 s; $p < 0.05$). The same observation was made for the characteristic relaxation time, τ (3.7 ± 1.0 s and 6.0 ± 2.6 s, respectively; $p < 0.05$). As opposed to BNC, which is electrically neutral, cartilage contains charged groups by way of the GAG content in the ECM. These charged groups play a role in the relaxation behavior of cartilage, via charge-dependent osmotic swelling pressures enhanced during compression.¹⁴³ Therefore, the introduction of electrical charge into the BNC network could provide mechanical properties that better mimic those of native cartilage, in particular improved relaxation kinetics (higher $t_{1/2}$ and τ). In chondrocyte-seeded BNC constructs, the introduction of electrical charges could be achieved by the GAGs produced by the seeded cells. Alternatively, the presence of charged GAGs in BNC can be mimicked by chemical modifications such as sulfonation or phosphorylation of the material, as demonstrated by Svensson et al.⁸¹

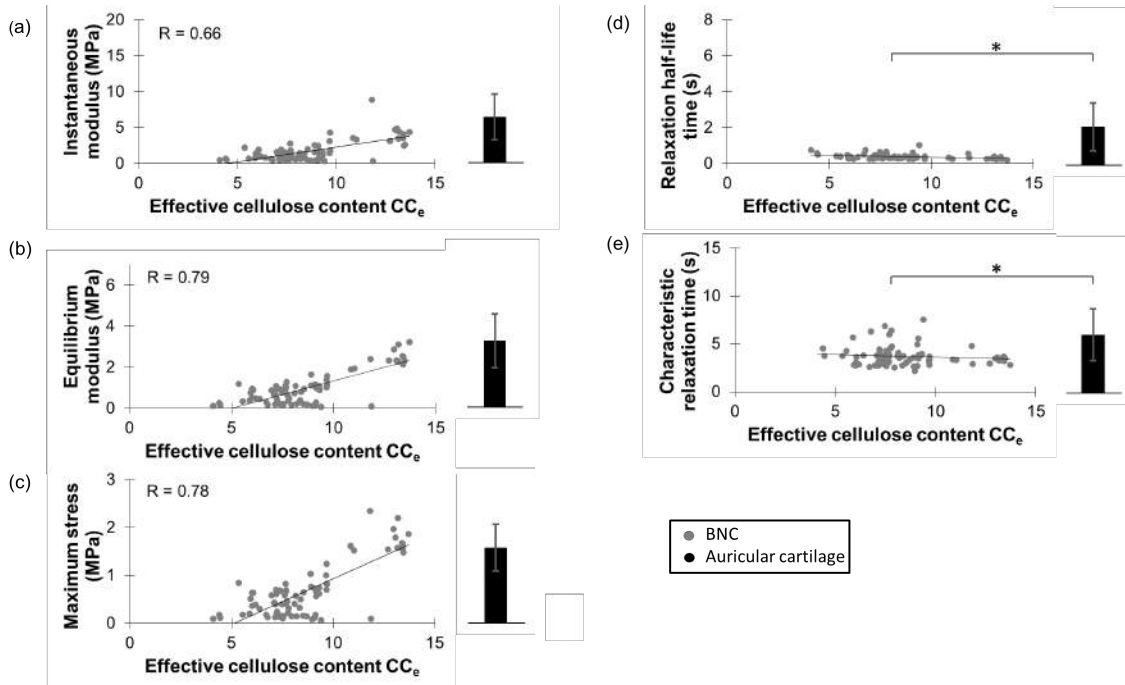


Figure 5 – (a) Instantaneous modulus, E_{in} , of BNC ($n_{total} = 78$) correlates with cellulose content ($R = 0.66$), 6.4 ± 3.2 MPa is measured for E_{in} of auricular cartilage ($n = 17$). (b) Equilibrium modulus, E_{eq} , of BNC correlates with cellulose content ($R = 0.79$), 3.3 ± 1.3 MPa is measured for E_{eq} of auricular cartilage. (c) Maximum stress, σ_{max} , of BNC correlates with cellulose content ($R = 0.78$), 1.6 ± 0.5 MPa is measured for σ_{max} of auricular cartilage. (d) Relaxation half-life time, $t_{1/2}$, of BNC is not influenced by the cellulose content, significant differences ($p < 0.05$) are observed between BNC and auricular cartilage (0.4 ± 0.1 s and 2.1 ± 1.3 s, respectively) (e) Characteristic relaxation time, τ , of BNC is not influenced by the cellulose content, significant differences ($p < 0.05$) are observed between BNC and auricular cartilage (3.7 ± 1.0 s and 6.0 ± 2.6 s, respectively).^(Paper 1)

SEM images of the network structure of native (1% cellulose content) and densified (5% and 10%) BNC are shown in **Figure 6**. As expected, a denser BNC network is observed in the

hydrogels with higher cellulose content. This densification of the BNC network occurs mostly along the z-direction. That is, the spacing between the cellulose fibrils, in z direction, is reduced as the material is compressed and the water is forced out of the hydrogel. When the hydrogel is completely dried the nanocellulose fibrils coalesce, forming hydrogen bonds that crosslink the nanocellulose network.

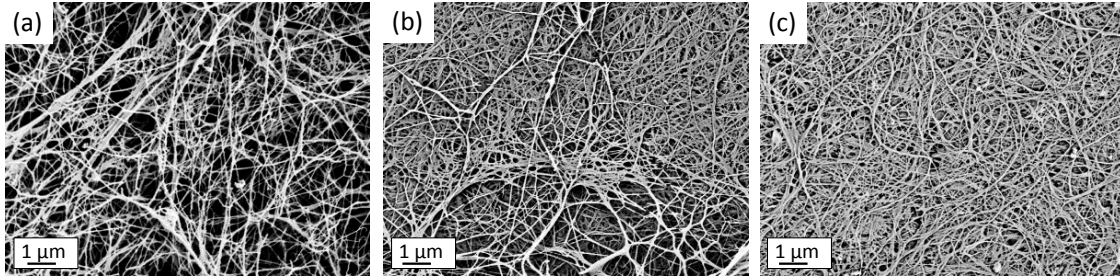


Figure 6 – SEM images of BNC with (a) 1%, (b) 5% and (c) 10% cellulose content. Densification of the BNC network occurs mostly along the z-direction. Spacing between the cellulose fibrils, in z direction, is reduced as the material is compressed and the water is forced out of the hydrogel. Width of dry nanocellulose fibrils is approximately 30 nm. ^(Paper I)

5.1.2 Biofabrication of patient-specific auricular bacterial nanocellulose implants

The auricular cartilage and external ear volume of a volunteer was successfully segmented and reconstructed from the MRI data (**Figure 7a-b**). A negative silicone mold was used to guide the bacteria during bacterial culture to reproduce the large-scale features of the outer ear; a process taking about 18 days (**Figure 7c**). Subsequently, a 3D patient-specific BNC implant prototype (1% cellulose content), mimicking the external ear shape, was successfully synthesized using this mold in a novel biofabrication process (**Figure 7d**). The auricular BNC implant prototype presented in **Paper I** demonstrates the ability of BNC to be shaped in more complex 3D structures than previously reported, i.e. blood vessels¹⁴⁹⁻¹⁵¹ and meniscus.¹⁵² This was made possible through the use of a bottom-up biofabrication approach, which requires a mold to guide the bacteria to reproduce the large-scale features of the tissue of interest. The method described here is a novel biofabrication process of microbially grown 3D auricular scaffolds.

It is key in the field of auricular cartilage replacement to control the external shape of the implant to obtain satisfying esthetic results. This outcome is often used as a measure of success for a potential biomaterial.^{18,19,22} Most efforts in auricular cartilage TE have used standardized auricular shapes.^{18,19,22,24} On the other hand, the auricular BNC implant prototype presented in this study was produced using patient MRI data, which yields a result compatible with the patient's expectation. An alternative method for the fabrication of patient-specific auricular scaffolds was presented by Liu et al.⁶⁵ who described the 3D printing of an auricular scaffold using computed-tomography data. The advantages of using MRI are, firstly the absence of potential radiation damage to the patient, and secondly a better soft tissue contrast and hence the direct visualization of cartilage. This makes it possible to produce patient-specific scaffolds that mimic the shape of auricular cartilage, rather than the whole outer ear (i.e. auricle). Consequently, in the following work we aimed at producing patient-specific BNC scaffolds with the shape of auricular cartilage.

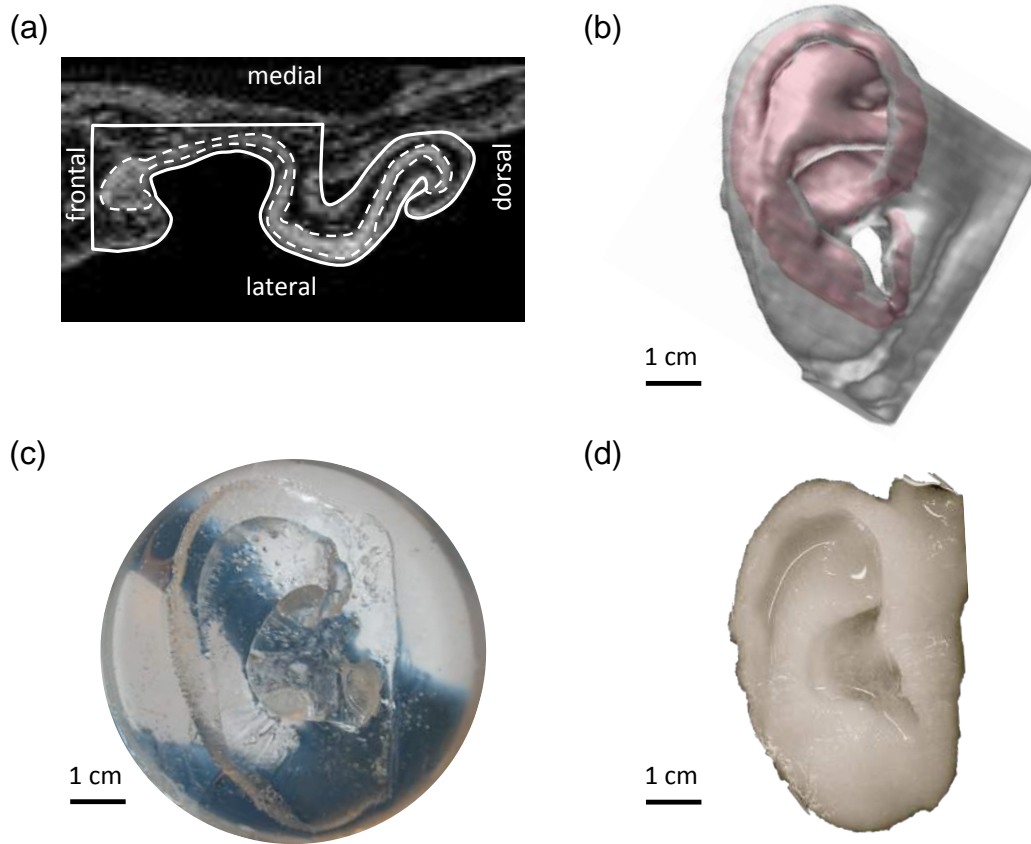


Figure 7 – (a) Transverse slice isolated from a spoiled gradient-echo MRI scan of volunteer’s left ear. Auricular cartilage is visible (dashed contour) surrounded by adipose tissue and skin. Plain contour indicates the external outline of the auricle. (b) 3D rendering of the auricle (gray color) and auricular cartilage (red color) obtained by manual segmentation of the previous MRI scan. (c) Negative silicone mold used to guide the bacteria during the bacterial culture to reproduce the large-scale features of the auricle. (d) Prototype of patient-specific auricular bacterial nanocellulose implant (1% cellulose content) produced using the dataset presented in (b).^(Paper I)

5.2 Biocompatibility evaluation of densified bacterial nanocellulose hydrogel

In **Paper I** we found that the compressive mechanical properties (E_{in} , E_{eq} , and σ_{max}) of densified BNC hydrogel with cellulose content of 13.7% covers the range of values observed for human auricular cartilage. Based on this, we propose BNC with high cellulose content (>14%) as a promising non-degradable implant material for auricular cartilage TE. In **Paper II**¹⁵³ we investigated the host tissue response to this modified BNC material. Moreover, we considered of utmost importance to first evaluate the purity, pyrogenicity and cytotoxicity of the material, before an *in vivo* biocompatibility study was conducted. Thus, a purification and depyrogenation process was developed and validated.

5.2.1 Validation of the depyrogenation process

The first purification step in the built-in house perfusion system extensively removed bacteria and its residues, particularly endotoxins, from the large BNC cylindrical structures. As shown by the

results from ESCA, the perfusion of BNC cylinders with 0.5 M NaOH for 28 days effectively reduced bacterial and medium residues, indicated by the removal of nitrogen from 6.9 to 0 %; reduced endotoxins (i.e. LPS), indicated by the reduction of the signal peak for C–C bonds; and improved the purity of the material, indicated by the oxygen to carbon ratio of 0.83 as found in pure cellulose (**Figure 8**). A solution of 0.5 M NaOH was first used in the purification process to lyse bacteria, in order to release the LPS from the cell wall and to hydrolyze the eight carbon sugar that links the lipid A to the core oligosaccharide. This action causes the separated lipid A to reduce its pyrogenic activity.^{93,95} The results from bacterial endotoxin analysis verified the effectiveness of the perfusion system to remove endotoxins from large BNC structures. The endotoxin content in the non-purified BNC cylinders decreased from 2,390 to 17.7 EU/ml after 14 days of perfusion and was further reduced to 5.7 EU/ml after 28 days of perfusion (**Figure 9**). Based on these results, we report a correlation between ESCA data on surface chemical composition and endotoxin content in BNC.

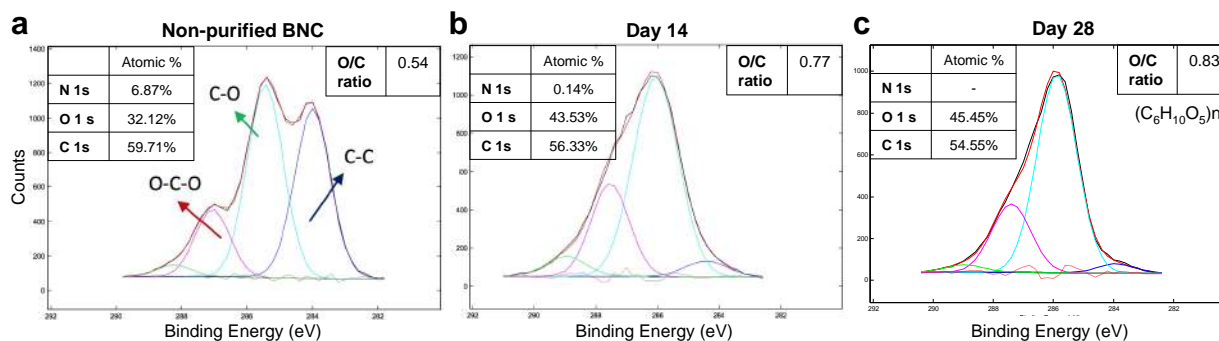


Figure 8 – High-resolution ESCA spectra of (a) non-purified BNC and BNC perfused with 0.5M NaOH after (b) 14 and (c) 28 days. The first depyrogenation process effectively reduced bacterial and medium residues, indicated by the removal of nitrogen from 6.9% to 0%; reduced lipopolysaccharides, indicated by the reduction of the signal peak for C-C bonds; and improved the purity of the material, indicated by the oxygen to carbon ratio of 0.83 as found in pure cellulose. (Paper II)

The first depyrogenation process, involving the perfusion of large BNC cylinders with alkaline solution, was not able to reduce the endotoxins in the BNC network to levels below the endotoxin limit set by the FDA for medical devices.⁹⁰ On the other hand, the second depyrogenation process, involving the rinsing of densified BNC hydrogel disks with endotoxin-free water for 14 days, was shown to reduce the amount of endotoxins to 0.10 EU/ml; five times lower than the endotoxin limit (0.5 EU/ml) for medical devices (**Figure 9**). The result from endotoxin analysis verified the effectiveness of the second purification process to remove endotoxins from the densified BNC hydrogel disks. This latter process for depyrogenation of BNC has not been investigated previously as a method to complement the depyrogenation processes based on hydrolysis and oxidation. All studies reporting washing BNC with water as the final step to remove the alkali and neutralize the pH have used either DI or Milli-Q water^{32,34,76,77,91,92} except for one study which used endotoxin-free water to wash the BNC scaffolds after sterilization.⁷⁵ However, this is the first study that quantifies the reduction of endotoxins in BNC throughout the depyrogenation process, during perfusion with alkaline solution and after washing with endotoxin-free water, and reports endotoxin levels well below the limit for medical devices in BNC with cellulose content of 17 %.

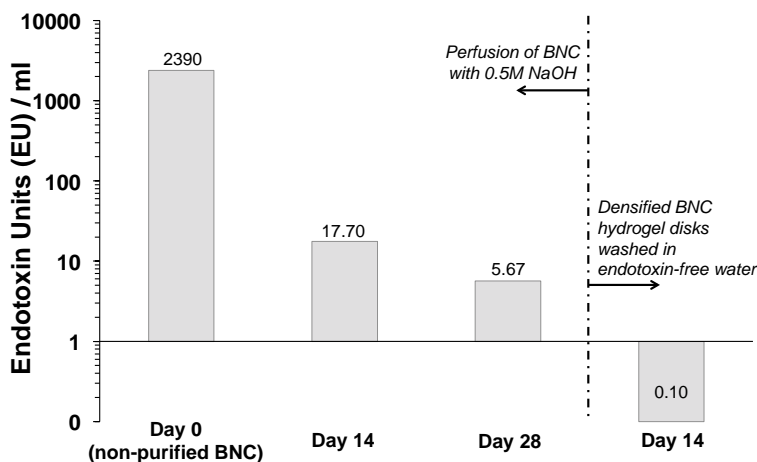


Figure 9 – Bacterial endotoxin testing of BNC during the first depyrogenation process of large BNC cylinders in perfusion system and after the second depyrogenation process in endotoxin-free water. ^(Paper II)

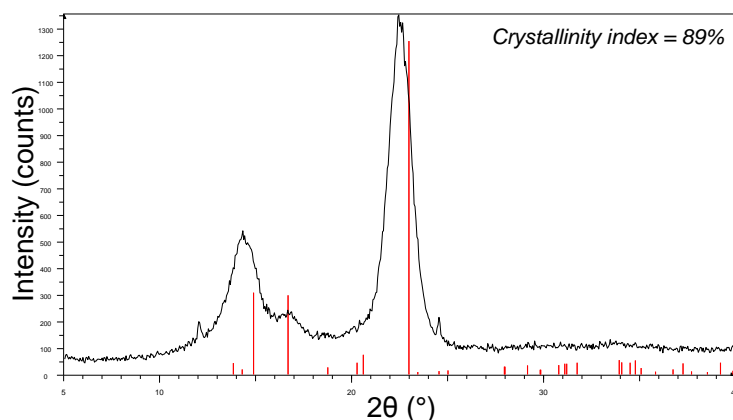


Figure 10 – X-ray diffraction pattern of densified BNC hydrogels after second purification process. The detected diffraction peaks at $2\theta = 14.7^\circ$, 16.2° and 22.4° , characteristic peaks of cellulose I; and the absence of the peaks at $2\theta = 12.1^\circ$ and 20.8° , characteristic peaks of cellulose II, gives substantial evidence that the perfusion of BNC with 0.5M NaOH for a period of 28 days did not change the crystalline structure of BNC fibrils from cellulose I to cellulose II. ^(Paper II)

The crystallinity of the densified BNC hydrogel after the purification process was investigated with XRD. The XRD pattern shows three major diffraction peaks located at $2\theta = 14.4^\circ$, 16.7° , and 22.6° (**Figure 10**). These peaks correspond to the primary diffraction of the (110), (110), and (200) planes of polymorph cellulose I.^{154,155} No peaks were observed at $2\theta = 12.1^\circ$ and 20.8° , which are characteristic peaks of cellulose II.¹⁵⁶ This demonstrates that the purification process did not induce any crystalline structure changes in the BNC fibrils from cellulose I to cellulose II. Moreover, the relative crystallinity determined from the XRD data was 89 % (**Figure 10**). Gea et al.⁹¹ reported a washing treatment for BNC with 2.5 wt% NaOH (0.625 M) followed by 2.5 wt% NaOCl, which also did not induce the transformation from cellulose I to II. Although the treatment with NaOH was much shorter in this previous study, the XRD patterns of the NaOH-treated BNC are very similar to our results.

Extracts of the non-pyrogenic densified BNC hydrogel disks were tested for *in vitro* cytotoxicity. The cultivation of sensitized L929 cells in BNC extracts revealed no cytotoxic effects, demonstrated by the high cell viability (108.4 ± 7.5 %). A cell viability between 70 and 100 % shows that there were no cytotoxic components in the extracts. As expected, the viability of L929 cells significantly decreased when incubated in 10 % DMSO (13.3 ± 1.5 %), which was used as positive control (**Figure 11**). Cell viability below 50 % reflects strong cytotoxic effects. Thus, biocompatibility testing according to standards set forth in ISO 10993-5 demonstrated that densified BNC hydrogel is non-cytotoxic after the purification process.

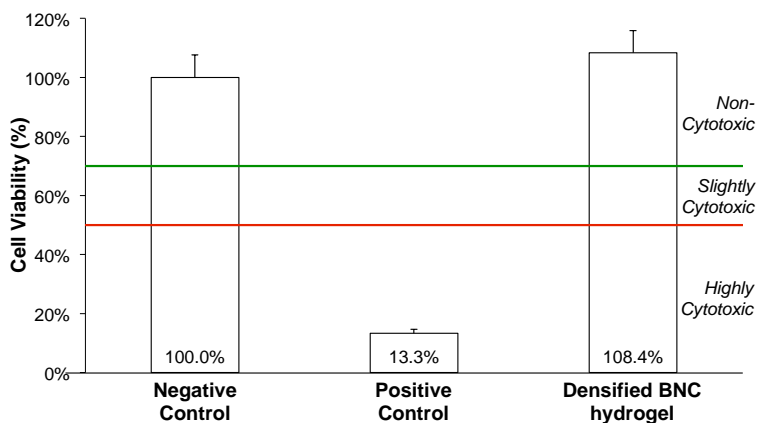


Figure 11 – *In vitro* cytotoxicity testing of densified BNC hydrogels after second depyrogenation process in endotoxin-free water. Biocompatibility testing according to standards set forth in ISO 10993-5 demonstrated that densified BNC hydrogel is non-cytotoxic after the purification process. ^(Paper II)

5.2.2 *In vivo* biocompatibility evaluation

The macroscopic assessment over the implantation period revealed no signs of inflammation around the implants. Furthermore, all implants showed an intimate integration with the surrounding soft tissue after 1-week intradermal implantation. Histological analysis was performed to evaluate the biocompatibility index of the three different materials. The score for neutrophil PMNCs and macrophages revealed a slightly higher occurrence of both cell types in the densified BNC hydrogel implants compared to autologous cartilage, but no significant differences were observed (**Figure 12a–b**). A moderate level of PMNCs and macrophages was detected in Gore-Tex implants, where a significant difference was observed compared to autologous auricular cartilage ($p < 0.05$). A total absence of lymphocytes and plasma cells was noted in all implanted groups (**Figure 12c–d**). There was a slight infiltration of giant cells in the Gore-Tex implants, whereas in densified BNC hydrogel and autologous cartilage implants, none to slight infiltration could be observed (**Figure 12e**). A significant difference ($p < 0.05$) in giant cell-infiltration was observed between Gore-Tex and densified BNC hydrogel implants (median scores: 1 and 0, respectively).

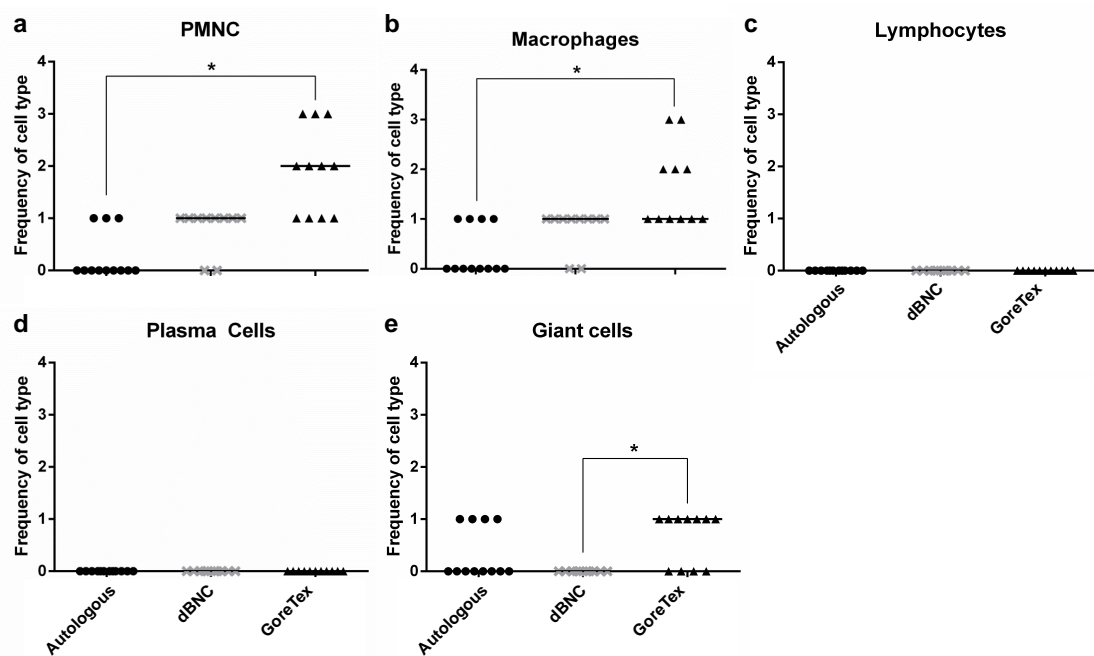


Figure 12 – Classification scores for evaluation of inflammatory reaction of autologous cartilage, densified BNC hydrogel (dBNC) and medical grade Gore-Tex after 1-week intradermal implantation. Median score indicated by line. Classification scores: 0 absent, 1 slight, 2 moderate, 3 marked, 4 severe (* $p < 0.05$). (Paper II)

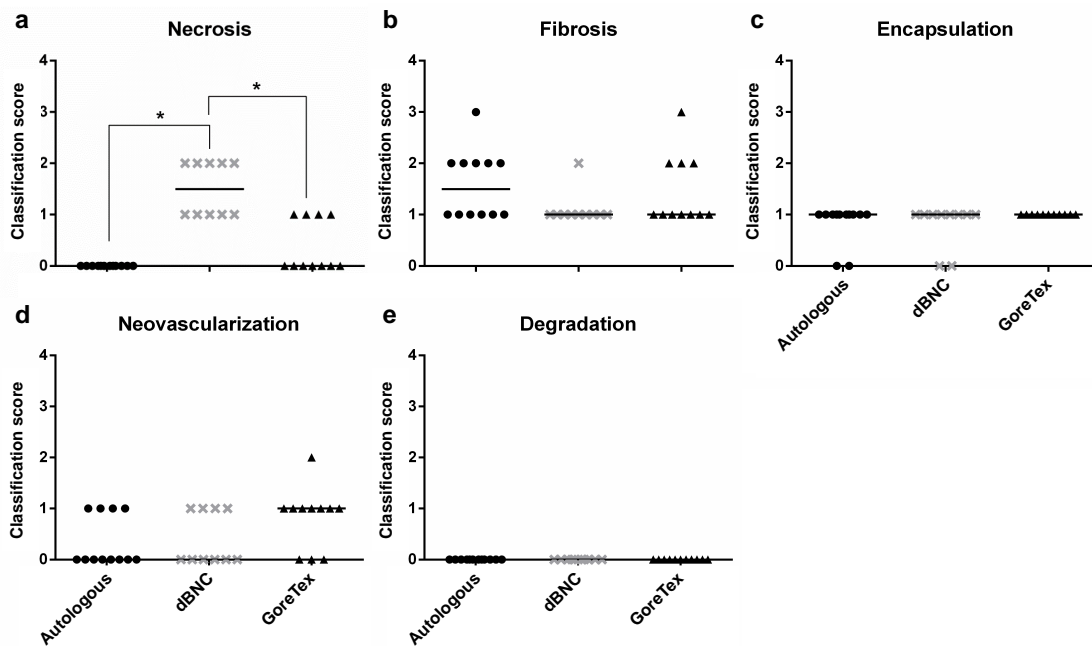


Figure 13 – Classification scores for evaluation of fibrotic reaction of autologous cartilage, densified BNC hydrogel (dBNC) and medical grade Gore-Tex after 1-week intradermal implantation. Median score for each implant group indicated by line. Classification scores: 0 absent, 1 slight, 2 moderate, 3 marked, 4 severe (* $p < 0.05$). (Paper II)

Regarding the level of necrosis, significant differences ($p < 0.05$) were observed in densified BNC implants compared to Gore-Tex and autologous cartilage implants. In autologous cartilage and Gore-Tex implants, no signs of necrosis were found. However, slight to moderate necrosis was observed in densified BNC hydrogel implants (**Figure 13a**). For all experimental groups, slight levels of fibrosis as well as encapsulation were detected. However, no significant differences were detected between the groups (**Figure 13b–c**). A slight level of neovascularization was detected in Gore-Tex implants, but none was detected in the other experimental groups. Moreover, none of the three materials demonstrated any signs of degradation (**Figure 13d–e**).

The biocompatibility testing revealed a significantly lower inflammatory reaction caused by the autologous cartilage (1.0 ± 1.0) implants compared to densified BNC hydrogel (6.0 ± 2.0) or Gore-Tex implants (10.0 ± 4.0) (**Figure 14a**). Regarding the fibrotic reaction, densified BNC hydrogel implants (1.5 ± 0.5) induced a lower reaction than autologous cartilage (2.0 ± 1.0) and Gore-Tex (2.0 ± 1.0), but no significant differences were detected (**Figure 14b**). On the basis of tissue and cellular responses, the biocompatibility index of the autologous cartilage group (3.5 ± 2.0) was significantly lower than the densified BNC hydrogel (7.5 ± 1.5) and Gore-Tex (12.0 ± 3.0) implant groups. Based on the recommendations of ISO 10993-6 Appendix E, autologous cartilage and BNC implant groups were considered a slight irritant to the host tissue, whereas the Gore-Tex group was considered a moderate irritant to the host tissue (**Figure 14c–f**).

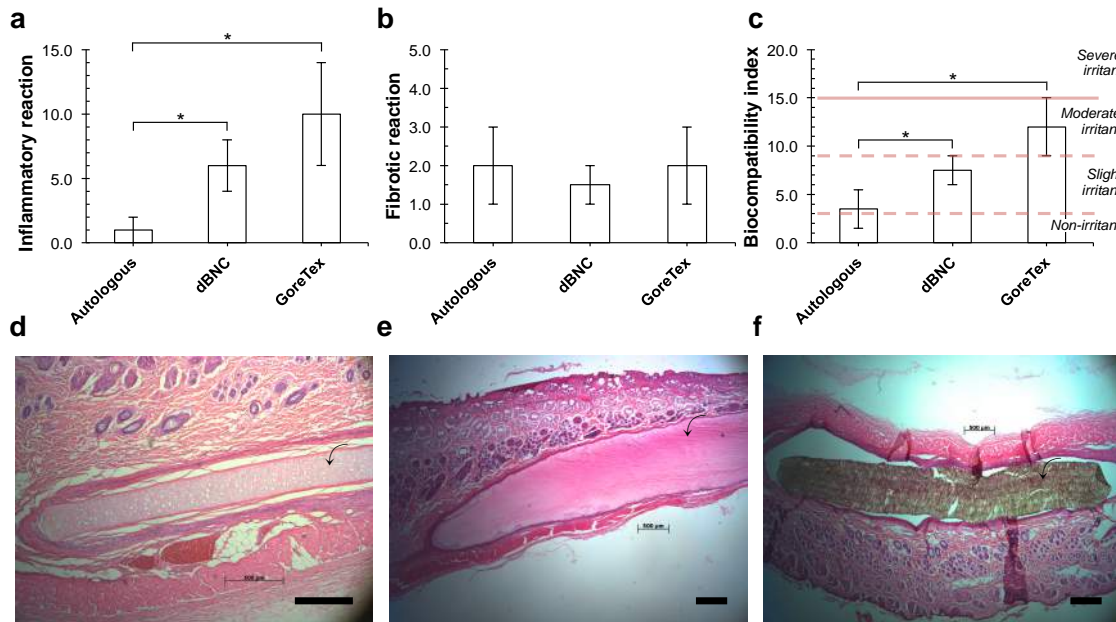


Figure 14 – *In vivo* biocompatibility evaluation: (a) inflammatory reaction, (b) fibrotic reaction and (c) biocompatibility index of autologous cartilage, densified BNC hydrogel (dBNC) and medical grade Gore-Tex after 1-week intradermal implantation. Representative hematoxylin and eosin-stained cross-sections of (d) autologous cartilage, (e) densified BNC hydrogel and (f) Gore-Tex explants (shown by arrows). Scale bar 500 μ m. The biocompatibility index of the autologous cartilage group (3.5 ± 2.0) was significantly lower than the densified BNC hydrogel (7.5 ± 1.5) and Gore-Tex (12.0 ± 3.0) implant groups. Autologous cartilage and BNC implant groups were considered a slight irritant to the host tissue, whereas the Gore-Tex group was considered a moderate irritant to the host tissue. ($*p < 0.05$) (Paper II)

The extent of the acute inflammatory response depends on the injury. In this context, it depends on the reactions caused by the material properties. The implantation of a biomaterial initially evokes tissue and cellular host responses to the locally applied defect and includes not only inflammatory reactions but also wound healing and foreign body responses.^{157,158} The scores for the inflammatory and fibrotic reactions take into account different cell types and tissue reactions involved in the acute inflammatory response and wound healing response. During inflammation, a complex multistage process involving numerous cell types, slight infiltration of neutrophil PMNCs and macrophages was observed in densified BNC hydrogel and Gore-Tex implants. Neutrophil PMNCs are rapidly recruited into the implantation site and characterized as cells of the short-lived (hours to days) acute inflammatory reactions induced by the implanted foreign material.^{157,159,160} In the normal wound healing sequence, the chronic inflammation follows the phase of acute inflammation and is also of short duration (days). It is characterized by macrophages as dominant cellular infiltrate in implanted biomaterials.^{157,160,161}

The rare presence of neutrophil PMNCs and macrophages in the autologous cartilage implants after 1-week intradermal implantation indicated a non-irritating effect on the surrounding tissue, whereas a significant increase of these cell types in the Gore-Tex implants revealed a persistent acute inflammatory phase (**Figure 12a, b**). On the basis of the detected significant differences in neutrophil PMNCs and macrophage infiltration between autologous cartilage and Gore-Tex implants, we hypothesize that the acute inflammation is not only caused by the implantation procedure but is also elicited by the implanted material itself (i.e. Gore-Tex). The slight presence of these two cell types in the densified BNC hydrogel implants suggests a slight foreign body reaction compared to Gore-Tex, which is advantageous for densified BNC hydrogel as a biomaterial.

As lymphocytes and plasma cells are known to be involved in immune reactions and in the chronic inflammatory phase,¹⁵⁷ their complete absence in our experiments may be explained by the short-term implantation period (**Figure 12c, d**). The assessment of tissue responses after short-term implantation may not fully reflect the biological response to the implanted material but can indicate the extent and progression to a chronic inflammation. As formation of granulation tissue is initiated within 1 day after implantation,^{159,162} the short-term implantation period applied in our study is temporally sufficient for the detection of granulation tissue and foreign body reaction.

In the granulation tissue response, the principle task of macrophages is to clear the implant site of tissue and cellular debris (phagocytosis), and participate in the foreign body reaction at the implant–tissue interface.¹⁵⁷ Additionally, in sequence of normal host response to implants, macrophages coalesce to form multinucleated foreign body giant cells. Giant cells are tightly associated with the foreign body response and typically can be detected on the surface of the implanted materials,^{161,162} as we could demonstrate for Gore-Tex implants. In contrast, no giant cells were observed on the surface of autologous cartilage and densified BNC hydrogel implants (**Figure 12e**). In line with this process, macrophages initiate tissue remodeling; accumulation of fibroblasts, inducing the formation of the fibrous capsule; and neovascularization by secreting various biologically active products.^{157,159,161,162} Based on experienced data known from

literature, we can conclude that the significant increase of giant cells as well as the slight levels of neovascularization and encapsulation (Figs. 6e and 7c, d) observed in Gore-Tex implants indicate a more distinct granulation tissue formation and foreign body reaction compared to the autologous cartilage and densified BNC hydrogel implants.

In support with our previous findings (**Paper I**), we conclude that densified BNC hydrogel with cellulose content of 17 % is a promising non-degradable biomaterial for auricular cartilage tissue engineering, due to its similarity with auricular cartilage in terms of mechanical strength and host tissue response.

5.3 Macroporous BNC-A composite scaffolds for auricular cartilage regeneration

When densified, BNC is a mechanically and biologically appropriate biomaterial for use in auricular cartilage reconstruction (**Paper I** and **II**). However, its dense nanocellulose network prevents cells from penetrating the material. To circumvent this problem, several techniques have been developed to support cell ingrowth in BNC scaffolds by tuning pore size and pore interconnectivity during biosynthesis of BNC,¹⁴⁹ via laser ablation⁷⁵ and freeze-dry processing.⁸⁵ In this study macroporous BNC-Alginate (BNC-A) composite scaffolds were fabricated by a freeze-drying process, and scaffolds with two different compositions were produced. Subsequently, we investigated cell ingrowth and redifferentiation capacity of hNCs seeded in macroporous BNC-A composite scaffolds *in vitro*, where the effect of scaffold composition on neocartilage formation was evaluated.

Two groups of BNC-A composite scaffolds, 50/50 and 90/10, were evaluated. As seen from SEM images, similar macroporous morphology with high degree of interconnectivity was observed in both types of BNC-A composite scaffolds (**Figure 15a** and **c**). Furthermore, the microstructure of the scaffolds was affected by the alginate concentration. That is, a low alginate content (i.e. 90/10) yielded a surface topography with nanofibrous structure, whereas a higher alginate content (i.e. 50/50) yielded scaffolds with a noticeably smoother surface topography (**Figure 15b** and **d**). Extracts of both BNC-A composite scaffolds were tested for endotoxin content and *in vitro* cytotoxicity. The LAL test detected an endotoxin content of <1.0 EU/ml in both scaffold types. This result is expected since the BNC pellicles were not purified in sterile and non-pyrogenic conditions. The cultivation of sensitized L929 cells and hNCs in these extracts revealed no cytotoxic effects, as demonstrated by the high cell viabilities (**Figure 16a, b**). As cell viabilities between 80% and 100% were observed, the cytotoxic potential of both BNC-A composite scaffolds was classified as non-cytotoxic (cell viability > 71%).

A significant increase in cell number was observed in 50/50 and 90/10 BNC-A composite scaffolds after 42 days ($1.09 \pm 0.11 \times 10^6$ and $1.04 \pm 0.05 \times 10^6$ cells/scaffold, respectively) of 3D culture compared to day 1 ($21.9 \pm 2.1 \times 10^3$ and $27.7 \pm 2.9 \times 10^3$ cells/scaffold, respectively). No differences were detected between the two BNC-A scaffold groups (**Figure 17a**). Furthermore, GAG content was significantly higher in the 50/50 BNC-A group ($66.24 \pm 18.29 \mu\text{g/mg}$) compared to the 90/10 BNC-A group ($38.64 \pm 11.67 \mu\text{g/mg}$) after 42 days of culture. A

significantly higher GAG content was found in both scaffold types after 42 days compared to 14 and 28 days of 3D culture (**Figure 17b**).

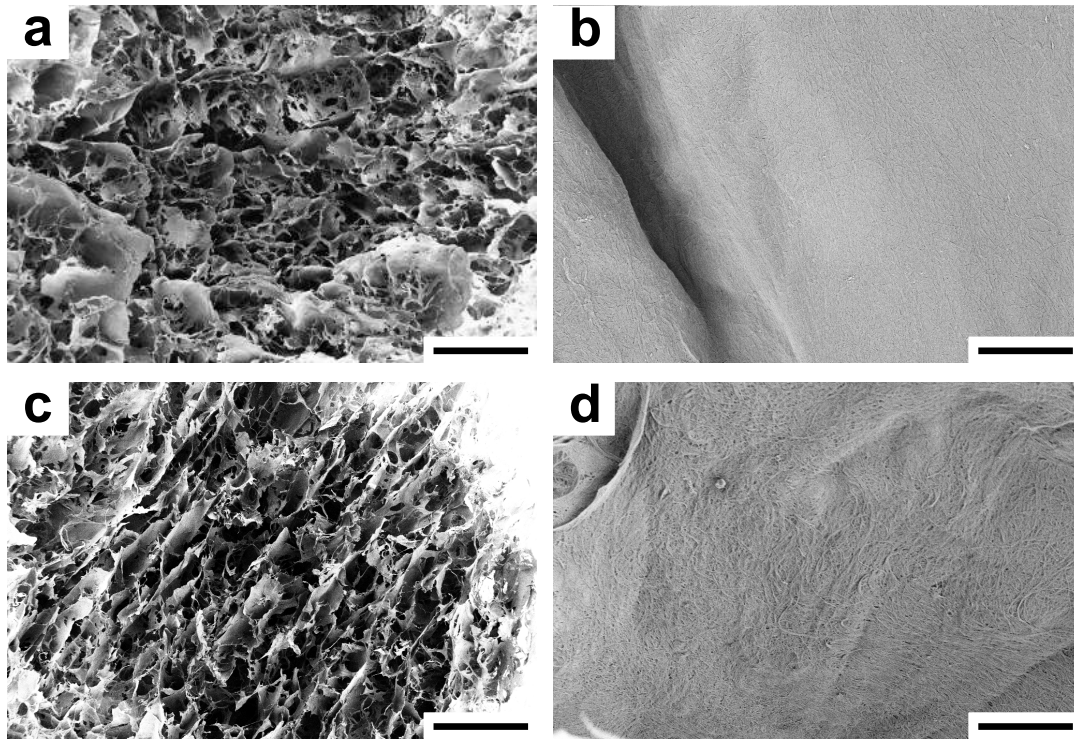


Figure 15 – SEM analyses of macroporous BNC-Alginate composite scaffolds (a, b) 50/50 and (c, d) 90/10 indicate a highly open porous structure in both composite scaffolds. (d) The BNC-A composite scaffolds with lower alginate content (90/10) preserved the nano-structured surface topography of pure BNC, whereby the BNC fibers are clearly visible. The scale bars indicate (a, c) 500 μm and (b, d) 5 μm .

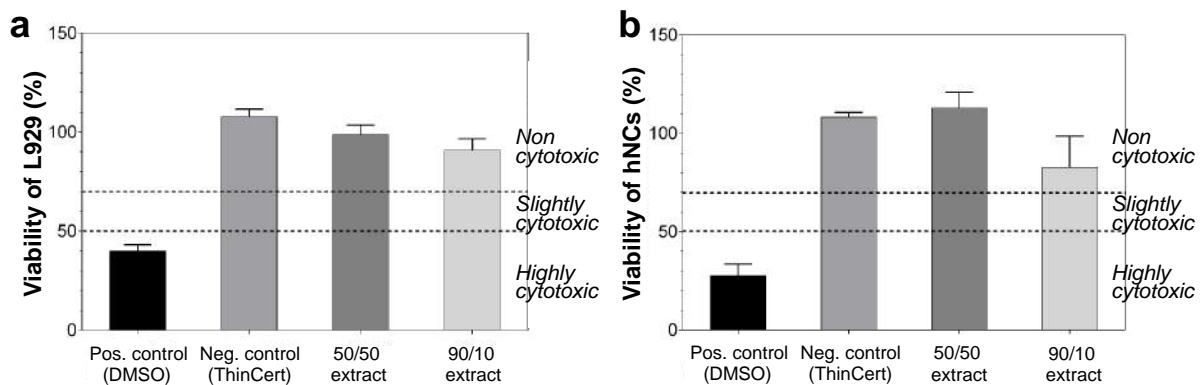


Figure 16 – In vitro cytotoxicity testing of BNC-Alginate composite scaffolds 50/50 and 90/10 ($n=12$ each). (a) L929 and (b) human nasoseptal chondrocytes (hNCs) were used as indicator cells to determine possible cytotoxic effects caused by the scaffold materials and production process. Both cell types show a high viability, indicating the non-cytotoxicity of the BNC-A composite scaffolds.

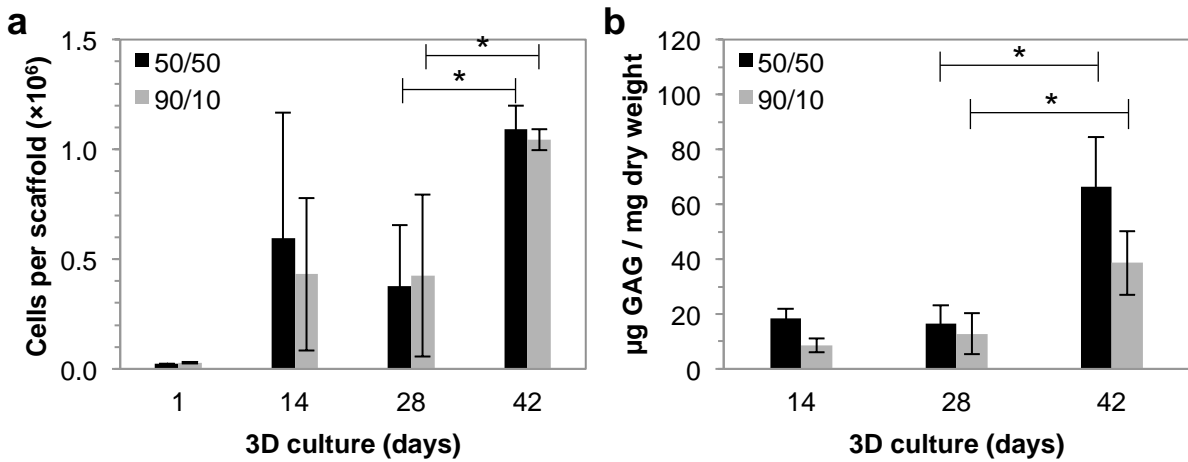


Figure 17 – (a) Proliferation of chondrocytes and (b) GAG content in 50/50 (black) and 90/10 (grey) BNC-A composite scaffolds ($n = 6$ per time point). During 3D culture cell proliferation and accumulation of GAGs were observed. No differences in cellularity were found between the two scaffold compositions, whereas GAG content was higher in 50/50 scaffolds. Error bars represent the standard deviation of the mean. $*p < 0.05$.

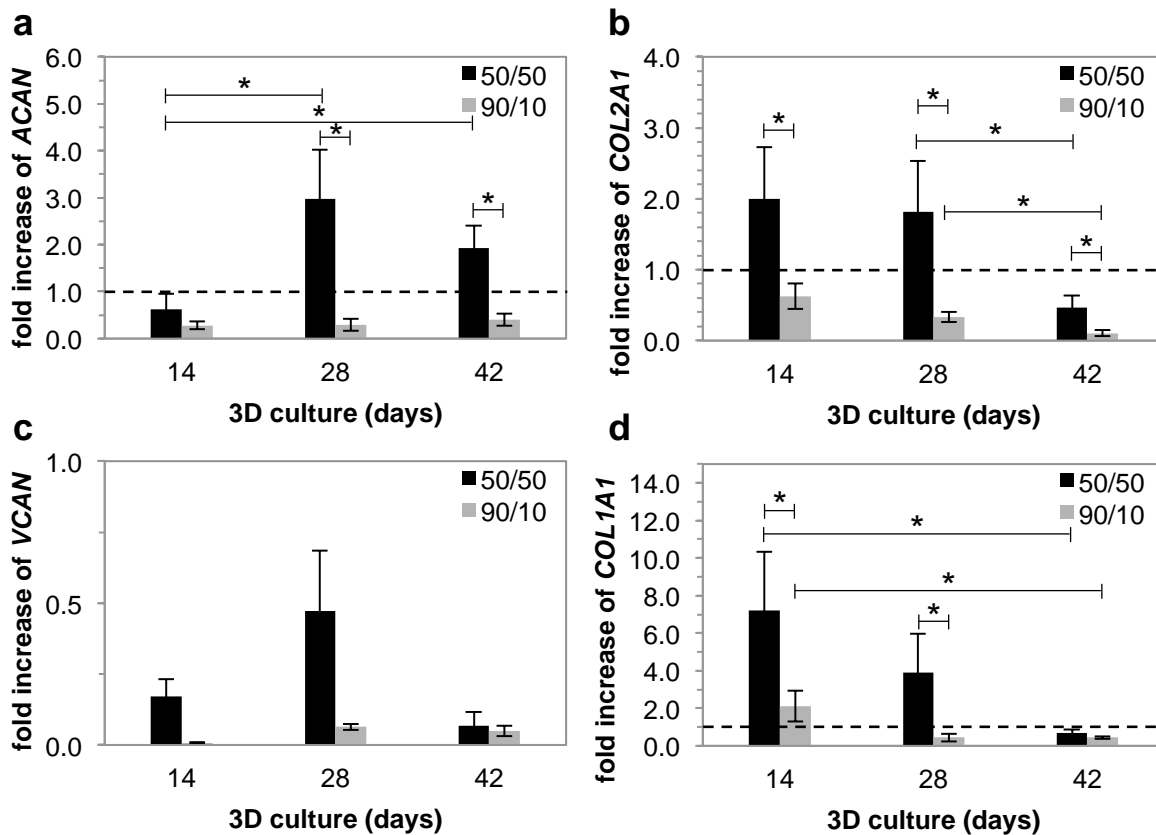


Figure 18 – Gene expression analyses of chondrogenic markers (a) ACAN, (b) COL2A1, and dedifferentiation markers (c) VCAN and (d) COL1A1 expressed in hNCs cultured in 50/50 (black) and 90/10 (grey) BNC-A composite scaffolds ($n = 6$ per time point). Gene expression was normalized to human nasoseptal cartilage (dashed line). The expression of evaluated marker genes was higher for hNCs cultured in 50/50 compared to 90/10 BNC-A composite scaffolds. Error bars represent the standard deviation of the mean. $*p < 0.05$.

Higher gene expression levels of chondrogenic markers *ACAN* and *COL2A1* were found in the 50/50 BNC-A group (**Figure 18a, b**). *ACAN* expression increased significantly between 14 days (0.62 ± 0.34 -fold) and 42 days (1.93 ± 0.47 -fold) of 3D culture in 50/50 BNC-A scaffolds and was significantly higher compared to the 90/10 BNC-A group after 42 days of culture (0.40 ± 0.13 -fold). The expression of *COL2A1* was maintained at higher levels in the 50/50 BNC-A group after 14 (1.99 ± 0.73 -fold) and 28 (1.81 ± 0.73 -fold) days of culture, but then decreased after 42 days (0.46 ± 0.17 -fold). Similarly, after 14 days *COL1A1* expression was significantly higher in the 50/50 BNC-A group (7.22 ± 3.10 -fold) compared to the 90/10 BNC-A group (2.11 ± 0.81 -fold), but it decreased significantly for both scaffold types after 42 days of culture (0.67 ± 0.21 -fold and 0.44 ± 0.06 -fold, respectively). Furthermore, lower expression levels of *VCAN* were found in hNCs cultured in both scaffold types compared to native cartilage (**Figure 18c, d**).

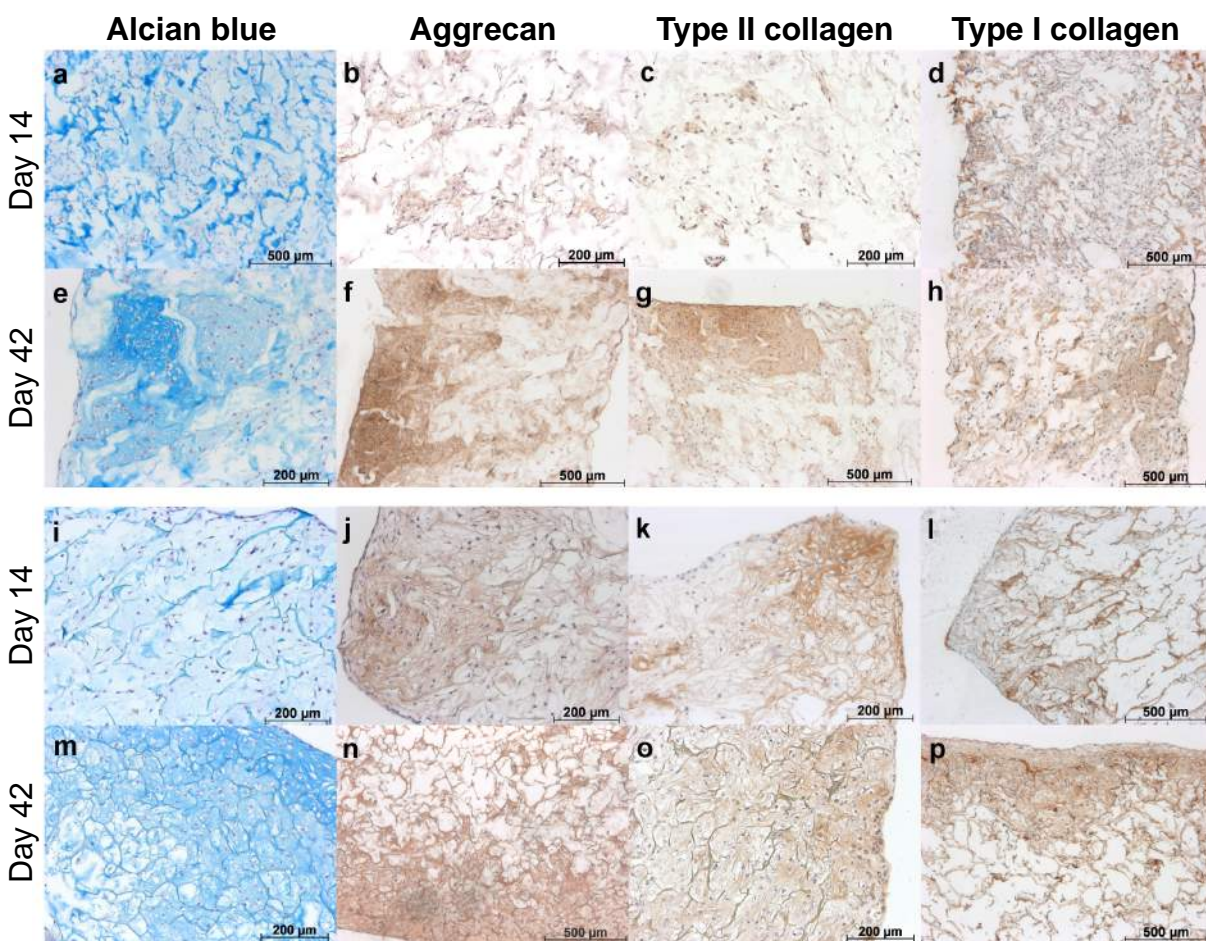


Figure 19 – Histological Alcian blue staining and immunohistochemical staining specific for the detection of aggrecan, type II collagen and type I collagen in chondrocyte-seeded (a-h) 50/50 and (i-p) 90/10 BNC-A composite scaffolds after 14 and 42 days in chondrogenic culture conditions. Positive immunostains for aggrecan and collagen type II were detected in both types of BNC-A composite scaffolds.

Chondrogenic matrix deposition was further confirmed by histological and immunohistological analyses. In 50/50 BNC-A composite scaffolds, only slight positive stains for GAGs, aggrecan and collagen type I and II were observed after 14 days of culture (**Figure 19 a–d**). On the other

hand, neocartilage accumulation in the form of aggrecan and collagen type II was found in the marginal areas of 90/10 BNC-A composite scaffolds after 14 days of culture. Although the central part of the scaffolds showed good cell infiltration, not much neocartilage was found in this area. A slight positive staining for GAGs and collagen type I was also detected in 90/10 BNC-A scaffolds (**Figure 19** i–l). After long-term 3D culture, neocartilage depositions (GAGs, aggrecan and collagen type II) were found notably in both BNC-A composite scaffolds, predominantly at the marginal areas of the scaffolds (**Figure 19** e–g, m–o).

Native BNC is known to be impenetrable to cells or at best the migration is limited to the surface.^{32,76,163,164} Thus, different fabrication methods to create macroporous BNC scaffolds that support cell infiltration have been investigated previously.^{75,85,149} As observed from our results, both macroporous BNC-A composite scaffolds provide an adequate environment that supports ingrowth, proliferation and redifferentiation of hNCs; in agreement with previous studies that have evaluated porous BNC scaffolds with human chondrocytes.^{75,83,165} After 42 days of 3D culture, depositions of cartilage-specific ECM such as GAGs, aggrecan and collagen type II were found notably in both BNC-A composite scaffolds. Moreover, macroporous BNC-A composite scaffolds with higher alginate content (i.e. 50/50) positively influenced the chondrogenic phenotype, as demonstrated by the higher gene expression levels of chondrogenic markers *ACAN* and *COL2A1*. However, the gene expression of the dedifferentiation markers *VCAN* and *COL1A1* was also higher in the hNCs seeded in this scaffold type. Although there was a higher expression of the evaluated chondrogenic markers in the 50/50 BNC-A scaffold, other aspects were also considered, i.e. sterilization capability, to select a scaffold composition for further studies. The 50/50 BNC-A scaffold could not be sterilized using an effective and reliable method, such as steam sterilization, due to the high alginate content. On the other hand, the 90/10 BNC-A composite scaffold could be sterilized by autoclaving without damaging the macroporous structure. hNCs seeded in 90/10 BNC-A scaffolds were shown to infiltrate the scaffold. Furthermore, the cells proliferate and produce neocartilage in such scaffold. Therefore, we concluded that the 90/10 BNC-A composite scaffold is suitable for auricular cartilage TE.

5.4 Bilayer bacterial nanocellulose scaffold for auricular cartilage regeneration

In **Paper III**¹⁶⁶ a novel BNC scaffold designed with a bilayer architecture that integrates mechanical stability and high porosity was evaluated for auricular cartilage TE, *in vitro* and *in vivo*. Bilayer BNC scaffolds with a dense and porous layer were successfully fabricated. SEM images revealed a compact BNC network structure in the dense layer and a macroporous structure in the porous layer (**Figure 20**). The dense and porous layers were stable and firmly attached, which facilitated the handling of the scaffolds during the purification process and throughout the study. 3D morphometric analysis showed that bilayer BNC scaffolds have a porosity of 75% and mean pore size of $50 \pm 25 \mu\text{m}$ (**Figure 20f, g**).

The ionic liquid EMIMAc offers a novel cellulose solvent system to achieve a strong interfacial molecular bonding between the cellulosic dense and porous layers. We are not aware of any other methods that can achieve such result. On the other hand, using EMIMAc increases the risk of having cytotoxic compounds in the bilayer BNC scaffolds, if these residues are not properly

removed during the purification process. Since the toxicity of ionic liquids is not well understood, the use of EMIMAc to fabricate the bilayer BNC scaffolds was investigated with precaution. The cytotoxicity of imidazole ionic liquids has been studied in a human lung carcinoma epithelial cell line model, and it was found that the alkyl-chain length of the ionic liquid has an influence on cytotoxicity.¹⁶⁷ However, the cytotoxicity of EMIMAc, in particular, has not been studied in eukaryotes. Consequently, we analyzed the removal of EMIMAc from the bilayer BNC scaffolds with ATR-FTIR spectroscopy, followed by *in vitro* cytotoxicity testing with sensitized L929 cells. The strong peak at wavenumber 1566 cm^{-1} was used to detect EMIMAc residues in the ATR spectra of bilayer BNC scaffolds, as it has been shown that this peak is composed of two overlapped peaks that correspond to the carboxyl group of the acetate and an underlying ring mode of the cation.^{122,123} Since the peak at 1566 cm^{-1} was found in the ATR spectra of bilayer BNC scaffolds that had been washed for 1 and 7 days, it was considered necessary to continue washing the scaffolds in endotoxin-free water. The washing process proved to be successful in removing the EMIMAc residues, as first observed in the ATR spectra of samples that were washed for 14 days. The absence of this peak confirmed the removal of EMIMAc residues from the BNC bilayer scaffolds (**Figure 21a**).

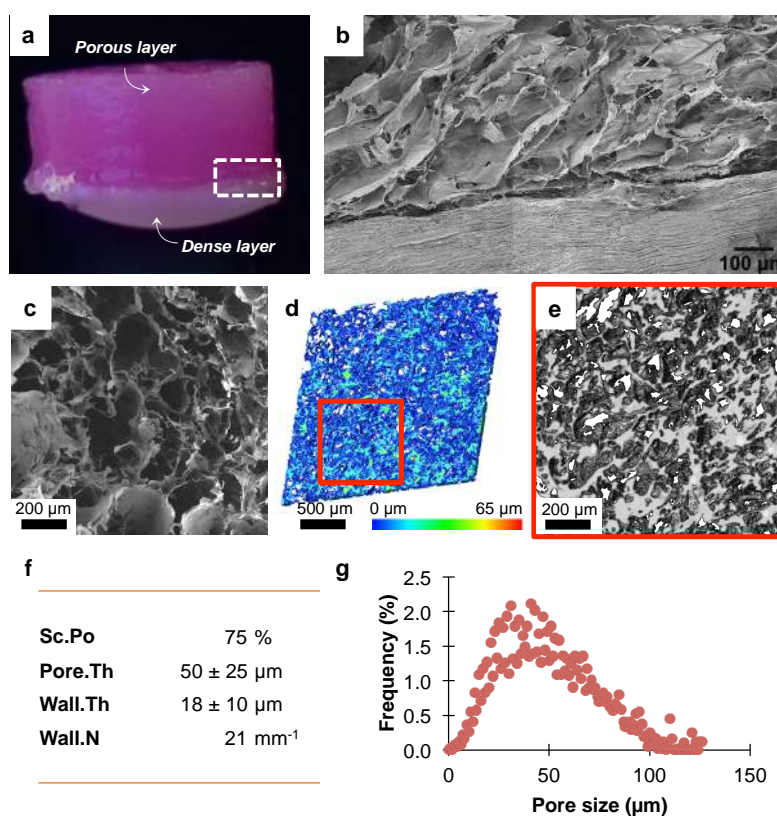


Figure 20 – (a) Photograph of bilayer BNC scaffold (side view). Comparison between (b, c) scanning electron microscopy images of bilayer BNC scaffolds and (d) 3D reconstructed model of the porous layer using microtomography. Similar honeycomb arrangement of sheet-like structures is visible in both images. (e) Higher magnification of the area marked red in (d). Morphometric analysis of segmented porous layer: (f) Morphometric parameters (Sc.Po: scaffold porosity, Pore.Th: volume-weighted mean pore size, Wall.Th: scaffold wall thickness, and Wall.N: scaffold wall number) and (g) Histogram of pore size distribution. ^(Paper III)

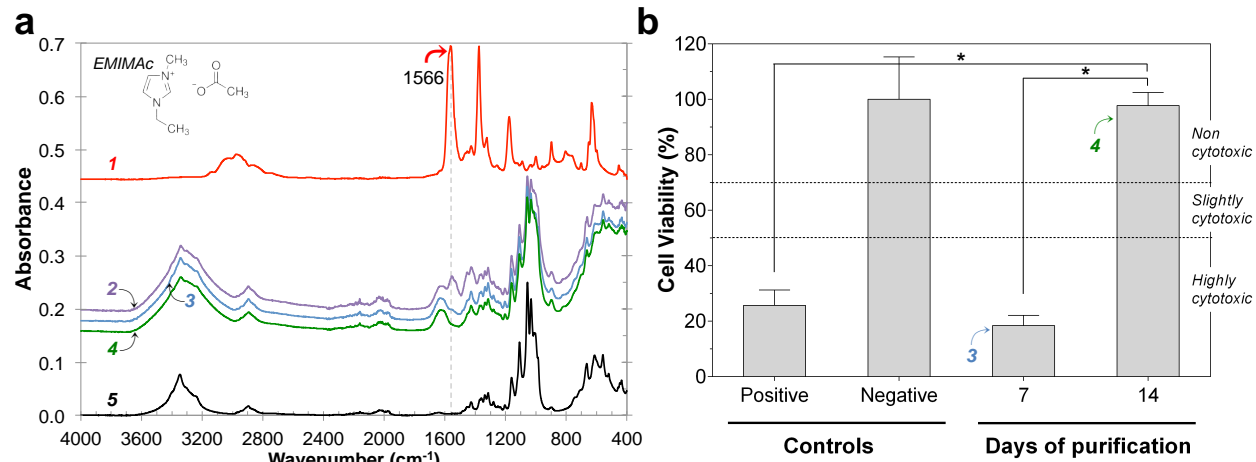


Figure 21 – (a) ATR spectra of (1) 1-Ethyl-3-methylimidazolium acetate (EMIMAc); bilayer BNC scaffolds after (2) 1 day, (3) 7 days and (4) 14 days of purification in endotoxin-free water; and (5) pure bacterial nanocellulose (BNC). (b) *In vitro* cytotoxicity testing of bilayer BNC scaffolds after 7 and 14 days of purification in endotoxin-free water ($n=4$ per time point). Post hoc comparisons using the Tukey HSD test indicated that the mean cell viability for the 14-day condition ($97.8 \pm 4.7\%$) was significantly higher than the 7-day ($18.4 \pm 3.6\%$) and positive control conditions ($25.6 \pm 5.5\%$) at the $*p<0.05$ level. Furthermore, there was no significant difference between the negative control and 14-day conditions. Thus, the cytotoxic potential of bilayer BNC scaffolds was classified as non-cytotoxic. Error bars represent the standard deviation of the mean. ^(Paper III)

In vitro cytotoxicity testing supported our findings from ATR-FTIR. Bilayer BNC scaffolds washed for 7 days still had residues of EMIMAc that were highly cytotoxic to L929 cells (cell viability: $18.4 \pm 3.6\%$). However, these residues were further reduced after the purification process with endotoxin-free water; yielding non-cytotoxic bilayer BNC scaffolds (cell viability: $97.8 \pm 4.7\%$; **Figure 21b**). These results are in good agreement with our previous study, which evaluated the cytotoxic potential of pure densified BNC hydrogel disks (i.e. dense BNC layer, **Paper II**¹⁵³) and found the material to be non-cytotoxic. All together, the results from ATR-FTIR and *in vitro* cytotoxicity testing demonstrated that EMIMAc residues were successfully removed from the bilayer BNC scaffolds after the purification process with endotoxin-free water; whereat no peak at 1566 cm^{-1} and no cytotoxic effects were observed. Furthermore, endotoxin analysis revealed that the produced bilayer BNC scaffolds were non-pyrogenic ($0.15 \pm 0.09\text{ EU/ml}$) after the purification process. The endotoxin content found in the scaffolds is three times lower than the endotoxin limit (0.5 EU/ml) set by the FDA for medical devices.⁹⁰ This low endotoxin content found in the bilayer BNC scaffolds is in good agreement with our previous results (0.10 EU/ml , **Paper II**¹⁵³), where densified BNC hydrogel disks (i.e. dense layer) of similar dimensions were considered non-pyrogenic after purification with endotoxin-free water for 14 days.

Gross examination of the hNC-seeded constructs throughout the 6 weeks of *in vitro* culture revealed a stable adhesion between the dense and porous layers. Moreover, the size and shape of the bilayer BNC scaffolds remained stable during the cell culture. The compact BNC network structure of the dense layer provided a good mechanical stability, while the interconnected high porosity layer supported the ingrowth of hNCs throughout this layer. As demonstrated in Alcian blue-stained images, the porous layer supported the ingrowth of hNCs and facilitated a

homogeneous cell distribution (**Figure 22a**). However, it took 4 weeks of *in vitro* culture to get a dense and homogenous cell distribution. After 6 weeks of *in vitro* culture, a rich and homogenous distribution of hNCs and neocartilage was observed throughout the porous layer of the scaffold, even in the center, which is known to be a critical region in static 3D culture due to the limited supply of nutrients and oxygen. This outcome could have been accelerated by increasing the percentage of cells retained in the scaffolds after cell seeding, as there was a substantial loss of cells when these were seeded in medium. Thus, for the *in vivo* study the cells were embedded in alginate to improve cell retention in the scaffolds after seeding. Alginate was chosen, since it has been successfully used to seed chondrocytes in a scaffold for *in vivo* implantation^{168,169} and this hydrogel is well known to maintain a chondrogenic phenotype of human chondrocytes and stimulate neocartilage formation.¹⁷⁰

Deposition of ECM by the hNCs seeded in bilayer BNC scaffolds was assessed qualitatively by immunohistological staining. During 3D culture, hNCs produced and accumulated cartilage-specific ECM components in the bilayer BNC scaffolds. A positive staining for s-GAGs was found around clusters of chondrocytes in the porous layer after 2 weeks of culture, as shown by the Alcian blue staining (**Figure 22a**). Moreover, synthesis and accumulation of s-GAGs, aggrecan as well as type II collagen increased visibly during 3D culture (**Figure 22a-c**). After 6 weeks of *in vitro* culture, a rich and homogenous distribution of cells and neocartilage was observed throughout the porous layer of the scaffold, even in the center, which is known to be a critical region in static 3D culture due to the limited supply of nutrients and oxygen. However, fibrocartilage ECM was also synthesized by the hNCs in the bilayer BNC scaffolds, as demonstrated by the positive immunostaining of type I collagen (**Figure 22d**).

The chondrogenic potential of the hNCs in the bilayer BNC scaffolds was also investigated on the basis of the expression of the chondrogenic marker genes *ACAN* and *COL2A1*. Dedifferentiation markers, *VCAN* and *COL1A1*, were also analyzed. Gene expression analyses confirmed the positive immunostains of aggrecan, type II and type I collagen. *ACAN* and *COL2A1* expression after 6 weeks was 3.4- and 4.9-fold higher, respectively, compared to gene expression levels at week 2. Expression of *COL1A1* was also upregulated during 3D culture, where after 6 weeks was 1.7-fold higher compared to gene expression levels at week 2. On the other hand, expression of *VCAN* remained relatively close to zero during the 6 weeks of 3D culture (**Figure 22e, f**). The upregulation of the chondrogenic markers *ACAN* and *COL2A1* was clearly enhanced compared to the expression of dedifferentiation markers, revealing the chondrogenic potential of the hNCs in the bilayer BNC scaffolds.

The stability and neocartilage formation in MNC/hNC-seeded and cell-free bilayer BNC scaffolds were evaluated after 8 weeks of subcutaneous implantation in nude mice. The mice survived until the end of the study period, during which no extrusion of constructs was observed. At 8 weeks post-implantation, a thin fibrous capsule surrounded all MNC/hNC-seeded and cell-free bilayer BNC scaffolds; considered a normal non-pathological foreign body reaction. Macroscopic examination of the explants revealed that the shape and size of the bilayer BNC scaffolds remained stable and no delamination of the dense and porous layers was observed in

any of the constructs. Furthermore, bilayer BNC scaffolds seeded with MNCs and hNCs encapsulated in alginate had a macroscopically cartilage-like appearance (**Figure 23a**).

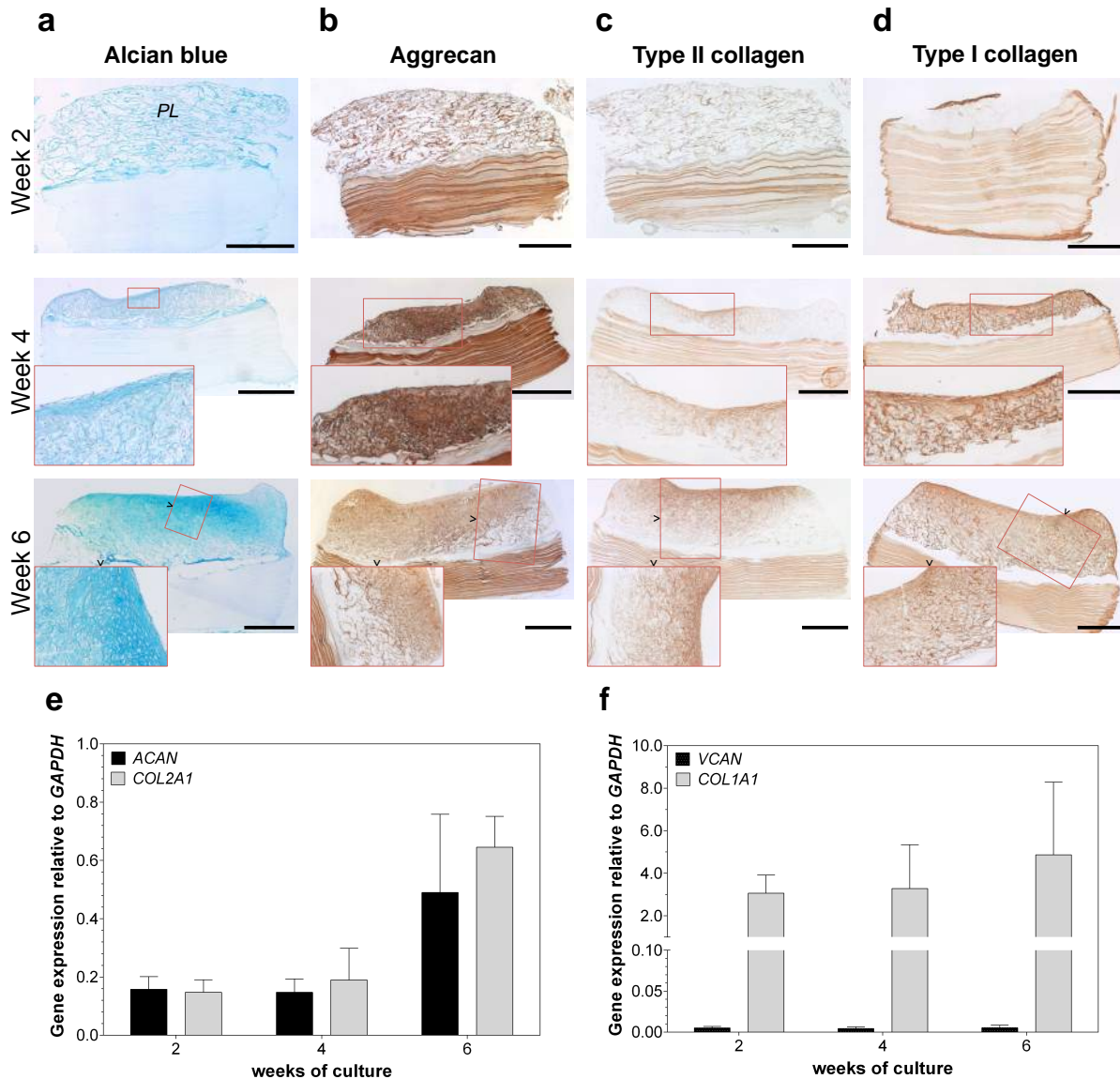


Figure 22 – Histological and immunohistochemical analysis of human nasoseptal chondrocytes (hNC) after 2, 4 and 6 weeks of culture in vitro in chondrogenic medium. Representative images of ECM produced in bilayer bacterial nanocellulose (BNC) scaffolds. Samples were stained with (a) Alcian blue to detect deposition of sulfated glycosaminoglycans (PL =porous layer). Immunohistochemical staining was used to detect cartilage-specific proteins such as (b) aggrecan, (c) type II collagen and (d) the dedifferentiation marker type I collagen. (e and f) Gene expression analysis of hNCs seeded in bilayer BNC scaffolds and cultured in vitro for 2, 4 and 6 weeks (n=4 per time point). Gene expression levels of ACAN, COL2A1, COL1A1 and VCAN relative to the housekeeping gene Glyceraldehyde 3-phosphate dehydrogenase (GAPDH). Error bars represent the standard deviation of the mean. The scale bar indicates 1 mm (a-d). ^(Paper III)

These MNC/hNC-seeded constructs were stiffer and more stable upon handling, compared to bilayer BNC scaffolds seeded with cell-free alginate solution. Based on gross morphological

examination, there were no signs of adhesive failure in the bilayer BNC scaffolds after the *in vitro* and *in vivo* studies. We postulate that the interfacial bonding between the layers is like a molecular welding process. As the BNC-EMIMAc solution partly dissolves both surfaces at the interface, this makes it possible for the long chains of BNC to diffuse into both layers. Once the dissolved BNC is precipitated in ethanol, the interface structure is locked, which results in a stable interfacial bonding. We have observed that when pulling the dense and porous layers apart, the scaffold breaks at the porous layer, similar to a structural failure. In contrast, a weak adhesion would have had resulted in an adhesive or cohesive failure at the interface. Based on this observation we speculate that the interfacial bonding between the layers is stronger than the structure of the porous layer, although in this study the interfacial strength of the bilayer BNC scaffolds was not measured.

In the *in vivo* study we explored the application of a clinically relevant strategy, by seeding bilayer BNC scaffolds with a low number of freshly isolated hNCs combined with freshly isolated human MNCs, in order to test the translation of this auricular cartilage TE technology to the clinic. At 8 weeks post-implantation, the cells encapsulated in alginate were homogeneously distributed in the porous layer of the scaffolds (**Figure 23b, c**). Moreover, deposition of cartilage matrix components such as proteoglycan and type II collagen were observed predominantly in MNC/hNC-seeded constructs. The strong Safranin O staining surrounding the cells showed the presence of proteoglycans in the newly synthesized ECM, while the presence of type II collagen was confirmed by immunohistochemistry (**Figure 23b, c**). These results, showing the formation of neocartilage in the porous layer, were further confirmed by biochemical analysis. A Kolmogorov-Smirnov test indicated a significant difference ($p < 0.05$) between mean GAG content for MNC/hNC-seeded ($0.87 \pm 0.65 \mu\text{g GAG/mg wet weight}$) and cell-free bilayer BNC scaffolds ($0.07 \pm 0.11 \mu\text{g GAG/mg wet weight}$). GAG-production in the MNC/hNC group was almost 12-fold higher compared to the control condition (**Figure 23d**).

A typical stress relaxation behavior was observed in all bilayer BNC scaffolds (MNC/hNC-seeded and cell-free controls), and the following measurements were determined for the MNC/hNC-seeded constructs at 8 weeks post-implantation; $0.76 \pm 0.19 \text{ MPa}$ for E_{in} , $0.19 \pm 0.08 \text{ MPa}$ for E_{eq} , $0.16 \pm 0.07 \text{ MPa}$ for σ_{max} and 7.1 ± 3.4 seconds for $t_{1/2}$. A one-way ANOVA was conducted to compare the effect of implantation and seeding of MNC/hNCs on initial matrix stiffness (i.e. E_{in}) of the constructs at 8 weeks post-implantation. There was a significant effect of implantation and seeding of MNC/hNCs on instantaneous modulus for the three conditions, $F(2, 23) = 16.10$, $p < 0.0001$, $\omega = 0.73$. Post hoc comparisons using the Tukey HSD test indicated that the mean E_{in} for the MNC/hNC condition ($0.76 \pm 0.19 \text{ MPa}$) was significantly higher than the non-implanted ($0.42 \pm 0.15 \text{ MPa}$) and cell-free conditions ($0.32 \pm 0.10 \text{ MPa}$) at the $p < 0.05$ level. The cell-free implanted condition did not significantly differ from the non-implanted condition (**Figure 23e**).

Moreover, a Kruskal–Wallis test was conducted to compare the effect of implantation and seeding of MNC/hNCs on relaxation kinetics (i.e. $t_{1/2}$) and intrinsic properties (i.e. E_{eq} and σ_{max}) of the constructs at 8 weeks post-implantation. The median $t_{1/2}$ values of the constructs were significantly affected by the implantation and seeding of MNC/hNCs, $H(2) = 17.46$, $p < 0.001$.

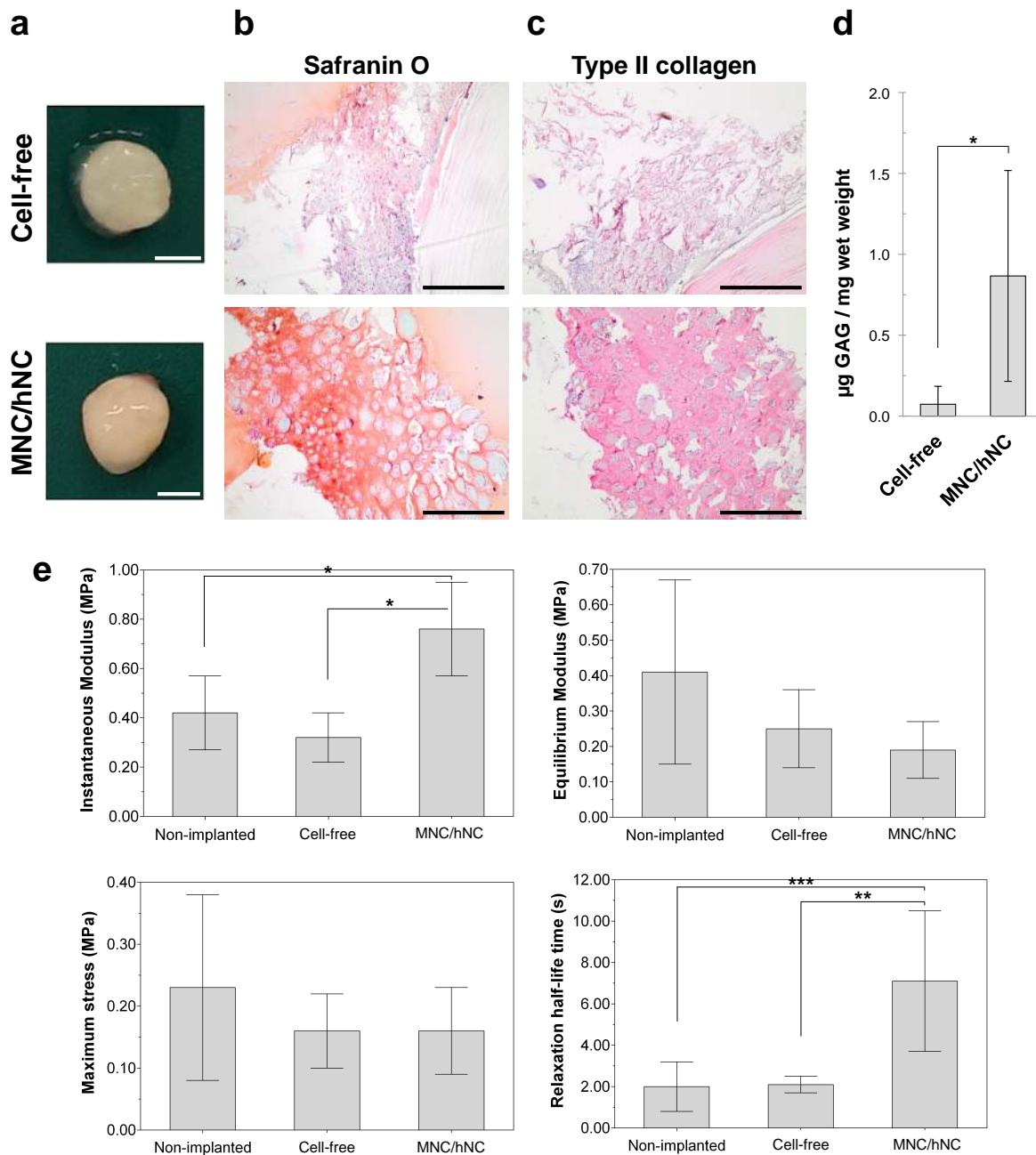


Figure 23 – (a) Photographs of cell-free and MNC/hNC-seeded bilayer BNC scaffolds after 8 weeks of subcutaneous implantation in nude mice. Histological evaluation of ECM in bilayer bacterial nanocellulose (BNC) scaffolds seeded with a combination of freshly isolated human nasoseptal chondrocytes (hNC) and bone marrow mononuclear cells (MNC) in alginate after 8 weeks of subcutaneous implantation. (b) Safranin O stain was used to examine proteoglycans present in the newly synthesized ECM, (c) whereas immunohistochemical analysis was used to detect type II collagen. (d) Cell-free and MNC/hNC-seeded bilayer BNC scaffolds were also analyzed for glycosaminoglycan (GAG) content after 8 weeks of subcutaneous implantation ($n=4$ per group). (e) Biomechanical evaluation of cell-free and MNC/hNC-seeded constructs after 8 weeks of subcutaneous implantation ($n=4$ per group), and non-implanted bilayer BNC scaffolds with cell-free alginate solution ($n=5$). Error bars represent the standard deviation of the mean. *, ** or *** indicates p -values less than 0.05, 0.01 or 0.001, respectively. The scale bars indicate 4 mm (a) and 1 mm (b, c). ^(Paper III)

However, E_{eq} and σ_{max} were not significantly affected by the tested conditions, $H(2) = 4.19$, $p = 0.12$ and $H(2) = 1.12$, $p = 0.57$, respectively. Post hoc comparisons using the Mann–Whitney tests indicated that the median $t_{1/2}$ for the MNC/hNC condition was significantly higher than the non-implanted ($U = 3$, $p < 0.001$, $r = -0.74$) and cell-free conditions ($U = 48$, $p < 0.01$, $r = -0.66$). No significant differences in $t_{1/2}$ were detected between the cell-free and non-implanted conditions. A 2.4- and 3.4-fold higher E_{in} and $t_{1/2}$, respectively, were observed in the MNC/hNC-seeded constructs compared to the cell-free group. Likewise, a 1.8- and 3.6-fold higher E_{in} and $t_{1/2}$, respectively, was observed in the MNC/hNC-seeded constructs compared to the non-implanted group (**Figure 23e**).

The presence of cartilage matrix in the bilayer BNC scaffolds was also supported by biomechanical analysis. At 8 weeks post-implantation, a significantly higher initial matrix stiffness and improved relaxation kinetics (i.e. higher E_{in} and $t_{1/2}$ values) were observed in the MNC/hNC-seeded scaffolds compared to the non-implanted and cell-free conditions. In fact, the effect size (i.e. ω and $r > 0.5$) obtained from the E_{in} and $t_{1/2}$ data represents a large effect by the MNC/hNC condition. However, there was no significant difference in E_{eq} and σ_{max} for the three conditions. Considering the improved relaxation kinetics in the MNC/hNC-seeded constructs, we conclude that the ability of the constructs to attract and trap water was enhanced through the production and accumulation of proteoglycans and glycosaminoglycans in the bilayer BNC scaffolds. Nevertheless, since the intrinsic scaffold properties did not improve in the MNC/hNC-seeded constructs compared to the cell-free control (no difference in E_{eq}), it implies that collagen matrix was not effectively produced in the porous layer. To put the results from the biomechanical analysis in a clinical context, the E_{in} and E_{eq} of the MNC/hNC-seeded constructs after 8 weeks of implantation were 8.4- and 17.4-fold lower, respectively, compared to human auricular cartilage (6.4 ± 3.2 MPa for E_{in} and 3.3 ± 1.3 MPa for E_{eq} ; **Paper I**¹⁴³) Therefore, the engineered cartilage as such would not be suitable for immediate ear cartilage replacement; rather modifications in cell concentration and perhaps a longer implantation period needs to be considered.

The present study has certain limitations. Firstly, cell density plays a critical role when engineering functional and stable cartilage. Others have demonstrated that cell densities greater than 20×10^6 cells/ml are desirable, while low cell densities resulted in decreased cartilage formation.¹⁷¹ In order to enhance the outcome of tissue-engineered auricular cartilage, a higher cell density is needed to benefit from increased cell–cell contacts signaling chondrogenic ECM deposition and preventing the dedifferentiation process. Despite the limitations already stated, our findings support that bilayer BNC scaffolds in combination with alginate provide a suitable environment for MNCs and hNCs to support the synthesis of neocartilage. Of equal importance, the use of freshly isolated hNCs and MNCs in the *in vivo* study gave us an indication of the potential of this strategy to advance the translation of cell-aided treatments to the clinic.

Most auricular cartilage TE strategies have revolved around biodegradable scaffolds, where the hypothetical optimum has been the scaffold's degradation orchestrated by the neo-tissue formation. It would be ideal if the scaffold could be degraded by the time the neocartilage has reached full mechanical strength. However, fine-tuning this intricate play has proven to be a

challenge in TE. If the material degrades too rapidly, the neocartilage will collapse. Whereas if it degrades too late, it could induce a continuous inflammation that would affect the cartilage formation. Thus, we aim for a hybrid implant—BNC well integrated with the host and neo-tissue—that supports cell ingrowth, neocartilage formation and long-term structural integrity after implantation. The non-degradable BNC will provide long-term structural integrity after implantation, and has previously shown remarkable integration with the host tissue in different animal models.^{32-34,153}

5.5 *In vivo* evaluation of patient-specific BNC scaffold for auricular cartilage regeneration

It is key in the field of auricular reconstructive surgery to control the external shape of the implant to obtain satisfying esthetic results. This outcome is often used as a measure of success for a potential scaffold.^{18,19,22} However, most efforts in auricular cartilage TE have used standardized auricular shapes.^{18,19,22,24} In this study, patient-specific auricular BNC scaffolds, with a bilayer architecture that integrates mechanical stability and high porosity, were successfully fabricated by combining the methods developed in **Papers I-III (Figure 24)**. We believe that the optimal esthetic outcome would come from an implant that mimics the shape of the patient’s own auricle. The auricular BNC scaffold presented in this study was obtained from MRI data, which produces a result compatible with the patient’s expectation (**Figure 24a, g**). An advantage of using MRI over X-ray computed tomography is the better soft tissue contrast provided by the former and hence, the direct visualization of articular cartilage.¹⁷² This makes it possible to produce patient-specific scaffolds that mimic the shape of auricular cartilage, rather than the whole outer ear (**Figure 24g**).

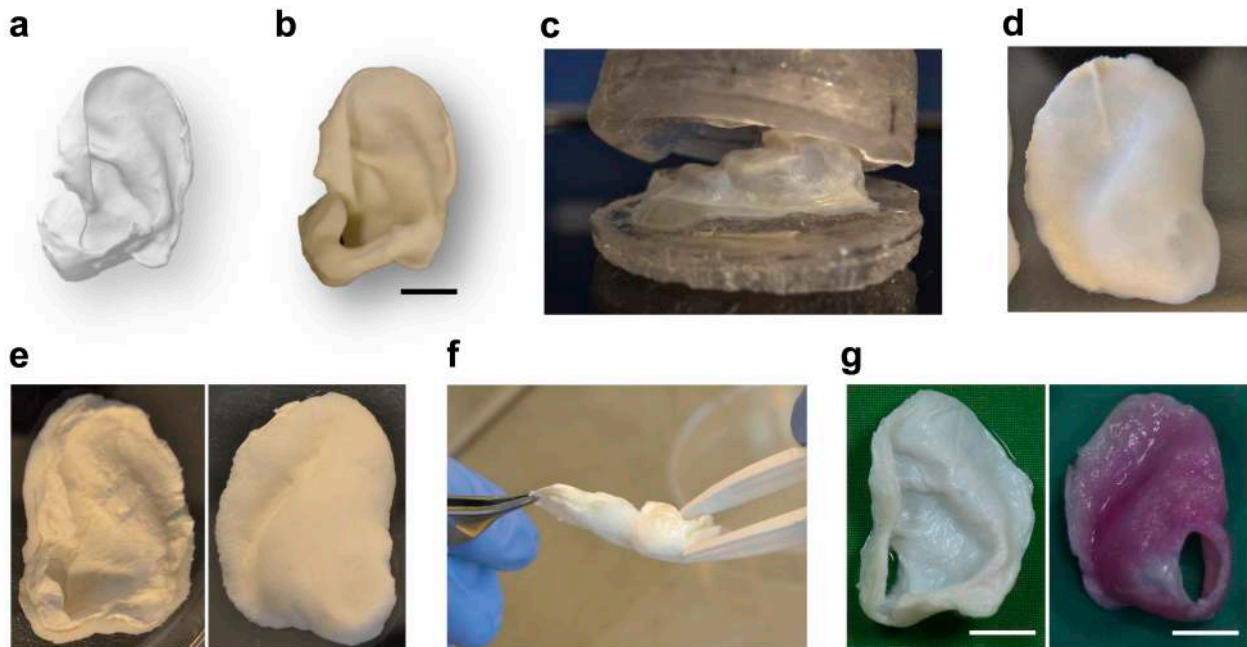


Figure 24 – Fabrication of patient-specific auricular BNC scaffolds with a bilayer architecture composed of a dense BNC layer and a macroporous BNC-A composite layer. (a) First, a 3D model of human auricular cartilage was rapid prototyped (b) to make a negative auricular mold (c), which was then used to form and auricular dense BNC

layer. (d) The BNC-A porous layer was molded on top of the dense layer, followed by freeze-drying (e). (f) The ionic liquid EMIMAc was used to attach both layers to achieve a strong interfacial bonding. (g) After purification, patient-specific auricular BNC scaffolds with bilayer architecture were ready for implantation in a rabbit model.

SEM images revealed an intact macroporous structure in the auricular BNC scaffolds after the fabrication process. The height of the porous layer was about 1.5 mm. The dense BNC layer remained stable during the purification process, with an approximate height of 1 mm (**Figure 25**).

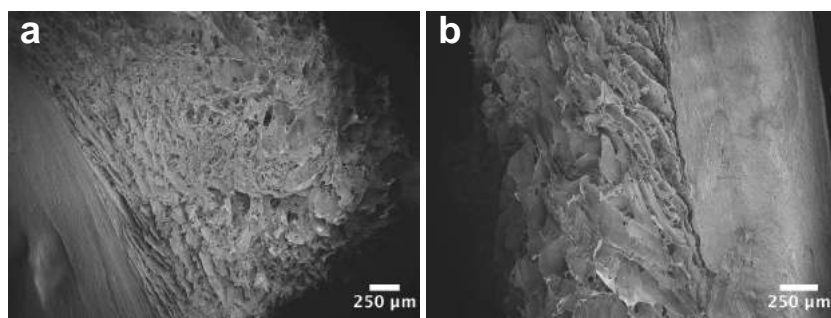


Figure 25 – Scanning electron microscopy images showing the bilayer architecture of auricular BNC scaffolds. The dense BNC layer provides the mechanical stability, while the macroporous BNC-A composite layer supports cell ingrowth.

In agreement with our previous results (**Paper III**), the dense and porous layers were stable and firmly attached, which facilitated the handling of the scaffolds during the purification process for 8 weeks. The removal of endotoxins from the auricular BNC scaffolds was confirmed by bacterial endotoxin testing (**Table 3**). After 5 weeks of purification, the scaffolds had an endotoxin content of 0.526 ± 0.192 EU/ml, slightly above the endotoxin limit (0.5 EU/ml) for medical devices.⁹⁰ Further washing with endotoxin-free water for 8 weeks yielded non-pyrogenic auricular BNC scaffolds (0.00658 ± 0.00214 EU/ml). The measured endotoxin content is in the same range as in the water used for purification (endotoxin specification <0.005 EU/ml) and 75 times lower than the endotoxin limit set by the FDA. Furthermore, *in vitro* cytotoxicity testing revealed that the auricular BNC scaffolds were non-cytotoxic after 5 weeks of purification (**Figure 26**). The cell viability for the auricular BNC scaffold group ($103.4 \pm 7.7\%$) was significantly higher than the positive control group ($31.2 \pm 4.2\%$) at the $p < 0.05$ level, and not significantly different to the negative control ($100 \pm 4.3\%$). This result confirmed the removal of EMIMAc residues from the auricular BNC scaffolds. Due to the large scaffold structures, the purification period of the auricular BNC scaffolds was much longer compared to the purification time of the bilayer BNC scaffolds presented in **Paper III**. Although the purification was lengthy, it was effective to yield non-pyrogenic and non-cytotoxic, patient-specific auricular BNC scaffolds ready for implantation in an immunocompetent rabbit model.

Table 3 – Endotoxin analysis of auricular BNC scaffolds after 5 and 8 weeks of purification in endotoxin-free water ($n=3$ per time point).

| Weeks of purification | Dilution | Spike recovery (%) | Endotoxin Units / ml |
|-----------------------|----------|--------------------|-----------------------|
| 5 | 1:10 | 137 ± 4 | 0.526 ± 0.192 |
| 8 | 1:1 | 69 ± 4 | 0.00658 ± 0.00214 |

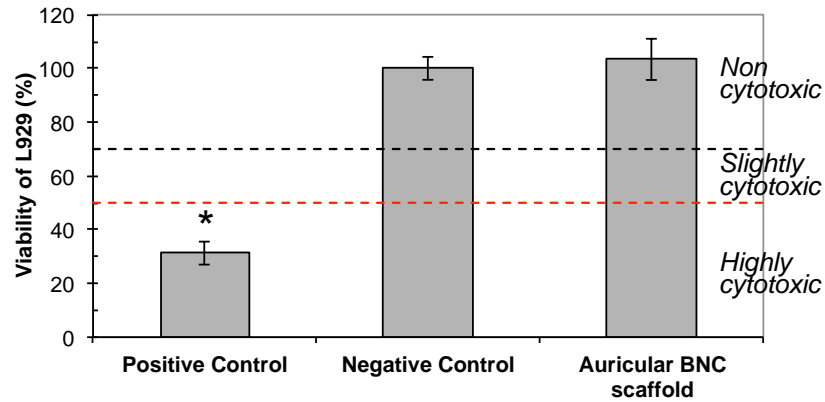


Figure 26 – *In vitro* cytotoxicity testing of auricular BNC scaffolds after 5 weeks of purification in endotoxin-free water (n=3). No significant differences were observed between the negative control and BNC scaffold groups, demonstrating the removal of cytotoxic ionic liquid residues from the auricular BNC scaffolds. Thus, the cytotoxic potential of such scaffolds was classified as non-cytotoxic. Error bars represent the standard deviation of the mean. * $p < 0.05$ compared to negative control.

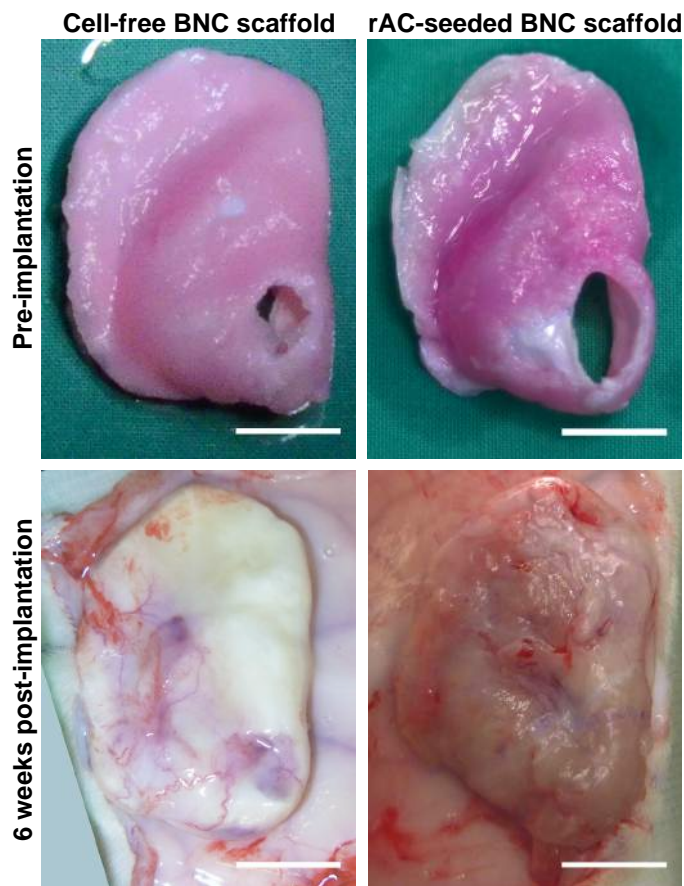


Figure 27 – Photographs showing gross morphology of cell-free and rAC-seeded auricular BNC scaffolds pre-implantation and after 6 weeks of subcutaneous implantation in immunocompetent autologous model. Auricular BNC scaffolds seeded with rabbit auricular chondrocytes. Scale bars indicate 1 cm.

Based on a qualitative assessment of shape and size of the implants, the cell-free auricular BNC scaffolds and the immunocompetent autologous tissue-engineered auricular grafts (i.e. rAC-seeded auricular BNC scaffolds) maintained a good structural integrity after 6 weeks of subcutaneous implantation in the immunocompetent rabbit model (**Figure 27**). On the other hand, the longest *in vivo* study that has evaluated immunocompetent autologous tissue-engineered auricular grafts with different polymeric scaffolds (PGA coated with PLA, PCL and P4HB) reported a severe foreign body reaction in all investigated scaffolds and a severe deformation and collapse of the implants at 3 months post-implantation.²² Most scaffold materials evaluated for auricular cartilage TE have been synthetic biodegradable polymers.^{16,22,65-67} Thus, many studies have resulted in poor shape and size stability of the auricular scaffold after implantation due to the short-lived chemical and mechanical stability of the scaffold materials. In agreement with our results, recent studies that have evaluated non-degradable biomaterials in immunocompromised mice models have also reported a better structural integrity of the implant.^{18,19,24} Although in this study the auricular BNC scaffolds were not evaluated for longer implantation times, we speculate that the implants would still retain their 3D structure since BNC is a non-degradable biomaterial with good chemical and mechanical stability. In a clinical context, the long-term structural integrity of auricular BNC scaffolds should not be compromised after implantation since humans do not produce enzymes capable of breaking down cellulose.⁷⁰ This would allow the BNC implants to retain the shape of the auricle after implantation.

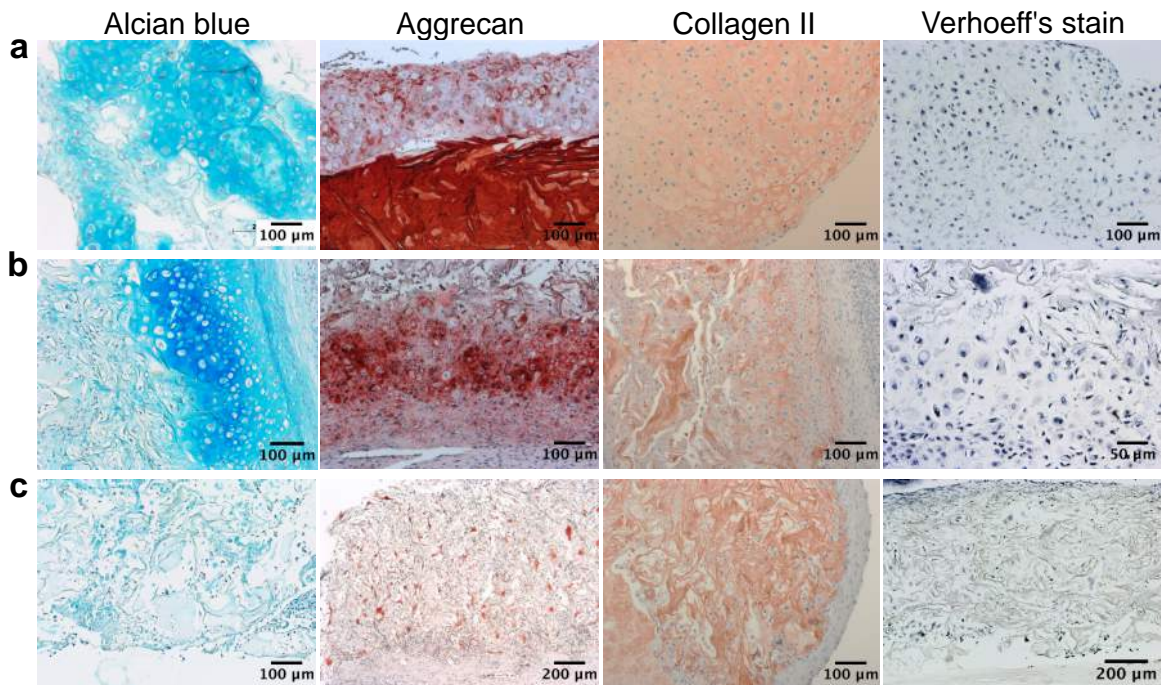


Figure 28 – Histological and immunohistochemical evaluation of ECM in auricular BNC scaffolds seeded with rabbit auricular chondrocytes. (a) RAC-seeded auricular BNC scaffolds after 2 weeks of *in vitro* culture, (b) followed by 6 weeks of subcutaneous implantation. (c) Cell-free auricular BNC scaffolds at 6 weeks post-implantation. Samples were stained with Alcian blue and Verhoeff's stain to detect deposition of sulfated glycosaminoglycans and elastic fibers, respectively. Immunohistochemical staining was used to detect aggrecan and type II collagen.

Besides maintaining a good structural integrity, the tissue-engineered auricular graft provided a scaffold architecture that is mechanically stable and porous to support cell ingrowth and neocartilage formation. As demonstrated in **Figure 28a**, the porous layer supported the ingrowth and homogenous distribution of rACs. A high cell density and positive stain for s-GAG were observed in the porous scaffold layer, especially at the top part, after 2 weeks of *in vitro* culture. Of particular interest is the arrangement of the chondrocytes in the porous layer, which were contained in cavities that resemble cartilage lacunae. Although the isotype control showed a non-specific background signal in the dense BNC layer caused by the anti-aggrecan antibody, areas around the lacunae were also stained positive for aggrecan after 2 weeks of *in vitro* culture. As expected, a stronger positive immunostain for aggrecan and staining for s-GAG were observed around the lacunae at 6 weeks post-implantation (**Figure 28b**). The same observation was made for type II collagen as in aggrecan. A non-specific immuno stain for collagen II was detected in the BNC. However, this important structural protein was also synthesized by the rACs in the auricular BNC scaffolds, as demonstrated by the positive immunostaining of type II collagen around the lacunae. A slight positive staining for elastic fibers was found in the lacunae within the porous layer at 6 weeks post-implantation, as shown by the Verhoeff's stain. The cell nuclei were stained black, whereas the fibrous-like structures inside the lacunae and around the cells were stained with a dark blue color (**Figure 28b**). The cell-free auricular BNC scaffolds supported the ingrowth of the surrounding cells from the host tissue. The surrounding cells infiltrated the porous layer completely or in some cases the ingrowth was mostly at the surface. As expected, ECM was synthesized by these cells and no cartilage cartilage-specific matrix was detected at 6 weeks post-implantation (**Figure 28c**).

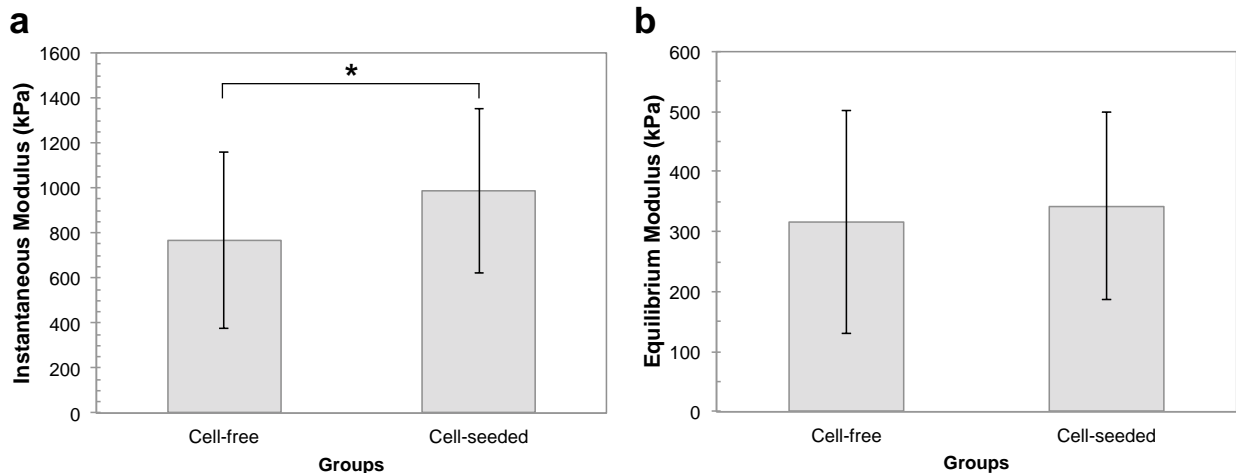


Figure 29 – Biomechanical evaluation. (a) Instantaneous and (b) equilibrium moduli of cell-free and rAC-seeded auricular BNC scaffolds at 6 weeks post-implantation ($n = 18$ per group). Error bars represent the standard deviation of the mean.

Biomechanical evaluation was performed on cell-free and rAC-seeded auricular BNC scaffolds after 6 weeks of subcutaneous implantation. A typical stress relaxation behavior was observed in both groups (cell-seeded and cell-free controls). The following measurements were determined for the rAC-seeded auricular BNC scaffolds at 6 weeks post-implantation: 986 ± 365 kPa for E_{in} and 343 ± 156 kPa for E_{eq} (**Figure 29**). A Wilcoxon–Mann–Whitney test indicated a significantly

higher ($p < 0.05$) E_{in} in the rAC-seeded group compared to the cell-free group (768 ± 391 kPa) at 6 weeks post-implantation. Furthermore, no significant differences in E_{eq} were detected between the cell-free (317 ± 186 kPa) and rAC-seeded groups. The significant increase of E_{in} in the rAC-seeded auricular BNC scaffolds implies an improved capacity of the tissue-engineered graft to retain water, which is likely due to the neo-synthesis of s-GAG and aggrecan. E_{in} describes the instantaneous incompressible behavior of the tissue-engineered construct.

In this study, we demonstrate a scaffold material and architecture as well as a biofabrication method of patient-specific tissue-engineered auricles with potential for auricular reconstruction. Patient-specific auricular BNC scaffolds, composed of a dense BNC layer and a macroporous BNC-A composite layer, were designed based on the mechanical requirements of human auricular cartilage and the porosity requirements for tissue growth. After 6 weeks of subcutaneous implantation in an immunocompetent rabbit model, we demonstrated that the auricular BNC scaffolds maintained a good structural integrity throughout the *in vivo* study and the porous layer supported the ingrowth of rACs and neocartilage formation. On the basis of these results, we propose BNC as a promising non-degradable scaffold biomaterial for auricular cartilage TE.

5.6 3D bioprinting of human chondrocyte-laden nanocellulose hydrogel for patient-specific auricular cartilage regeneration

In **Paper IV** 3D chondrocyte-laden auricular constructs with an open inner structure and high shape fidelity were successfully bioprinted with a novel bioink, composed of cellulose nanofibrils and alginate, and evaluated in long-term 3D culture for auricular cartilage TE. A crucial and important prerequisite for successful bioprinting is the innocuousness and cytocompatibility of the bioprinting process and the cell-carrier hydrogel, the bioink. The results from the indirect cytotoxicity test demonstrate that no cytotoxic effects were caused by the NFC-A bioink, bioprinting process and crosslinking solution on the indicator cells, hNCs and rACs (**Figure 30**). There were no significant differences in cell viability between the NFC-A and negative control groups. Furthermore, the viability for hNCs and rACs cultured with undiluted NFC-A extracts under standard ($96.0 \pm 6.2\%$ and $99.2 \pm 2.3\%$, respectively) and sensitizing ($94.5 \pm 5.9\%$ and $93.6 \pm 6.5\%$, respectively) culture conditions was not significantly different; verifying the non-cytotoxicity of the NFC-A bioink. These results are in good agreement with previous studies that have tested the cytocompatibility of NFC with human dermal fibroblasts¹⁷³ and hepatic progenitor HepaRG cells.¹⁷⁴

Another prerequisite for bioprinting is to be able to operate in an aqueous environment, which restricts the choice of materials.^{101,103} In this study, cell-laden NFC-A auricular constructs with high shape fidelity were successfully bioprinted due to the highly viscous, shear-thinning bioink (**Figure 31a** and **b**). It is well known that NFC exhibits a high zero-shear viscosity and shear-thinning behavior, even at low solid content. Moreover, the high viscosity is established instantaneously after shearing has stopped.^{124,174} All these important rheological properties combined with the rapid crosslinking property of alginate are required for easy dispensing of the

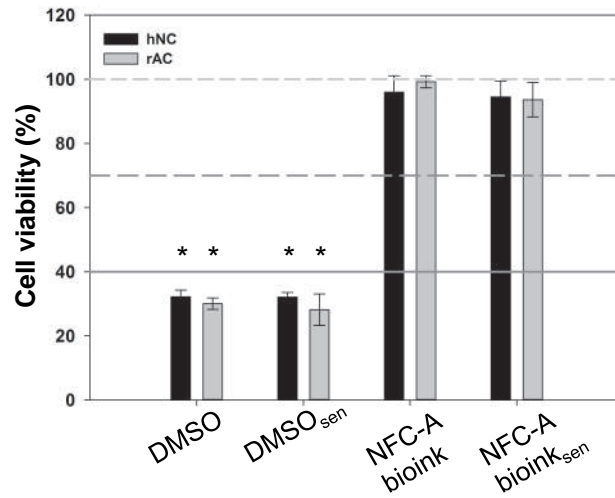


Figure 30 – *In vitro* cytotoxicity test of NFC-A bioink. Human nasal chondrocytes (hNC) and rabbit auricular chondrocytes (rAC) were used as indicator cells to determine cytotoxic effects potentially caused by bioink components, crosslinking or bioprinting process. 10% Dimethyl sulfoxide (DMSO) was used as positive control. HNCs and rACs cultured in the NFC-A bioink extracts demonstrate a high viability and reflect the non-cytotoxicity of NFC-A bioink. Error bars show 95.0% CI of mean. (* $p < 0.05$). (Paper IV)

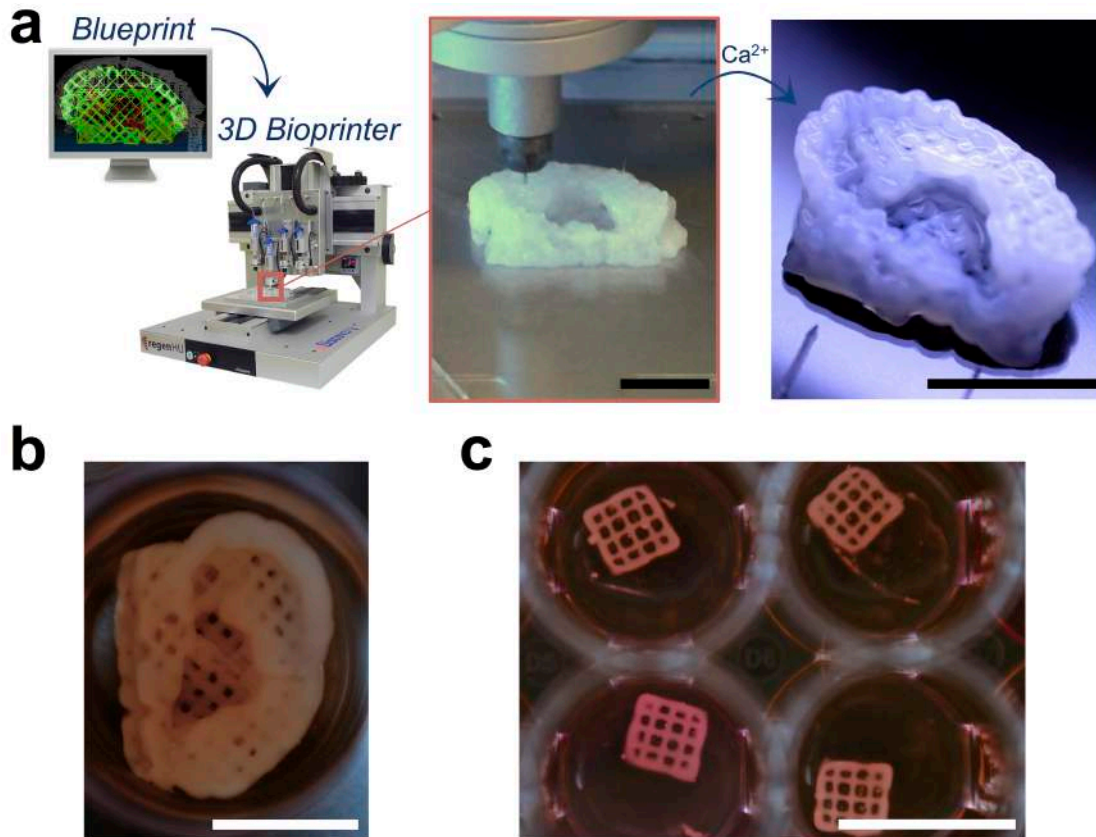


Figure 31 – (a) 3D bioprinting process of chondrocyte-laden NFC-A auricular constructs with open porosity. Blueprint shows the toolpaths of the support (PCL, white) and object (NFC-A, green) materials. (b) 3D bioprinted auricular and (c) lattice-structured constructs, laden with hNCs, after 28 days of culture. Scale bars indicate 1 mm. (Paper IV)

hydrogel at low pressures (< 40 kPa); maintaining a high shape fidelity during and after bioprinting; and keeping the cells in a 3D environment after crosslinking the cell-laden bioink constructs. Until now, hydrogels based on natural polymers have been regarded as having a sub-optimal printability compared to synthetic hydrogels such as pluronics.¹⁷⁵ A bioink with a high zero-shear viscosity and a fast response to re-establish the high viscosity after extrusion is required to avoid sedimentation of the cells and to keep a high shape fidelity during the bioprinting process. These two rheological properties are illustrated by the end results of the 3D cell-laden NFC-A auricular constructs presented in this study (**Figure 31a** and **b**). Furthermore, the cell-laden NFC-A constructs showed an excellent shape and size stability after bioprinting and 3D culture for up to 28 days, demonstrating the stability of the NFC-A network after crosslinking (**Figure 31b** and **c**).

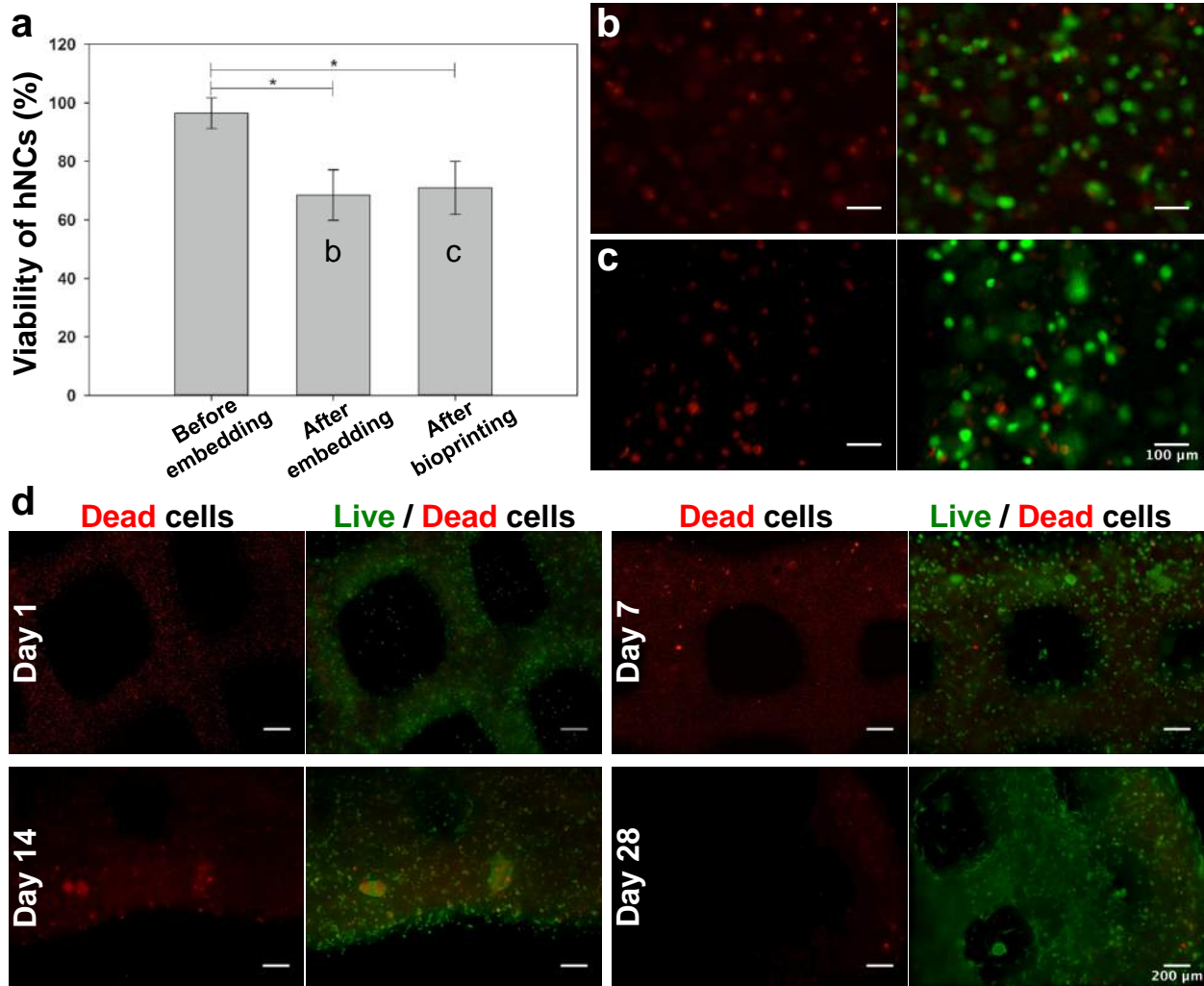


Figure 32 – Live/Dead cell imaging analysis. **a**) Percent viability of human nasoseptal chondrocytes (hNC) before and after embedding in NFC-A bioink and after bioprinting process. Error bars show 95.0% CI of mean. (* $p < 0.05$). Representative images showing live (green) and dead (red) hNCs **(b)** after embedding and crosslinking; **(c)** after 3D bioprinting and crosslinking of cell-laden NFC-A constructs; and **(d)** in 3D bioprinted constructs throughout 28 days of 3D culture. Scale bars indicate **(b, c)** 100 μm and **(d)** 200 μm . ^(Paper IV)

To assess the influence of embedding, bioprinting and crosslinking processes on cell viability, we performed a Live/Dead staining based on a cell-permeable dye for staining of live cells and a cell-impermeable dye for detection of dead cells. We examined the cell viability before embedding the hNCs in NFC-A bioink; after embedding and crosslinking; and after embedding, bioprinting and crosslinking the cell-laden NFC-A constructs (**Figure 32a**). A Kruskal–Wallis ANOVA on ranks was conducted to compare the effect of embedding and bioprinting on cell viability. There was a significant effect of the handling of the cells on levels of cell viability for the three tested conditions, $H(2, 10) = 6.49, p < 0.05$. Post hoc comparisons using the Dunn’s test indicated that the mean cell viability after embedding and crosslinking processes ($68.5 \pm 6.9\%$) was significantly lower than before embedding the hNCs ($96.5 \pm 2.1\%$) at the $p < 0.05$ level. Moreover, there was no significant difference between the after embedding and after bioprinting ($70.9 \pm 7.2\%$) conditions, indicating that the bioprinting process had no significant influence on cell vitality (**Figure 32a-c**).

A homogeneous cell distribution was observed after embedding the hNCs in NFC-A bioink and bioprinting the constructs, indicating a successful mixing process and capability of this bioink to keep the cells in suspension due to its high zero-shear viscosity (**Figure 32b-d**). Furthermore, we examined the viability of hNCs in the NFC-A constructs qualitatively, throughout the 28 days of culture, using live/dead cell imaging analysis. Directly after embedding, a loss of chondrocytes was detected, but these were able to recover during 3D culture. Less dead hNCs were present in the bioprinted constructs after day 7 compared to day 1, indicating a higher cell viability and cell recovery post-bioprinting. Moreover, cell recovery improved as the 3D culture progressed, as indicated by the decrease of dead cells embedded in the bioink. Also, an increase in cell numbers could be observed after 28 days of culture (**Figure 32d**).

The qualitative results from cell imaging, pointing towards cell proliferation in the NFC-A hydrogels, were confirmed by biochemical analysis. A Wilcoxon–Mann–Whitney test indicated a significantly higher ($p < 0.05$) cell number per construct after 28 days ($5.65 \times 10^5 \pm 1.11 \times 10^5$), compared to 14 days ($3.98 \times 10^5 \pm 1.05 \times 10^5$) of 3D culture (**Figure 33a**). Furthermore, hNCs demonstrated the capacity to synthesize GAGs in the NFC-A bioink after 14 and 28 days of culture in chondrogenic differentiation medium. A Wilcoxon–Mann–Whitney test showed a significant difference ($p < 0.05$) between mean GAG content per scaffold after 14 days ($21.0 \pm 9.1 \mu\text{g GAG}$) and 28 days ($40.6 \pm 11.8 \mu\text{g GAG}$) of culture (data not shown). Although total GAG-production was 2-fold higher at day 28 compared to day 14, the synthesis rate of GAGs—measured in chondroitin sulfate equivalents per cell—was not significantly different between day 14 ($54.6 \pm 24.8 \text{ pg/cell}$) and day 28 ($72.0 \pm 22.0 \text{ pg/cell}$) (**Figure 33b**).

Our results demonstrated the capacity of hNCs to build up neocartilage tissue, by synthesizing and accumulating sulfated GAGs in the NFC-A bioink during 3D culture in chondrogenic differentiation medium. We also investigated whether chondrocytes maintain their capacity for tissue remodeling and turnover. For this purpose, we analyzed the matrix regulatory agents MMP-2 and MMP-9 by gelatin zymography. The results revealed that the pro and active form of MMP-2 were abundantly expressed and secreted on day 14. After 28 days, the expression of pro-MMP2 per cell decreased, while the secretion of active-MMP2 remained stable. Both forms of

MMP-9 were secreted on at much lower levels compared to MMP-2 and remained stable between day 14 and 28 (**Figure 33c** and d). Matrix metalloproteinases (MMPs) are a family of Zn^{2+} -dependent endopeptidases, essential for the degradation and timely breakdown of ECM during development, morphogenesis, and tissue remodeling under pathological, as well as normal physiological conditions.^{176,177} It has been shown that both MMPs are expressed in moderate levels in hyaline cartilage and *in vitro*, where MMP-2 is expressed in higher levels than MMP-9.¹⁷⁸ Our results confirmed this finding and show that hNCs support tissue remodeling in NFC-A bioink.

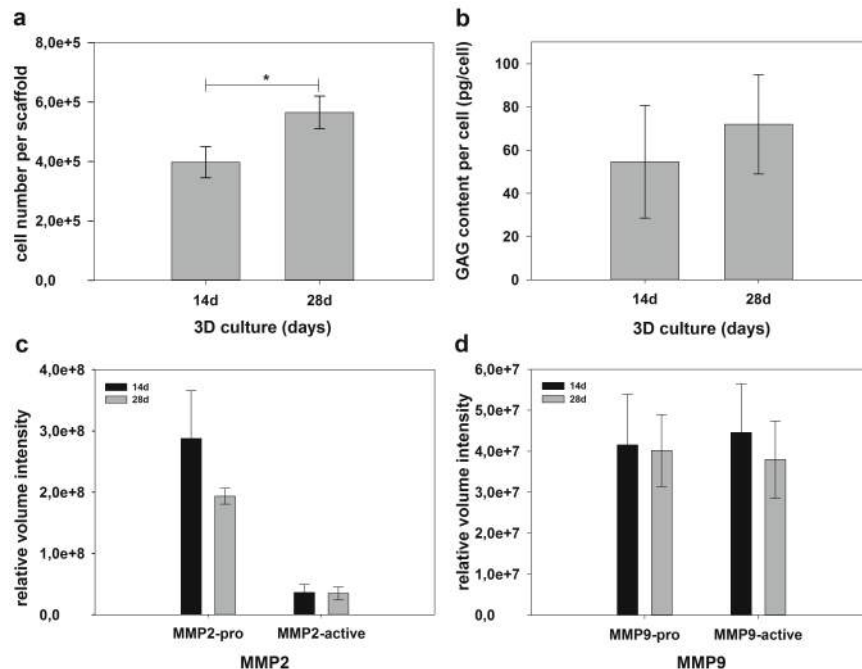


Figure 33 – Quantitative biochemical assays for characterization of hNC proliferation, GAG neo-synthesis and release of matrix metalloproteinases, MMP 2 and MMP9, during 3D culture for up to 28 days in NFC-A bioink. (a) Cell number per scaffold. HNCs proliferate in NFC-A bioink and a significant increase in cell number is observed after 28 days. (b) The GAG content per cell increases clearly from day 14 to day 28 in 3D culture. (c) Release of pro- and active-MMP2 and (d) pro- and active-MMP9 in 3D culture of hNC in NFC-A bioink. Error bars show 95.0% CI of mean. $n = 6$ per time point, $*p < 0.05$. (Paper IV)

The local environment provided to chondrocytes affects not only their morphological appearance but also their differentiation status.¹⁷⁹⁻¹⁸¹ The redifferentiation and re-organization of the gene expression pattern of hNCs, shown by the up-regulation of the examined chondrogenic markers at the gene and protein levels (**Figure 34**), could be attributed in part to the highly hydrated, fibrous 3D environment provided by the NFC-A bioink. This biologically relevant aqueous 3D environment, composed of cellulose nanofibrils with morphological similarity to collagen, provides the hNCs with a milieu that resembles their natural matrix; while the excellent printability of this bioink make it possible to bioprint complex, anatomically-shaped cell-laden constructs with a controlled cell density.

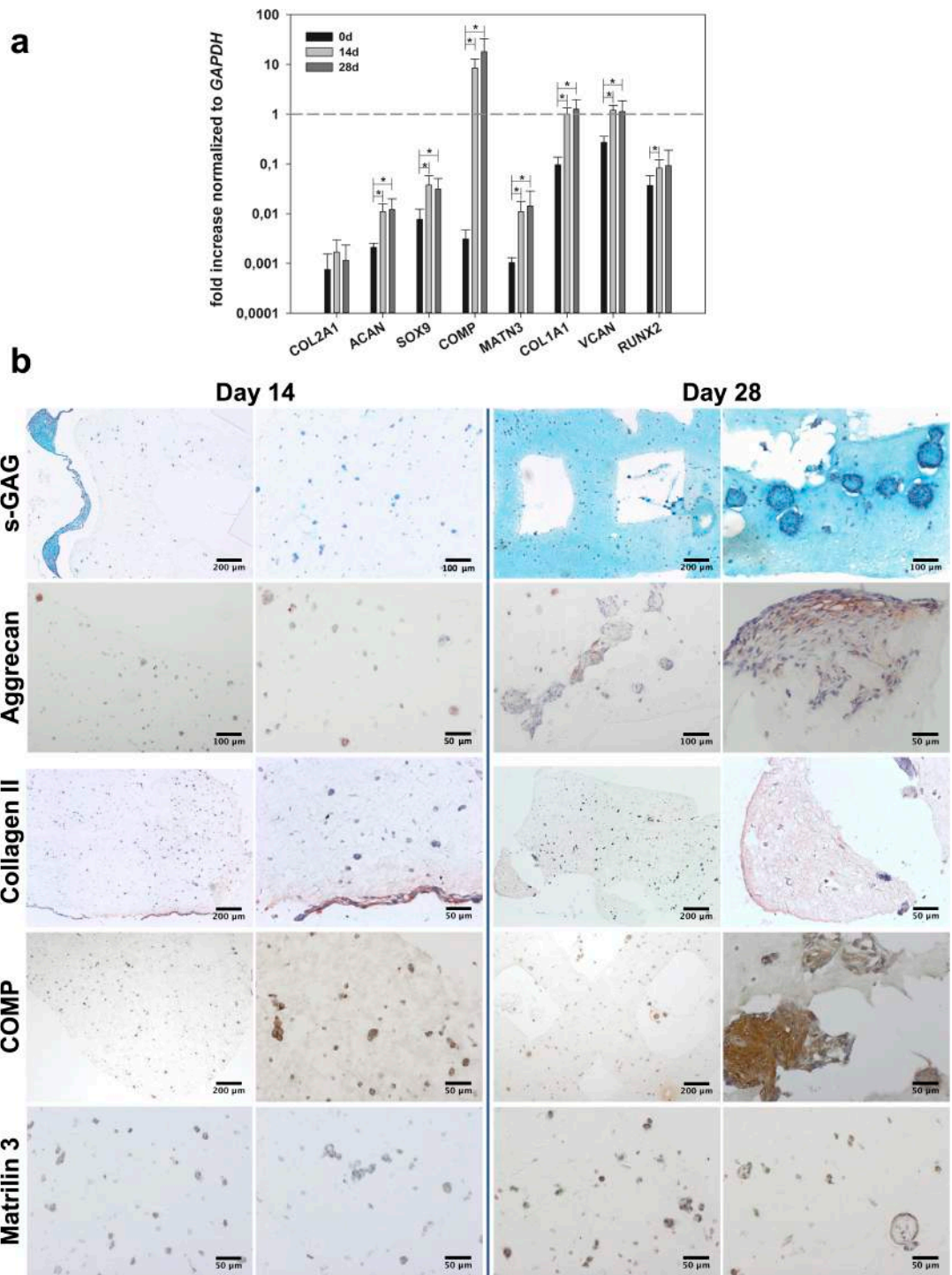


Figure 34 – (a) Comparative expression of redifferentiation and dedifferentiation marker genes in human nasoseptal cartilage and hNCs after monolayer expansion (day 0) and after 3D bioprinting in NFC-A bioink and cultured for 14 and 28 days. The data is presented as the fold change in gene expression normalized to GAPDH and relative to human nasoseptal cartilage (dashed line). Error bars show 95.0% CI of mean. (* $p < 0.05$). (b) Histological Alcian blue staining of sulfated glycosaminoglycans (s-GAG), and immunohistological staining specific for aggrecan, collagen type II, cartilage oligomeric protein (COMP) and matrilin-3 in hNC-laden NFC-A constructs after 14 and 28 days of culture. Nuclei are counterstained with Hematoxylin. ^(Paper IV)

As a consequence of hNC amplification in monolayer culture, gene expression of all examined markers was down-regulated and detectable only at very low levels (**Figure 34a**). When cultured-expanded hNCs were embedded and cultured in the NFC-A bioink the pattern of gene expression started to revert to a more differentiated state. During the first 14 days in 3D culture, the expression of the cartilage-specific markers *ACAN* ($1.09 \times 10^{-2} \pm 5.32 \times 10^{-3}$ -fold), *COMP* (8.381 ± 4.72 -fold), *MATN3* ($1.09 \times 10^{-2} \pm 7.12 \times 10^{-3}$ -fold) and *SOX9* ($3.75 \times 10^{-2} \pm 2.21 \times 10^{-2}$ -fold) was significantly (each $p < 0.05$) up-regulated compared to monolayer culture (day 0). The expression of *COL2A1* ($1.68 \times 10^{-3} \pm 1.41 \times 10^{-3}$ -fold) was also up-regulated, but not significantly. In addition, hNCs exhibited a significant (each $p < 0.05$) up-regulated expression of *COL1A1* ($9.98 \times 10^{-1} \pm 3.65 \times 10^{-1}$ -fold) and *VCAN* (1.20 ± 0.33 -fold), both generally accepted as markers for chondrocyte dedifferentiation, as well as *RUNX2* ($8.24 \times 10^{-2} \pm 4.11 \times 10^{-2}$ -fold). Although the increase in gene expression was significant between day 0 and 28, no significant changes occurred between day 14 and 28 (**Figure 34a**)

The results of gene expression were confirmed on protein level by histological and immunohistochemical stainings. The results shown in **Figure 34b** demonstrate a homogenous distribution of hNCs with round shape morphology in the NFC-A bioink during 3D culture. Furthermore, a homogeneous deposition of sulfated GAGs within the hNC-laden NFC-A constructs was clearly visualized together with large cell aggregates, where a strong positive stain for s-GAGs was detected around the clusters of hNCs after 28 days in 3D culture. A positive immunostain for aggrecan was also observed around single hNCs already after 14 days of culture, whereas an enhanced accumulation of aggrecan was observed in cell clusters after 28 days of 3D culture. Moreover, cells growing inside the pores of the gridded constructs were found along with neo-synthesized ECM components such as GAGs around the stretched hNCs. The out-growing cells built up a superficial layer on the bioink surface. These cells exhibited the capacity to produce GAGs, aggrecan and collagen type II. After 14 days of culture, a positive immunostain for collagen type II was observed mostly at the edges of the constructs and as the culture progressed larger areas positive for collagen II were found.

In agreement with gene expression, *de novo* synthesis of COMP by hNCs was already observed after 14 days in 3D culture. COMP was found around single cells, cell clusters and further away from the cells, in the bioink matrix surrounding the embedded hNCs, after 28 days of culture. COMP belongs to the major non-collagenous proteins in cartilage and is tightly regulated during chondrocyte de- and re-differentiation.¹⁸² COMP expression is abruptly down-regulated during dedifferentiation in monolayer expansion and is re-expressed in chondrocytes cultivated in 3D.^{182,183} Our results confirm the observations of earlier 3D studies with alginate beads.¹⁸² A significant increase of COMP was detected on gene expression and protein levels, already after 14 days in 3D culture (**Figure 34a** and **b**). Down-regulation of *COL2A1* and *COMP* during monolayer amplification has severe negative consequences on the assembly, integrity and stability of newly synthesized ECM.¹⁸² Therefore, the up-regulation of gene expression and increased deposition of COMP and collagen type II in hNCs after 3D culture in NFC-A bioink is an important finding, since it reveals the redifferentiation capacity of hNCs in NFC-A bioink (**Figure 34a** and **b**).

Our results show that the expression of *MATN3* in hNCs increased significantly during 3D culture in NFC-A bioink. Accompanied by the enhanced gene expression, we detected depositions of matrilin 3 as pericellular filamentous networks surrounding the hNCs embedded in the NFC-A bioink after 14 and 28 days of 3D culture (**Figure 34a** and **b**). Matrilin 3 possesses regulatory function for the maintenance of cartilage ECM and prevention of premature chondrocyte hypertrophy,¹⁸⁴ acts as modulator of collagen fibrillogenesis, and interacts with collagen type II and IX, proteoglycans and COMP.^{185,186} The expression and neosynthesis of GAGs, collagen type II, aggrecan, COMP and matrilin 3 by the hNCs, observed in the bioprinted cell-laden constructs during 3D culture, could be attributed in part to the biologically relevant aqueous 3D environment that the bioink provides to the cells—mimicking the morphology of their natural matrix while providing a more controlled and relevant cell density. According to Kaps et al., chondrocyte differentiation is initiated by 3D assembly, which subsequently results in the regulation of proliferation-associated genes and initiates re-differentiation.¹⁸³ In this context, the up-regulation of all cartilage-specific markers (*ACAN*, *COL2A1*, *COMP*, *MATN3* and *SOX9*) during 3D culture in NFC-A bioink suggests that the dedifferentiation of hNCs, following expansion in monolayer, is reversed by subsequent 3D assembly in an aqueous 3D environment that mimics the morphology of their natural matrix; whereat chondrogenic developmental sequences are re-initiated.

5.7 Mechanical stimulation of cell-seeded BNC scaffolds to enhance neo-tissue development

In **Paper V**⁸⁰ a compression bioreactor was utilized to apply dynamic mechanical stimulation to cell-seeded constructs as a means to enhance production of extracellular matrix *in vitro*. The SEM images of BNC scaffolds clearly confirmed that the macro-channels remained open after removal of the cylindrical porogens, where the diameter of the macro-channels was approximately 600–700 μm (**Figure 35**). The open macro-channeled architecture of the BNC scaffolds facilitated the seeding of the cells and the transport of nutrients inside the channels.

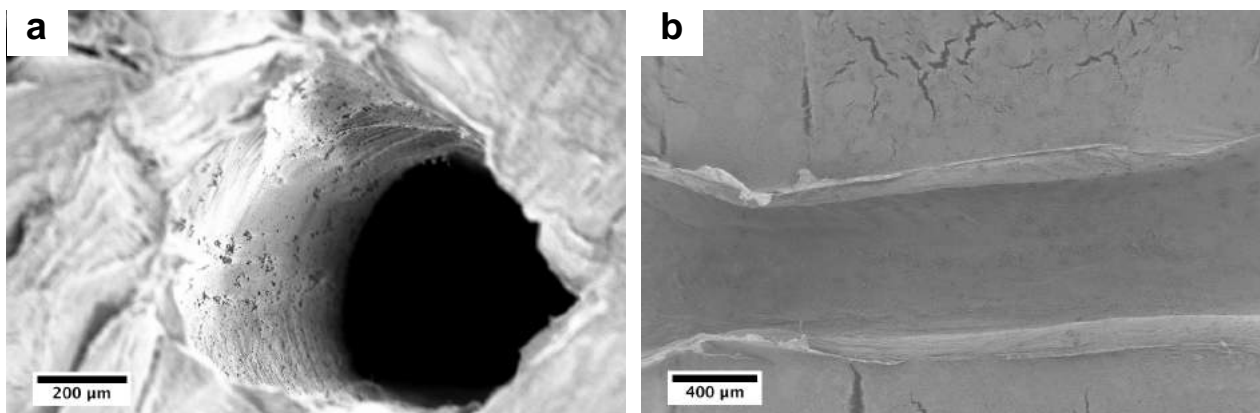


Figure 35 – SEM images of macro-channeled BNC scaffolds. (a) Cross-section and (b) top-view images of macro-channel. ^(Paper V)

As both cellulose and collagen are visualized with SHG microscopy, correct interpretation of SHG images requires differentiation between the materials. For this purpose, corresponding

SHG, CARS, and brightfield images from a macro-channel boundary region were compared. In brightfield images, it was generally easy to differentiate between the BNC and the macro-channel (μc)/cell regions (**Figure 36**). Although, individual cellulose fibers can be readily visualized with SHG microscopy,¹²⁸ the dense cellulose network appears rather homogeneous in the $200 \times 200 \mu\text{m}^2$ field of view of the acquired SHG images (**Figure 36b**, BNC). Furthermore, the cellulose gave a relatively constant background signal in the CARS image (**Figure 36c**, BNC). In contrast, SHG and CARS visualize the μc /cell region differently. The compact matrix of the μc /cell region gives a non-uniform signal in the CARS image, consistent with the morphology of the region and here shown in orange-brown color (**Figure 36c**, $\mu\text{c}/\text{cell}$). Moreover, a strong signal and high CARS image contrast is obtained from lipid droplets visualized in bright yellow color. The SHG image of the macro-channel (μc)/cell region shows a developed fiber network identified as SHG-active collagen because of its location and the dimensions of the fiber network, compared to the denser and homogenous cellulose shown in the lower right corner of the SHG image (**Figure 36b**). In addition, the fibers in the μc /cell region show higher SHG intensity compared to the cellulose; in agreement with the strong SHG signals generally obtained from collagen type I.¹²⁷ This confirms that the SHG signal obtained in the μc /cell region originates from collagen (**Figure 36b**).

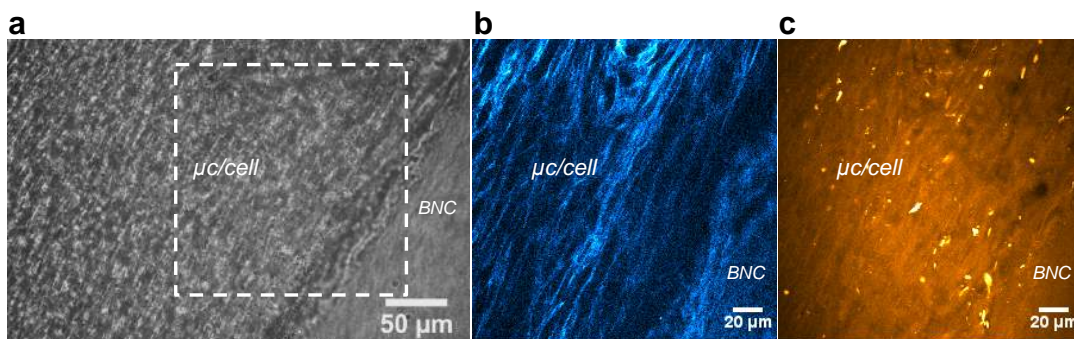


Figure 36 – Microscopy images of cell-seeded macro-channeled BNC scaffold after 14 days in static culture. (a) Brightfield image shows the overall cell arrangement in the macro-channel (μc)/cell region, where the boundary of the macro-channel is clearly identified. (b) Specific imaging of collagen fibers (blue color) in the indicated region of interest (inset in image a) is provided by SHG microscopy, which also visualizes the cellulose scaffold (BNC). (c) The fibroblasts can be probed by CARS microscopy, useful for confocal imaging of the cell matrix ($\mu\text{c}/\text{cell}$, orange-brown color). (Paper V)

Cells seeded on unmodified BNC scaffolds were able to align at local level, but were more randomly oriented at a larger scale after 14 days of culture (**Figure 37a**). The macro-channels were highly populated by fibroblasts and the cells were aligned at the local- and large-scale in the constructs cultured under static conditions already at 14 days; demonstrating the role of the macro-channels to guide cell growth (**Figure 37f-h**). For individual fibroblasts, cell orientation is locally determined by neighboring cells. As the cells proliferate and reach the boundaries of the macro-channels, it results in cell layers oriented parallel to the direction of the channels. SHG microscopy images revealed that this cell alignment also resulted in the synthesis of collagen fibers aligned along the channel. Comparison between SHG and brightfield images shows an alignment of collagen fibers and cells along the channel direction for construct cultured in static as well as dynamic conditions (**Figure 37f-j**, arrows).

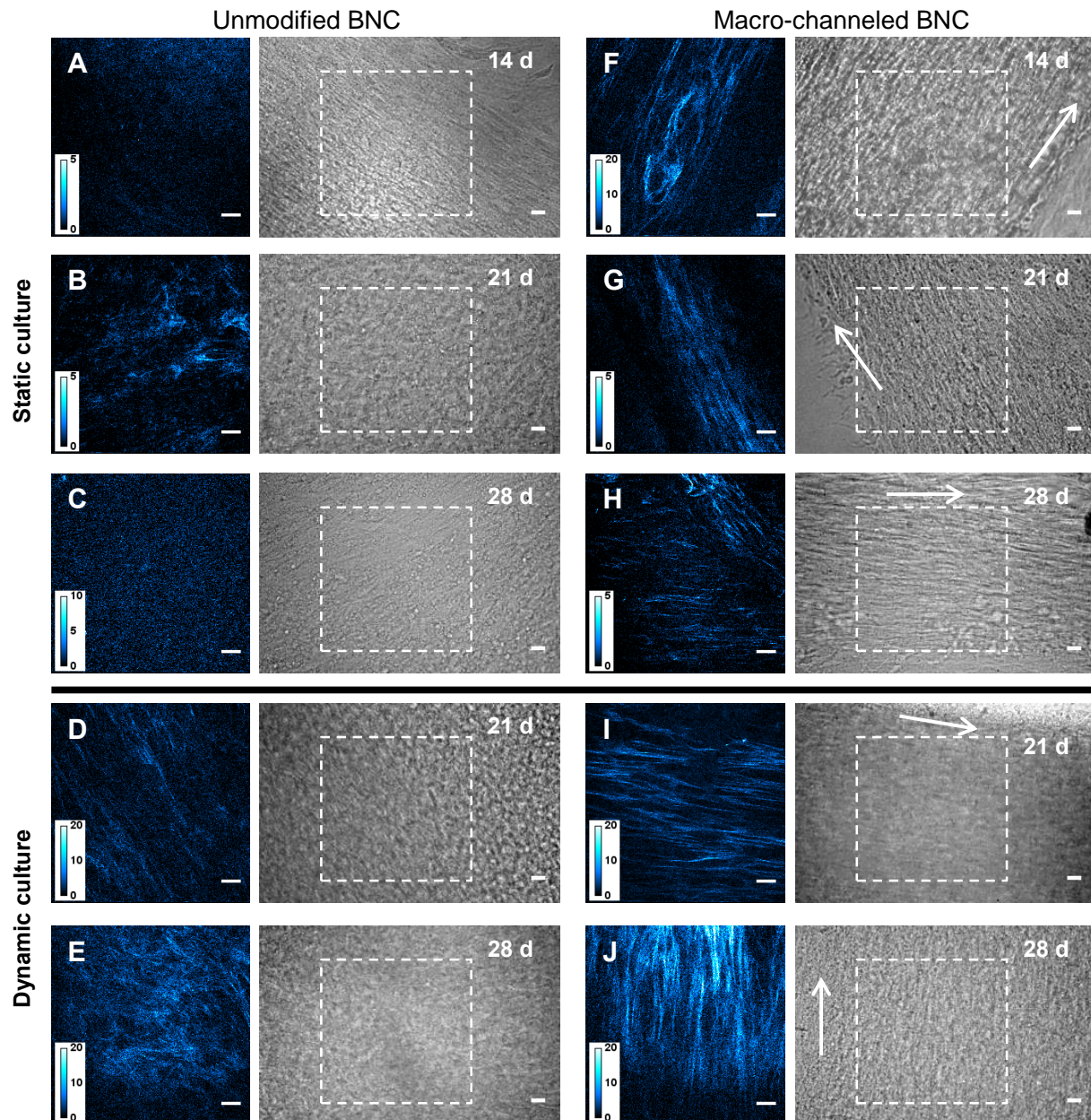


Figure 37 – SHG and brightfield microscopy images from cell-seeded (a–e) unmodified and (f–j) macro-channeled BNC scaffolds cultured in static (upper rows) and dynamic conditions (lower rows) at day 14, 21, and 28. The SHG images visualize collagen fibers and the brightfield images show cell pattern at a larger scale. Macro-channeled scaffolds show an alignment of cell pattern and collagen fibers along the channel (f–j). Samples from the dynamic culture show higher amount of collagen fiber networks compared to the static culture. Insets indicate regions of SHG images and the arrows indicate macro-channel directions. Scale bar size 20 μm . ^(Paper V)

Cells seeded in macro-channeled BNC scaffolds and cultured in static conditions showed collagen fiber networks after 14 days of culture (**Figure 37f**). However, weaker SHG signals were observed in samples collected at day 21 and 28 (**Figure 37b, c, g, h**). SHG signals positive for collagen were expected in samples from the static culture, as collagen secretion is a primary

task of fibroblasts. Thus, the static culture served as a base-line control for the dynamic culture. In contrast to the static culture, SHG images of constructs from the dynamic cultures showed stronger SHG signal and demonstrated collagen fiber networks (**Figure 37d, e, i, j**, see intensity scales). SHG microscopy has been used extensively for visualization of fibrillar collagen structures.¹⁸⁷⁻¹⁹⁰ On the basis of the amount of fibers and the signal strength in SHG images from the dynamic cultures, it is clear that the collagen production was enhanced by the mechanical stimulation (**Figure 37** and **Figure 38**). **Figure 38** shows three-dimensional arrangements of collagen fibers and cells in volume views rendered from stacks of SHG and CARS images measured on constructs during dynamic culture (days 21 and 28). In the overlay volume views (left), showing collagen fibers (blue) and cell layers (orange), it can be observed that the collagen fibers are embedded in the cell matrix and appear anchored to the cells (**Figure 38**, arrows). Furthermore, fiber alignment is maintained through multiple layers of cells in the macro-channeled BNC scaffolds, as shown by the box views (right) of the collagen fiber networks (**Figure 38c, d**).

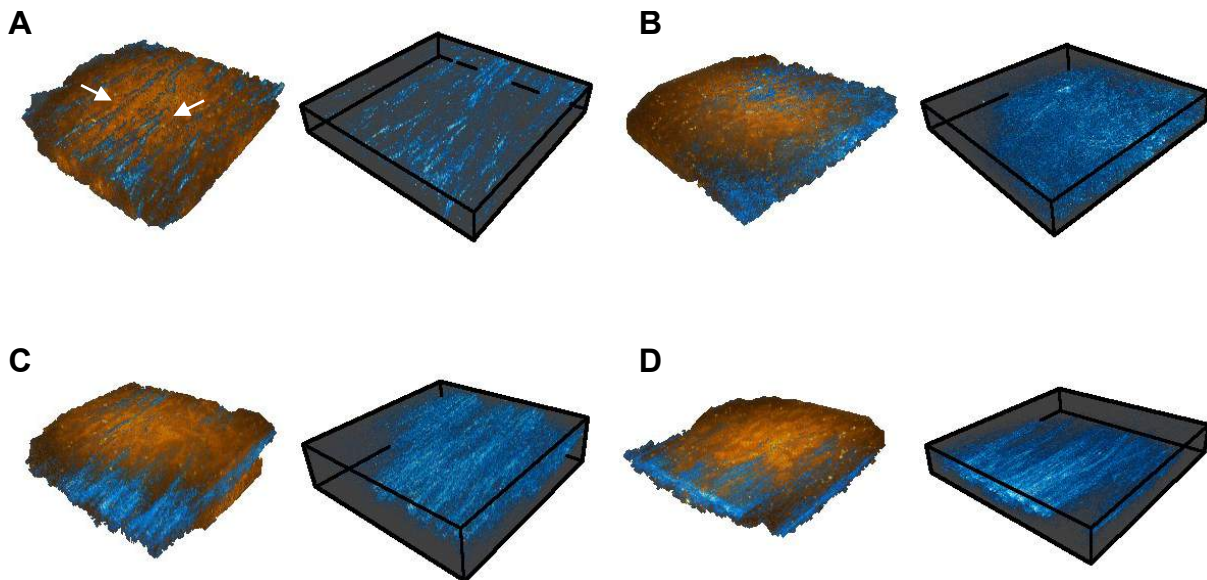


Figure 38 – SHG and CARS microscopy volume views of collagen fibers (blue) and fibroblasts (brown–orange) in (a, b) unmodified and (c, d) macro-channeled BNC scaffolds cultured under dynamic conditions at day 21 (a, c) and 28 (b, d). Overlay SHG and CARS volume views (left) show that fibers are embedded in the cell matrix (a, arrows). Separate visualization of the collagen fiber networks (box views, right) shows the multilayer arrangement of fibers. Note the alignment for the macro-channeled scaffolds (c, d). Lateral image dimensions $200 \times 200 \mu\text{m}^2$, vertical image dimensions $30 \mu\text{m}$ (a, b, d) and $50 \mu\text{m}$ (c). ^(Paper V)

Our findings show that the macro-channels facilitate the alignment of the cells along the channels, which results in the secretion of collagen fibers oriented in the same direction. Furthermore, collagen production is enhanced by dynamic mechanical stimulation under physiologically relevant loading conditions. The use of bioreactors is essential for the development of tissue-engineered cartilage *in vitro*, where mechanical stimulation can be easily applied to cell-seeded BNC scaffolds to aid in the development of the neo-tissue. Cell migration, ECM deposition, and complex tissue differentiation, among other forms of cell behavior, are regulated by mechanical stimuli. Mechanosensitive tissues, such as bone and cartilage, are known

to adapt their developmental programs in response to applied mechanical stresses. This smart feature allows our tissues to specifically adapt to their working conditions.^{191,192} Thus, it is of extreme importance to develop tissue-engineered constructs under a physiologically relevant mechanical environment

CHAPTER 6

CONCLUDING REMARKS

In **Paper I** we aimed to assess whether BNC is a mechanically appropriate implant material for auricular cartilage replacement. For the first time, mechanical properties of human auricular cartilage were determined in order to define a benchmark required for BNC and other scaffold materials aimed at auricular cartilage TE. Although tissue samples from only 4 donors were tested, this benchmark was considered more appropriate than using published mechanical properties of hyaline cartilage or fibrocartilage. The compressive mechanical properties of BNC materials could be tuned (E_{eq} : 0.06 to 3.2 MPa) to match the mechanical requirements of human auricular cartilage (E_{eq} : 3.3 ± 1.3 MPa) by increasing the cellulose content to 14%. Additionally, we demonstrated a novel biofabrication process to produce patient-specific BNC implants with complex 3D shapes such as a human auricle. Based on these results, it was concluded that BNC shows promise for engineering non-degradable auricular implants with tunable, patient-specific mechanical properties and shapes. Based on the mechanical requirements of auricular cartilage and the porosity requirements for tissue growth, this study led to the design of a BNC scaffold with a bilayer architecture that combines mechanical stability (i.e. dense BNC layer) and high porosity (i.e. macroporous BNC-A composite layer).

In **Paper II**, we investigated the host tissue response to densified BNC hydrogel with cellulose content of 17 %, since this material was considered a mechanically appropriate scaffold material for auricular cartilage TE (**Paper I**). It was considered of utmost importance to first evaluate the purity, pyrogenicity and cytotoxicity of the densified BNC hydrogel, before an *in vivo* biocompatibility study was conducted. Thus, a purification and depyrogenation process was developed and validated. As shown by the results from ESCA and bacterial endotoxin analysis, the first depyrogenation process extensively removed bacteria and its residues, particularly endotoxins, from the large BNC structures. The second depyrogenation process, consisting of rinsing with endotoxin-free water, was shown to reduce the endotoxin content in the densified BNC hydrogels down to 0.10 EU/ ml; well below the endotoxin limit for medical devices. Furthermore, biocompatibility testing according to standards set forth in ISO 10993 demonstrated that the purified and densified BNC hydrogel is non-cytotoxic and causes minimal foreign body response. Based on the recommendations of ISO 10993-6 Appendix E, autologous auricular cartilage and densified BNC implant groups were considered a slight irritant to the host tissue in a rabbit model. In support with our previous findings, in **Paper II** we concluded that the tested densified BNC hydrogel is a promising non-degradable biomaterial for auricular cartilage TE, due to its similarity with auricular cartilage in terms of mechanical strength (**Paper I**) and host tissue response.

Since native and densified BNC hydrogels are impenetrable to cells, due to the lack of macroporosity, different methods were investigated to create porous BNC scaffolds that support cell ingrowth. A freeze-drying process was used to fabricate macroporous scaffolds composed of BNC and alginate, where the latter served as the binder of the scaffold matrix. The redifferentiation capacity of hNCs was studied in macroporous BNC-A composite scaffolds *in*

vitro, where the effect of scaffold composition on neocartilage formation was evaluated. Two groups of BNC-A composite scaffolds, 50/50 and 90/10, with similar macro-architecture but different pore surface topographies were investigated. Our results demonstrate that both composite scaffolds possess morphological properties appropriate for cell ingrowth, proliferation and neocartilage formation. After 42 days of 3D culture, depositions of cartilage-specific ECM such as GAGs, aggrecan and collagen type II were found notably in both BNC-A composite scaffolds. Although there was a higher expression of the evaluated chondrogenic markers in the 50/50 BNC-A scaffold type, we selected the 90/10 BNC-A composite scaffold for further studies since it can be sterilized using an effective and reliable method, such as steam sterilization, without damaging the macroporous structure.

In **Paper III** a novel BNC scaffold designed with a bilayer architecture that integrates mechanical stability and high porosity was successfully fabricated and evaluated for auricular cartilage TE, *in vitro* and *in vivo*. To achieve a strong interfacial molecular bonding between the scaffold layers, we used a novel cellulose solvent system consisting of the ionic liquid EMIMAc. This study demonstrates that non-pyrogenic and non-cytotoxic bilayer BNC scaffolds can be successfully produced. Furthermore, such scaffolds together with alginate provide a suitable environment for culture-expanded hNCs as well as freshly isolated hNCs and MNCs to form cartilage *in vitro* and *in vivo*. Most studies that have used biodegradable materials to engineer auricular cartilage have resulted in poor structural integrity of the scaffold after implantation due to the short-lived chemical stability of the scaffold material. This study found that bilayer BNC scaffolds offer a good mechanical stability and maintain a structural integrity while providing a porous architecture that supports cell ingrowth and neocartilage formation, as demonstrated by gene expression, immunohistochemical, biochemical and biomechanical analyses. This work, together with previous studies (**Papers I and II**), lead to the development of bilayer BNC scaffolds in the shape of a human auricle, with the aim to provide an effective treatment to serious auricular defects.

Patient-specific auricular BNC scaffolds, composed of a dense BNC layer and a macroporous BNC-A composite layer, were designed and produced based on the mechanical requirements of human auricular cartilage and the porosity requirements for tissue growth. These scaffolds were fabricated by combining the methods developed in previous studies (**Papers I–III**), and evaluated in an immunocompetent rabbit model for six weeks. In this study, we demonstrated the capacity of rabbit auricular chondrocytes to synthesize cartilage-specific ECM components in the immunocompetent autologous grafts. Additionally the auricular shape of the BNC scaffolds was maintained throughout the *in vivo* study. We demonstrate a scaffold material and architecture as well as a biofabrication method of patient-specific tissue-engineered auricles with potential for auricular reconstruction.

A bioprinting method of patient-specific auricular BNC scaffolds was first described in **Paper I**. However, the biofabrication of porous, auricular BNC scaffolds was not successful with this method. In **Paper IV** patient-specific, chondrocyte-laden auricular constructs with an open inner structure and high shape fidelity were successfully bioprinted using a novel bioink composed of cellulose nanofibrils and alginate, and evaluated for auricular cartilage TE. This study

demonstrates that NFC-A bioink is non-cytotoxic. Furthermore, the cell-laden NFC-A constructs showed increased cell viability and proliferation as well as an excellent shape and size stability throughout 3D culture for 28 days. Moreover, hNCs embedded in the bioink redifferentiated and underwent chondrogenesis, which resulted in neo-synthesis and accumulation of cartilage-specific extracellular matrix around the cells—as demonstrated by gene expression, immunohistochemical and biochemical analyses. Based on these results we can conclude that NFC-A bioink provides a biologically relevant environment that supports redifferentiation of human chondrocytes *in vitro*, while offering excellent printability—making it a promising bioink for auricular cartilage TE.

The use of bioreactors is essential for the development of tissue-engineered cartilage *in vitro*. In **Paper V** a compression bioreactor was utilized to apply dynamic mechanical stimulation to cell-seeded constructs as a means to enhance production of extracellular matrix *in vitro*. The three-dimensional distributions of collagen fibers and fibroblasts in the cellulose scaffolds were studied under native, soft-matter conditions by combined second harmonic generation and coherent anti-Stokes Raman scattering microscopy. The results revealed that macro-channels incorporated in BNC scaffolds facilitate the alignment of fibroblasts and, thus, the neo-synthesized collagen fibers. Furthermore, collagen production is enhanced by dynamic mechanical stimulation under physiologically relevant loading conditions for native cartilage. These two factors have made it possible to engineer a composite biomaterial consisting of oriented collagen fibers embedded in a cellulose matrix.

In this thesis, we evaluated nanocellulose-based scaffold materials, purification methods, scaffold architectures and biofabrication methods of patient-specific tissue-engineered auricles with potential for auricular reconstruction. Based on the evidence from multiple studies, we propose BNC as a promising non-degradable biomaterial for auricular cartilage TE. Although the primary focus of this thesis has been on auricular reconstruction, the methods developed are also applicable in the regeneration of other cartilage tissues such as those found in the nose, trachea, spine and articular joints.

6.1 SUGGESTIONS FOR FUTURE RESEARCH

The compressive mechanical properties of BNC materials can be tuned to match the mechanical requirements of human auricular cartilage. However, the relaxation kinetics of the material need to be further improved. In future work it would be appropriate to introduce negative-charged groups in the BNC network to better mimic the relaxation behavior of native cartilage. It was expected that the GAGs produced by the seeded chondrocytes would be enough to improve the relaxation kinetics (higher $t_{1/2}$ and τ) of the tissue-engineered constructs. However, this was only observed in the *in vivo* studies. The presence of charged GAGs in BNC can be mimicked by chemical modifications such as sulfonation or phosphorylation of the material, as demonstrated by Svensson et al.⁸¹ The importance of having negative-charged groups is not only to bind water, and hence improve relaxation kinetics, but also to bind the growth factors in the culture medium or those produced by the cells.

Macroscopic examination of the bilayer BNC scaffolds revealed a stable adhesion between the dense and porous layers, with no signs of adhesive failure after the *in vitro* and *in vivo* studies (**Paper III**). However, we also observed that when pulling the dense and porous layers apart the scaffold breaks at the porous layer, similar to a structural failure. We speculate that the interfacial bonding between the layers is stronger than the structure of the porous layer, since the mechanical stability of the BNC-A layer is dependent on the crosslinked alginate in the composite matrix. Thus, to improve the mechanical stability of the bilayer scaffold, the macroporous BNC-A layer would need to be replaced with a macroporous layer made of BNC only. Such macroporous BNC scaffolds can be produced during the biosynthesis of BNC using the techniques developed by Bäckdahl et al.¹⁴⁹ or by post-processing techniques using laser ablation.⁷⁵ The biofabrication of macroporous BNC scaffolds during the biosynthesis process is preferred, since it would yield macroporous scaffolds with a continuous network of cellulose nanofibrils. When combined with a dense BNC layer, it would most likely result in bilayer BNC scaffolds with better mechanical stability and interfacial strength.

As cartilage is a mechanosensitive tissue, it would be necessary to culture tissue-engineered auricular constructs under a physiologically relevant mechanical environment, if these are to be matured *in vitro* before implantation. Thus, the physiological loading conditions for auricular cartilage must first be assessed to design an appropriate bioreactor for mechanical stimulation. Static and dynamic mechanical stimulation applied to chondrocyte-laden scaffolds would enhance cell proliferation and neocartilage formation, and thus, improve the neo-tissue's mechanical properties. Also, elastic fibers play a major role in the mechanical properties of auricular cartilage. This underlines the importance of elastin synthesis in auricular cartilage TE attempts. Since auricular chondrocytes are necessary to produce elastic fibers, it would be appropriate to use a combination of auricular and nasoseptal chondrocytes to incorporate elastic fibers in the neocartilage.

3D bioprinting offers endless possibilities to the future of tissue and organ regeneration. Using this technology it is possible to biofabricate chondrocyte-laden auricular constructs surrounded by a perichondrium-like layer, and covered by a layer with keratinocytes; mimicking more closely the native tissue architecture.

ACKNOWLEDGMENTS

This thesis work was performed within the framework of the EuroNanoMed ERA-NET initiative (EAREG-406340-131009/1) and the Swedish Research Council (Grant 2009-7838) is gratefully acknowledged for financing this work. This work was carried out at Biopolymer Technology, Department of Chemistry and Chemical Engineering, Chalmers University of Technology, Gothenburg, Sweden; Institute for Biomechanics, ETH Zurich, Zurich, Switzerland; Department of Otorhinolaryngology, Ulm University Medical Center, Ulm, Germany; and Department of Otorhinolaryngology, Head and Neck Surgery, Erasmus MC, University Medical Center, Rotterdam, The Netherlands.

I would like to express my gratitude to all who have been involved and helped during the years of my doctoral studies. Without their continued efforts and support, I would have not been able to bring my work to a successful completion.

- Professor Paul Gatenholm, my supervisor, for taking me under your mentorship, providing me with many opportunities to grow, giving me the freedom to explore my ideas and for your contagious enthusiasm! Thank you for challenging me, never accepting anything less than my best efforts, and encouraging me throughout these years as your student.
- Professors Nicole Rotter at Ulm University Medical Center and Ralph Müller at ETH Zurich for hosting me in your labs on repeated occasions and for the fruitful collaboration we have had during these years.
- Dr. Kathryn Stok, my unofficial co-supervisor, for your guidance, advice and excellent discussions about research and life. Thank you for making me feel part of your research group, the memorable teambuilding activities, your priceless feedback on our manuscripts and for the fun Mexican parties we had!
- Dr. Silke Schwarz for being a great host and teacher every time I visited Ulm. We had long days at the lab but they always ended with very interesting and insightful talks about research and life. It was great hanging out with you and Ludwig in Schwabach and its surroundings!
- Professor Gerjo J.V.M. van Osch at Erasmus MC, for all the valuable and insightful comments when writing our manuscript.
- All the members of the EAREG consortium for making it a very pleasant and fruitful research collaboration and for hosting great meetings! Paul Gatenholm, Johan Sundberg, Athanasios Mantas, Nicole Rotter, Silke Schwarz, Eva-Maria Feldmann, Ralph Müller, Kathryn Stok, Luc Nimeskern, Gerjo van Osch, Mieke Pleumeekers, Anette Jork, Jens Riesle, Jeanine Hendriks and Willem de Jong.
- Julie Gold for your excellent lectures on biomaterials, which inspired me to embark on this field of research. Your way of teaching and engaging with students sparks motivation. I have really enjoyed our talks!

- Former and current colleagues at BBV Lab for sharing your knowledge and for making it such a great environment to work! Johan, thank you for the great discussions and for sharing your ideas with me. You have a very creative way of thinking! Magdalena, thank you for your patience in teaching this, at times crazy, mechanical engineer how to behave in a chemistry lab. Katia, thank you for all the hearty Mexican meals we cooked in the lab. My master students: Gopal, Shruti, Manuela, Thanos and Simona, thank you for your hard work and contribution to this work. It's been a very rewarding experience supervising all of you and learning from and with you. Sara and Daniel, I'm grateful to you for your readiness to help, kindness and for managing this lab so smoothly. Volo and Guillermo, thanks for the great discussions and for always cheering me up with your jokes. The CELL-INK group – Kajsa, Thanos, Ivan, Theo, Daniel and Paul – it's been fun working with you and learning so much in the past months. Karl and Daniel, thank you for proofreading my thesis.
- Colleagues at the polymer floor for always being so helpful and kind. Anne Wendel and Anders Mårtensson for your willingness to always help me with experimental analysis and for the great discussions. Your expertise has contributed in many ways to this work.
- Esa Väänänen at the mechanical workshop for improving my designs and always being so helpful to build them in a short time.
- Colleagues at the Institute for Biomechanics, ETH Zurich – Kathryn, Luc, Silke W, Jolanda, Steve, Ana, Willy and Ben – for making my time there very pleasant and fruitful. Colleagues at Ulm University Medical Center – Silke, Eva, Alex, Katia, Hanna, Monika and Gaby – for making my time there very memorable and for your excellent technical support with histology, immunohistochemistry and PCR.
- Co-authors for their valuable contributions to this work, insightful comment and for being instrumental in my scientific formation.
- Friends, for your continued support through words of encouragement and for reminding me that there is a life after work. Hans, Unni, Stig, Birgitta, Mickael, Karin, Sofia and David, for your friendship and for being like a family to me.
- I want to commend my parents for their hard work in raising eight children with a resolute and unswerving vision of giving us all the gift of a higher education. Words cannot express my gratitude to mom and dad. Thank you for your unwavering devotion to us, for putting every ounce of soul into your vision and for giving us a fresh start into adult life. Watching you struggle with a can-do attitude has been a blessing for us. I have learned by your example how to deal with problems that seem “insurmountable”. Brothers and sisters, you have been of priceless support throughout my life and I admire all of you for who you are.
- Lastly, I want to thank my love, Linnea, for being part of my life. Your love, laugh and smile bring joy to my life. It's been a wonderful journey by your side!

Héctor

REFERENCES

- 1 Carey, J. C., Park, A. H. & Muntz, H. R. in *Human malformations and related anomalies* (eds Roger E. Stevenson & Judith G. Hall) 329–338 (Oxford University Press, 2006).
- 2 Luquetti, D. V., Heike, C. L., Hing, A. V., Cunningham, M. L. & Cox, T. C. Microtia: Epidemiology and genetics. *American Journal of Medical Genetics Part A* **158A**, 124-139, doi:10.1002/ajmg.a.34352 (2012).
- 3 Li, D. *et al.* Psychosocial outcomes among microtia patients of different ages and genders before ear reconstruction. *Aesthetic Plast Surg* **34**, 570-576, doi:10.1007/s00266-010-9502-1 (2010).
- 4 Steffen, A., Wollenberg, B., Konig, I. R. & Frenzel, H. A prospective evaluation of psychosocial outcomes following ear reconstruction with rib cartilage in microtia. *J Plast Reconstr Aesthet Surg* **63**, 1466-1473, doi:10.1016/j.bjps.2009.09.005 (2010).
- 5 Ishimoto, S. *et al.* Hearing levels in patients with microtia: correlation with temporal bone malformation. *Laryngoscope* **117**, 461-465, doi:10.1097/MLG.0b013e31802ca4d4 (2007).
- 6 Suutarla, S. *et al.* Microtia in Finland: comparison of characteristics in different populations. *International journal of pediatric otorhinolaryngology* **71**, 1211-1217, doi:10.1016/j.ijporl.2007.04.020 (2007).
- 7 Walton, R. L. & Beahm, E. K. Auricular reconstruction for microtia: Part II. Surgical techniques. *Plast Reconstr Surg* **110**, 234-249; quiz 250-231, 387 (2002).
- 8 Ohara, K., Nakamura, K. & Ohta, E. Chest wall deformities and thoracic scoliosis after costal cartilage graft harvesting. *Plast Reconstr Surg* **99**, 1030-1036 (1997).
- 9 Cenzi, R., Farina, A., Zuccarino, L. & Carinci, F. Clinical outcome of 285 Medpor grafts used for craniofacial reconstruction. *J Craniofac Surg* **16**, 526-530 (2005).
- 10 Constantine, K. K., Gilmore, J., Lee, K. & Leach, J., Jr. Comparison of microtia reconstruction outcomes using rib cartilage vs porous polyethylene implant. *JAMA Facial Plast Surg* **16**, 240-244, doi:10.1001/jamafacial.2014.30 (2014).
- 11 Sterodimas, A., de Faria, J., Correa, W. E. & Pitanguy, I. Tissue engineering and auricular reconstruction: a review. *J Plast Reconstr Aesthet Surg* **62**, 447-452, doi:10.1016/j.bjps.2008.11.046 (2009).
- 12 Bichara, D. A. *et al.* The tissue-engineered auricle: past, present, and future. *Tissue Eng Part B Rev* **18**, 51-61, doi:10.1089/ten.TEB.2011.0326 (2012).
- 13 Langer, R. & Vacanti, J. P. Tissue engineering. *Science* **260**, 920-926 (1993).
- 14 Griffith, L. G. & Naughton, G. Tissue engineering--current challenges and expanding opportunities. *Science* **295**, 1009-1014, doi:10.1126/science.1069210 (2002).
- 15 Vacanti, C. A., Cima, L. G., Ratkowski, D., Upton, J. & Vacanti, J. P. in *Mater Res Soc Symp Proc.* 367–374 (1992;252).
- 16 Cao, Y., Vacanti, J. P., Paige, K. T., Upton, J. & Vacanti, C. A. Transplantation of chondrocytes utilizing a polymer-cell construct to produce tissue-engineered cartilage in the shape of a human ear. *Plast Reconstr Surg* **100**, 297-302; discussion 303-294 (1997).
- 17 Yanaga, H., Imai, K., Fujimoto, T. & Yanaga, K. Generating Ears from Cultured Autologous Auricular Chondrocytes by Using Two-Stage Implantation in Treatment of Microtia. *Plast Reconstr Surg* **124**, 817-825 810.1097/PRS.1090b1013e3181b1017c1090e (2009).
- 18 Lee, S. J., Broda, C., Atala, A. & Yoo, J. J. Engineered cartilage covered ear implants for auricular cartilage reconstruction. *Biomacromolecules* **12**, 306-313, doi:10.1021/bm100856g (2011).
- 19 Zhou, L. *et al.* Engineering ear constructs with a composite scaffold to maintain dimensions. *Tissue Eng Part A* **17**, 1573-1581, doi:10.1089/ten.TEA.2010.0627 (2011).

- 20 Haisch, A., Klaring, S., Groger, A., Gebert, C. & Sittinger, M. A tissue-engineering model for the manufacture of auricular-shaped cartilage implants. *Eur Arch Otorhinolaryngol* **259**, 316-321, doi:10.1007/s00405-002-0446-1 (2002).
- 21 Isogai, N. *et al.* Tissue engineering of an auricular cartilage model utilizing cultured chondrocyte-poly(L-lactide-epsilon-caprolactone) scaffolds. *Tissue Eng* **10**, 673-687, doi:10.1089/1076327041348527 (2004).
- 22 Shieh, S. J., Terada, S. & Vacanti, J. P. Tissue engineering auricular reconstruction: in vitro and in vivo studies. *Biomaterials* **25**, 1545-1557 (2004).
- 23 Kusuhara, H. *et al.* Tissue engineering a model for the human ear: assessment of size, shape, morphology, and gene expression following seeding of different chondrocytes. *Wound Repair Regen* **17**, 136-146, doi:10.1111/j.1524-475X.2008.00451.x (2009).
- 24 Ruzsyzmah, B. H. I., Chua, K. H., Mazlyzam, A. L. & Aminuddin, B. S. Formation of tissue engineered composite construct of cartilage and skin using high density polyethylene as inner scaffold in the shape of human helix. *International journal of pediatric otorhinolaryngology* **75**, 805-810 (2011).
- 25 Nimeskern, L. *et al.* Magnetic Resonance Imaging of the Ear for Patient-Specific Reconstructive Surgery. *PLoS One* **9**, e104975, doi:10.1371/journal.pone.0104975 (2014).
- 26 Van Osch, G. J. *et al.* Considerations on the use of ear chondrocytes as donor chondrocytes for cartilage tissue engineering. *Biorheology* **41**, 411-421 (2004).
- 27 van Osch, G. J., Marijnissen, W. J., van der Veen, S. W. & Verwoerd-Verhoef, H. L. The potency of culture-expanded nasal septum chondrocytes for tissue engineering of cartilage. *Am J Rhinol* **15**, 187-192 (2001).
- 28 Pittenger, M. F. *et al.* Multilineage potential of adult human mesenchymal stem cells. *Science* **284**, 143-147 (1999).
- 29 Zuk, P. A. *et al.* Human adipose tissue is a source of multipotent stem cells. *Mol Biol Cell* **13**, 4279-4295, doi:10.1091/mbc.E02-02-0105 (2002).
- 30 Hendriks, J., Riesle, J. & van Blitterswijk, C. A. Co-culture in cartilage tissue engineering. *J Tissue Eng Regen Med* **1**, 170-178, doi:10.1002/term.19 (2007).
- 31 de Windt, T. S. *et al.* Concise review: unraveling stem cell cocultures in regenerative medicine: which cell interactions steer cartilage regeneration and how? *Stem Cells Transl Med* **3**, 723-733, doi:10.5966/sctm.2013-0207 (2014).
- 32 Helenius, G. *et al.* In vivo biocompatibility of bacterial cellulose. *J Biomed Mater Res A* **76**, 431-438, doi:10.1002/jbm.a.30570 (2006).
- 33 Malm, C. J. *et al.* Small calibre biosynthetic bacterial cellulose blood vessels: 13-months patency in a sheep model. *Scandinavian Cardiovascular Journal* **46**, 57-62, doi:doi:10.3109/14017431.2011.623788 (2012).
- 34 Andrade, F. K. *et al.* Studies on the biocompatibility of bacterial cellulose. *J Bioact Compat Pol* **28**, 97-112, doi:Doi 10.1177/0883911512467643 (2013).
- 35 Rotter, N., Bücheler, M., Haisch, A., Wollenberg, B. & Lang, S. Cartilage tissue engineering using resorbable scaffolds. *J Tissue Eng Regen Med* **1**, 411-416, doi:10.1002/term.52 (2007).
- 36 Hunter, A. *et al.* Elements of morphology: standard terminology for the ear. *Am J Med Genet A* **149A**, 40-60, doi:10.1002/ajmg.a.32599 (2009).
- 37 Harris, J., Kallen, B. & Robert, E. The epidemiology of anotia and microtia. *J Med Genet* **33**, 809-813 (1996).
- 38 Shaw, G. M., Carmichael, S. L., Kaidarova, Z. & Harris, J. A. Epidemiologic characteristics of anotia and microtia in California, 1989-1997. *Birth Defects Res A Clin Mol Teratol* **70**, 472-475, doi:10.1002/bdra.20042 (2004).
- 39 Forrester, M. B. & Merz, R. D. Descriptive epidemiology of anotia and microtia, Hawaii, 1986-2002. *Congenit Anom (Kyoto)* **45**, 119-124, doi:10.1111/j.1741-4520.2005.00080.x (2005).

- 40 Canfield, M. A., Langlois, P. H., Nguyen, L. M. & Scheuerle, A. E. Epidemiologic features and clinical subgroups of anotia/microtia in Texas. *Birth Defects Res A Clin Mol Teratol* **85**, 905-913, doi:10.1002/bdra.20626 (2009).
- 41 Du, J. M. *et al.* Psychological status of congenital microtia patients and relative influential factors: analysis of 410 cases. *Zhonghua Yi Xue Za Zhi* **87**, 383-387 (2007).
- 42 Tanzer, R. C. Total reconstruction of the auricle: a 10-year report. *Plast Reconstr Surg* **40**, 547-550 (1967).
- 43 Brent, B. Auricular repair with autogenous rib cartilage grafts: two decades of experience with 600 cases. *Plast Reconstr Surg* **90**, 355-374; discussion 375-356 (1992).
- 44 Nagata, S. A new method of total reconstruction of the auricle for microtia. *Plast Reconstr Surg* **92**, 187-201 (1993).
- 45 Firmin, F. Ear reconstruction in cases of typical microtia. Personal experience based on 352 microtic ear corrections. *Scand J Plast Reconstr Surg Hand Surg* **32**, 35-47 (1998).
- 46 Cronin, T. D. & Ascough, B. M. Silastic ear construction. *Clin Plast Surg* **5**, 367-378 (1978).
- 47 Ohmori, S. Reconstruction of microtia using the Silastic frame. *Clin Plast Surg* **5**, 379-387 (1978).
- 48 Williams, J. D., Romo, T., 3rd, Sclafani, A. P. & Cho, H. Porous high-density polyethylene implants in auricular reconstruction. *Arch Otolaryngol Head Neck Surg* **123**, 578-583 (1997).
- 49 Romo, T., 3rd, Fozo, M. S. & Sclafani, A. P. Microtia reconstruction using a porous polyethylene framework. *Facial Plast Surg* **16**, 15-22 (2000).
- 50 Wilkes, G. H. & Wolfaardt, J. F. Osseointegrated alloplastic versus autogenous ear reconstruction: criteria for treatment selection. *Plast Reconstr Surg* **93**, 967-979 (1994).
- 51 Thorne, C. H. *et al.* Auricular reconstruction: indications for autogenous and prosthetic techniques. *Plast Reconstr Surg* **107**, 1241-1252 (2001).
- 52 Pan, B. *et al.* Microtia: ear reconstruction using tissue expander and autogenous costal cartilage. *Journal of Plastic, Reconstructive & Aesthetic Surgery* **61**, S98-S103, doi:10.1016/j.bjps.2007.07.012 (2008).
- 53 Gray, H. *Anatomy of the Human Body*. 20 edn, (Lea & Febiger, Bartleby.com, 1918, 2000).
- 54 Ha, R. Y. & Trovato, M. J. in *Selected Readings in Plastic Surgery* Vol. 11 1-45 (Selected Readings in Plastic Surgery, Inc., Dallas, 2011).
- 55 Tortora, G. J. & Derrickson, B. *Essentials of anatomy and physiology*. 8th edn, (John Wiley & Sons, 2010).
- 56 Naumann, A. *et al.* Immunochemical and Mechanical Characterization of Cartilage Subtypes in Rabbit. *Journal of Histochemistry & Cytochemistry* **50**, 1049-1058, doi:10.1177/002215540205000807 (2002).
- 57 Britberg, M. & Lindahl, A. in *Tissue Eng* Vol. Academic Press Series in Biomedical Engineering (ed Clemens van Blitterswijk) Ch. 18, 533-557 (Academic Press, 2008).
- 58 Spiller, K. L., Maher, S. A. & Lowman, A. M. Hydrogels for the repair of articular cartilage defects. *Tissue Eng Part B Rev* **17**, 281-299, doi:10.1089/ten.TEB.2011.0077 (2011).
- 59 Archer, C. W. & Francis-West, P. The chondrocyte. *The International Journal of Biochemistry & Cell Biology* **35**, 401-404 (2003).
- 60 Eyre, D. R. & Muir, H. The distribution of different molecular species of collagen in fibrous, elastic and hyaline cartilages of the pig. *Biochem J* **151**, 595-602 (1975).
- 61 Cotta-Pereira, G., Del-Caro, L. M. & Montes, G. S. Distribution of elastic system fibers in hyaline and fibrous cartilages of the rat. *Acta Anat (Basel)* **119**, 80-85 (1984).
- 62 Hardingham, T. E., Fosang, A. J. & Dudhia, J. The structure, function and turnover of aggrecan, the large aggregating proteoglycan from cartilage. *Eur J Clin Chem Clin Biochem* **32**, 249-257 (1994).
- 63 Roughley, P. J. & Lee, E. R. Cartilage proteoglycans: structure and potential functions. *Microsc Res Tech* **28**, 385-397, doi:10.1002/jemt.1070280505 (1994).

- 64 Rotter, N., Steiner, A. & Scheithauer, M. Reconstruction of auricular cartilage using tissue-engineering techniques. *Operative Techniques in Otolaryngology-Head and Neck Surgery* **19**, 278-284, doi:10.1016/j.otot.2008.10.004 (2008).
- 65 Liu, Y. *et al.* In vitro engineering of human ear-shaped cartilage assisted with CAD/CAM technology. *Biomaterials* **31**, 2176-2183, doi:10.1016/j.biomaterials.2009.11.080 (2010).
- 66 Cao, Y. *et al.* Comparative study of the use of poly(glycolic acid), calcium alginate and pluronics in the engineering of autologous porcine cartilage. *J Biomater Sci Polym Ed* **9**, 475-487 (1998).
- 67 Kamil, S. H., Eavey, R. D., Vacanti, M. P., Vacanti, C. A. & Hartnick, C. J. Tissue-engineered cartilage as a graft source for laryngotracheal reconstruction: a pig model. *Arch Otolaryngol Head Neck Surg* **130**, 1048-1051, doi:10.1001/archotol.130.9.1048 (2004).
- 68 Isogai, N. *et al.* Combined chondrocyte-copolymer implantation with slow release of basic fibroblast growth factor for tissue engineering an auricular cartilage construct. *Journal of Biomedical Materials Research Part A* **74A**, 408-418, doi:10.1002/jbm.a.30343 (2005).
- 69 Isogai, N. *et al.* Cytokine-Rich Autologous Serum System for Cartilaginous Tissue Engineering. *Ann Plast Surg* **60**, 703-709, doi:10.1097/SAP.0b013e31814b2cb5 (2008).
- 70 Béguin, P. & Aubert, J.-P. The biological degradation of cellulose. *FEMS Microbiology Reviews* **13**, 25-58, doi:10.1016/0168-6445(94)90099-X (1994).
- 71 Brown, A. J. On an acetic ferment which forms cellulose. *Journal of the Chemical Society, Transactions* **49**, 432-439, doi:10.1039/ct8864900432 (1886).
- 72 Fink, H. P., Purz, H. J., Bohn, A. & Kunze, J. Investigation of the supramolecular structure of never dried bacterial cellulose. *Macromol Symp* **120**, 207-217, doi:Doi 10.1002/Masy.19971200121 (1997).
- 73 Mello, L. R., Feltrin, L. T., Neto, P. T. F. & Ferraz, F. A. P. Duraplasty with biosynthetic cellulose: An experimental study. *J Neurosurg* **86**, 143-150, doi:Doi 10.3171/Jns.1997.86.1.0143 (1997).
- 74 Pertile, R. A. *et al.* Bacterial Cellulose: Long-Term Biocompatibility Studies. *J Biomater Sci Polym Ed*, doi:10.1163/092050611X581516 (2011).
- 75 Ahrem, H. *et al.* Laser-structured bacterial nanocellulose hydrogels support ingrowth and differentiation of chondrocytes and show potential as cartilage implants. *Acta Biomater* **10**, 1341-1353, doi:10.1016/j.actbio.2013.12.004 (2014).
- 76 Bäckdahl, H. *et al.* Mechanical properties of bacterial cellulose and interactions with smooth muscle cells. *Biomaterials* **27**, 2141-2149 (2006).
- 77 Bodin, A. *et al.* Tissue-engineered conduit using urine-derived stem cells seeded bacterial cellulose polymer in urinary reconstruction and diversion. *Biomaterials* **31**, 8889-8901, doi:Doi 10.1016/J.Biomaterials.2010.07.108 (2010).
- 78 Feldmann, E. M. *et al.* Description of a novel approach to engineer cartilage with porous bacterial nanocellulose for reconstruction of a human auricle. *J Biomater Appl*, doi:10.1177/0885328212472547 (2013).
- 79 Kowalska-Ludwicka, K. *et al.* Modified bacterial cellulose tubes for regeneration of damaged peripheral nerves. *Arch Med Sci* **9**, 527-534, doi:10.5114/aoms.2013.33433 (2013).
- 80 Martínez Ávila, H., Brackmann, C., Enejder, A. & Gatenholm, P. Mechanical stimulation of fibroblasts in micro-channeled bacterial cellulose scaffolds enhances production of oriented collagen fibers. *J Biomed Mater Res A* **100**, 948-957, doi:10.1002/jbm.a.34035 (2012).
- 81 Svensson, A. *et al.* Bacterial cellulose as a potential scaffold for tissue engineering of cartilage. *Biomaterials* **26**, 419-431 (2005).
- 82 Zaborowska, M. *et al.* Microporous bacterial cellulose as a potential scaffold for bone regeneration. *Acta Biomaterialia* **6**, 2540-2547, doi:10.1016/j.actbio.2010.01.004 (2010).

- 83 Andersson, J., Stenhamre, H., Bäckdahl, H. & Gatenholm, P. Behavior of human chondrocytes in engineered porous bacterial cellulose scaffolds. *J Biomed Mater Res A* **94**, 1124-1132, doi:10.1002/jbm.a.32784 (2010).
- 84 Rosen, C. L. *et al.* Results of the prospective, randomized, multicenter clinical trial evaluating a biosynthesized cellulose graft for repair of dural defects. *Neurosurgery* **69**, 1093-1103, doi:10.1227/NEU.0b013e3182284aca (2011).
- 85 Chiaoprakobkij, N., Sanchavanakit, N., Subbalekha, K., Pavasant, P. & Phisalaphong, M. Characterization and biocompatibility of bacterial cellulose/alginate composite sponges with human keratinocytes and gingival fibroblasts. *Carbohydrate Polymers* **85**, 548-553, doi:10.1016/j.carbpol.2011.03.011 (2011).
- 86 Silipo, A. & Molinaro, A. in *Bacterial Lipopolysaccharides* (eds Yuriy A. Knirel & Miguel A. Valvano) Ch. 1, 1-20 (Springer Vienna, 2011).
- 87 Williams, K. L. in *Endotoxins Drugs and the Pharmaceutical Sciences* (ed Kevin L. Williams) 47-66 (CRC Press, 2007).
- 88 Heine, H., Rietschel, E. T. & Ulmer, A. J. The biology of endotoxin. *Mol Biotechnol* **19**, 279-296, doi:10.1385/MB:19:3:279 (2001).
- 89 Hold, G. L. & Bryant, C. E. in *Bacterial Lipopolysaccharides* (eds Yuriy A. Knirel & Miguel A. Valvano) Ch. 12, 371-387 (Springer Vienna, 2011).
- 90 Administration, U. S. F. a. D. (ed U.S. Department of Health & Human Services) 8 (U.S. Food and Drug Administration, Silver Spring, 2012).
- 91 Gea, S. *et al.* Investigation into the structural, morphological, mechanical and thermal behaviour of bacterial cellulose after a two-step purification process. *Bioresource technol* **102**, 9105-9110, doi:10.1016/j.biortech.2011.04.077 (2011).
- 92 Grobelski, B. *et al.* Biocompatibility of modified bionanocellulose and porous poly(ϵ -caprolactone) biomaterials. *Int J Polymer Mater Polymer Biomat* **63**, 518-526, doi:10.1080/00914037.2013.854223 (2014).
- 93 Sandle, T. A Practical Approach to Depyrogenation Studies Using Bacterial Endotoxin. *J GXP Compliance* **15**, 90-96 (2011).
- 94 Williams, K. *Endotoxins: Pyrogens, LAL Testing and Depyrogenation*. (Informa Healthcare, 2007).
- 95 Williams, K. L. in *Endotoxins Drugs and the Pharmaceutical Sciences* (ed Kevin L. Williams) 301-327 (CRC Press, 2007).
- 96 Boland, T., Mironov, V., Gutowska, A., Roth, E. A. & Markwald, R. R. Cell and organ printing 2: fusion of cell aggregates in three-dimensional gels. *Anat Rec A Discov Mol Cell Evol Biol* **272**, 497-502, doi:10.1002/ar.a.10059 (2003).
- 97 Mironov, V., Boland, T., Trusk, T., Forgacs, G. & Markwald, R. R. Organ printing: computer-aided jet-based 3D tissue engineering. *Trends in Biotechnology* **21**, 157-161, doi:10.1016/S0167-7799(03)00033-7 (2003).
- 98 Wilson, W. C., Jr. & Boland, T. Cell and organ printing 1: protein and cell printers. *Anat Rec A Discov Mol Cell Evol Biol* **272**, 491-496, doi:10.1002/ar.a.10057 (2003).
- 99 Ilkhanizadeh, S., Teixeira, A. & Hermanson, O. Inkjet printing of macromolecules on hydrogels to steer neural stem cell differentiation. *Biomaterials* **28**, 3936-3943, doi:10.1016/j.biomaterials.2007.05.018 (2007).
- 100 Lee, Y. B. *et al.* Bio-printing of collagen and VEGF-releasing fibrin gel scaffolds for neural stem cell culture. *Exp Neurol* **223**, 645-652, doi:10.1016/j.expneurol.2010.02.014 (2010).
- 101 Malda, J. *et al.* 25th anniversary article: Engineering hydrogels for biofabrication. *Advanced Materials* **25**, 5011-5028, doi:10.1002/adma.201302042 (2013).
- 102 Murphy, S. V. & Atala, A. 3D bioprinting of tissues and organs. *Nat Biotechnol* **32**, 773-785, doi:10.1038/nbt.2958 (2014).

- 103 Pati, F. *et al.* Printing three-dimensional tissue analogues with decellularized extracellular matrix bioink. *Nat Commun* **5**, 3935, doi:10.1038/ncomms4935 (2014).
- 104 Seol, Y. J., Kang, H. W., Lee, S. J., Atala, A. & Yoo, J. J. Bioprinting technology and its applications. *Eur J Cardiothorac Surg* **46**, 342-348, doi:10.1093/ejcts/ezu148 (2014).
- 105 Giannitelli, S. M., Accoto, D., Trombetta, M. & Rainer, A. Current trends in the design of scaffolds for computer-aided tissue engineering. *Acta Biomaterialia* **10**, 580-594, doi:10.1016/j.actbio.2013.10.024 (2014).
- 106 Sun, W., Starly, B., Nam, J. & Darling, A. Bio-CAD modeling and its applications in computer-aided tissue engineering. *Computer-Aided Design* **37**, 1097-1114, doi:10.1016/j.cad.2005.02.002 (2005).
- 107 Cohen, D. L., Malone, E., Lipson, H. & Bonassar, L. J. Direct freeform fabrication of seeded hydrogels in arbitrary geometries. *Tissue Eng* **12**, 1325-1335, doi:10.1089/ten.2006.12.1325 (2006).
- 108 Jia, J. *et al.* Engineering alginate as bioink for bioprinting. *Acta Biomaterialia* **10**, 4323-4331, doi:10.1016/j.actbio.2014.06.034 (2014).
- 109 Murphy, S. V., Skardal, A. & Atala, A. Evaluation of hydrogels for bio-printing applications. *J Biomed Mater Res A* **101**, 272-284, doi:10.1002/jbm.a.34326 (2013).
- 110 Cui, X., Breitenkamp, K., Finn, M. G., Lotz, M. & D'Lima, D. D. Direct human cartilage repair using three-dimensional bioprinting technology. *Tissue Eng Part A* **18**, 1304-1312, doi:10.1089/ten.TEA.2011.0543 (2012).
- 111 Duan, B., Hockaday, L. A., Kang, K. H. & Butcher, J. T. 3D bioprinting of heterogeneous aortic valve conduits with alginate/gelatin hydrogels. *J Biomed Mater Res A* **101**, 1255-1264, doi:10.1002/jbm.a.34420 (2013).
- 112 Duan, B., Kapetanovic, E., Hockaday, L. A. & Butcher, J. T. Three-dimensional printed trileaflet valve conduits using biological hydrogels and human valve interstitial cells. *Acta Biomaterialia* **10**, 1836-1846, doi:10.1016/j.actbio.2013.12.005 (2014).
- 113 Fedorovich, N. E. *et al.* Biofabrication of osteochondral tissue equivalents by printing topologically defined, cell-laden hydrogel scaffolds. *Tissue Eng Part C Methods* **18**, 33-44, doi:10.1089/ten.TEC.2011.0060 (2012).
- 114 Kolesky, D. B. *et al.* 3D bioprinting of vascularized, heterogeneous cell-laden tissue constructs. *Advanced Materials* **26**, 3124-3130, doi:10.1002/adma.201305506 (2014).
- 115 Lee, J. S. *et al.* 3D printing of composite tissue with complex shape applied to ear regeneration. *Biofabrication* **6**, 024103, doi:10.1088/1758-5082/6/2/024103 (2014).
- 116 Schuurman, W. *et al.* Gelatin-methacrylamide hydrogels as potential biomaterials for fabrication of tissue-engineered cartilage constructs. *Macromol Biosci* **13**, 551-561, doi:10.1002/mabi.201200471 (2013).
- 117 Matsuoka M, T. T., Matsushita K, Adachi O, Yoshinaga F. A synthetic medium for bacterial cellulose production by *Acetobacter xylinum* subsp. sucrofermentation. *Biosci Biotechnol Biochem* **60**, 575-579 (1996).
- 118 Bartel, D. L., Davy, D. T. & Keaveny, T. M. Orthopaedic Biomechanics: Mechanics and Design in Musculoskeletal Systems. (2006).
- 119 Little, C. J., Bawolin, N. K. & Chen, X. Mechanical properties of natural cartilage and tissue-engineered constructs. *Tissue Eng Part B Rev* **17**, 213-227, doi:10.1089/ten.TEB.2010.0572 (2011).
- 120 Stok, K. S., Lisignoli, G., Cristino, S., Facchini, A. & Muller, R. Mechano-functional assessment of human mesenchymal stem cells grown in three-dimensional hyaluronan-based scaffolds for cartilage tissue engineering. *J Biomed Mater Res A* **93**, 37-45, doi:10.1002/jbm.a.32503 (2010).

- 121 Segal, L., Creely, J. J., Martin, A. E. & Conrad, C. M. An Empirical Method for Estimating the Degree of Crystallinity of Native Cellulose Using the X-Ray Diffractometer. *Text Res J* **29**, 786-794, doi:10.1177/004051755902901003 (1959).
- 122 Dhumal, N. R., Kim, H. J. & Kiefer, J. Molecular interactions in 1-ethyl-3-methylimidazolium acetate ion pair: a density functional study. *J Phys Chem A* **113**, 10397-10404, doi:10.1021/jp907394v (2009).
- 123 Viell, J. & Marquardt, W. Concentration measurements in ionic liquid-water mixtures by mid-infrared spectroscopy and indirect hard modeling. *Applied Spectroscopy* **66**, 208-217, doi:10.1366/11-06427 (2012).
- 124 Pääkkö, M. *et al.* Enzymatic hydrolysis combined with mechanical shearing and high-pressure homogenization for nanoscale cellulose fibrils and strong gels. *Biomacromolecules* **8**, 1934-1941, doi:10.1021/bm061215p (2007).
- 125 Waters, R. L., Lunsford, B. R., Perry, J. & Byrd, R. Energy-speed relationship of walking: standard tables. *J Orthop Res* **6**, 215-222, doi:10.1002/jor.1100060208 (1988).
- 126 Petrović, M. *et al.* A novel bioreactor with mechanical stimulation for skeletal tissue engineering. *Chemical Industry & Chemical Engineering Quarterly* **15**, 41-44 (2009).
- 127 Campagnola, P. J. *et al.* Three-Dimensional High-Resolution Second-Harmonic Generation Imaging of Endogenous Structural Proteins in Biological Tissues. *Biophysical Journal* **81**, 493-508 (2002).
- 128 Brown, R. M., Millard, A. C. & Campagnola, P. J. Macromolecular structure of cellulose studied by second-harmonic generation imaging microscopy. *Optics Letters* **28**, 2207-2209 (2003).
- 129 Cheng, J.-X. Coherent anti-Stokes Raman Scattering Microscopy. *Applied Spectroscopy* **91**, 197-208 (2007).
- 130 Hendriks, J. A. A., Riesle, J. U., Wilson, C. E. & Van Den Doel, M. A. Cartilage cell processing system. US patent (2014).
- 131 Blaney Davidson, E. N., van der Kraan, P. M. & van den Berg, W. B. TGF-beta and osteoarthritis. *Osteoarthritis Cartilage* **15**, 597-604, doi:10.1016/j.joca.2007.02.005 (2007).
- 132 Worster, A. A. *et al.* Chondrocytic differentiation of mesenchymal stem cells sequentially exposed to transforming growth factor-beta1 in monolayer and insulin-like growth factor-I in a three-dimensional matrix. *J Orthop Res* **19**, 738-749, doi:10.1016/S0736-0266(00)00054-1 (2001).
- 133 Fortier, L. A., Barker, J. U., Strauss, E. J., McCarrel, T. M. & Cole, B. J. The role of growth factors in cartilage repair. *Clin Orthop Relat Res* **469**, 2706-2715, doi:10.1007/s11999-011-1857-3 (2011).
- 134 Longobardi, L. *et al.* Effect of IGF-I in the chondrogenesis of bone marrow mesenchymal stem cells in the presence or absence of TGF-beta signaling. *J Bone Miner Res* **21**, 626-636, doi:10.1359/jbmr.051213 (2006).
- 135 Sah, R. L., Chen, A. C., Grodzinsky, A. J. & Trippel, S. B. Differential effects of bFGF and IGF-I on matrix metabolism in calf and adult bovine cartilage explants. *Arch Biochem Biophys* **308**, 137-147, doi:10.1006/abbi.1994.1020 (1994).
- 136 Tyler, J. A. Insulin-like growth factor 1 can decrease degradation and promote synthesis of proteoglycan in cartilage exposed to cytokines. *Biochemical Journal* **260**, 543-548 (1989).
- 137 Livak, K. J. & Schmittgen, T. D. Analysis of relative gene expression data using real-time quantitative PCR and the 2(-Delta Delta C(T)) Method. *Methods* **25**, 402-408, doi:10.1006/meth.2001.1262 (2001).
- 138 Schmittgen, T. D. & Livak, K. J. Analyzing real-time PCR data by the comparative C(T) method. *Nat Protoc* **3**, 1101-1108 (2008).

- 139 Enobakhare, B. O., Bader, D. L. & Lee, D. A. Quantification of sulfated glycosaminoglycans in chondrocyte/alginate cultures, by use of 1,9-dimethylmethylene blue. *Anal Biochem* **243**, 189-191, doi:10.1006/abio.1996.0502 (1996).
- 140 Farndale, R. W., Sayers, C. A. & Barrett, A. J. A direct spectrophotometric microassay for sulfated glycosaminoglycans in cartilage cultures. *Connect Tissue Res* **9**, 247-248 (1982).
- 141 Barbosa, I. *et al.* Improved and simple micro assay for sulfated glycosaminoglycans quantification in biological extracts and its use in skin and muscle tissue studies. *Glycobiology* **13**, 647-653, doi:10.1093/glycob/cwg082 (2003).
- 142 McGowan, K. B., Kurtis, M. S., Lottman, L. M., Watson, D. & Sah, R. L. Biochemical quantification of DNA in human articular and septal cartilage using PicoGreen and Hoechst 33258. *Osteoarthritis Cartilage* **10**, 580-587 (2002).
- 143 Nimeskern, L. *et al.* Mechanical evaluation of bacterial nanocellulose as an implant material for ear cartilage replacement. *J Mech Behav Biomed* **22**, 12-21, doi:10.1016/j.jmbbm.2013.03.005 (2013).
- 144 Mow, V. C. & Guo, X. E. Mechano-electrochemical properties of articular cartilage: their inhomogeneities and anisotropies. *Annu Rev Biomed Eng* **4**, 175-209, doi:10.1146/annurev.bioeng.4.110701.120309 (2002).
- 145 Rotter, N. *et al.* Age dependence of biochemical and biomechanical properties of tissue-engineered human septal cartilage. *Biomaterials* **23**, 3087-3094 (2002).
- 146 Joshi, M. D., Suh, J. K., Marui, T. & Woo, S. L. Interspecies variation of compressive biomechanical properties of the meniscus. *Journal of Biomedical Materials Research* **29**, 823-828, doi:10.1002/jbm.820290706 (1995).
- 147 Lee, T. C., Midura, R. J., Hascall, V. C. & Vesely, I. The effect of elastin damage on the mechanics of the aortic valve. *Journal of Biomechanics* **34**, 203-210 (2001).
- 148 Oxlund, H., Manschot, J. & Viidik, A. The role of elastin in the mechanical properties of skin. *Journal of Biomechanics* **21**, 213-218 (1988).
- 149 Bäckdahl, H., Esguerra, M., Delbro, D., Risberg, B. & Gatenholm, P. Engineering microporosity in bacterial cellulose scaffolds. *J Tissue Eng Regen Med* **2**, 320-330, doi:Doi 10.1002/Term.97 (2008).
- 150 Bodin, A. *et al.* Modification of nanocellulose with a xyloglucan-RGD conjugate enhances adhesion and proliferation of endothelial cells: implications for tissue engineering. *Biomacromolecules* **8**, 3697-3704, doi:10.1021/bm070343q (2007).
- 151 Klemm, D., Schumann, D., Udhardt, U. & Marsch, S. Bacterial synthesized cellulose - artificial blood vessels for microsurgery. *Prog Polym Sci* **26**, 1561-1603 (2001).
- 152 Bodin, A., Concaro, S., Brittberg, M. & Gatenholm, P. Bacterial cellulose as a potential meniscus implant. *J Tissue Eng Regen Med* **1**, 406-408 (2007).
- 153 Martínez Ávila, H. *et al.* Biocompatibility evaluation of densified bacterial nanocellulose hydrogel as an implant material for auricular cartilage regeneration. *Appl Microbiol Biotechnol* **98**, 7423-7435, doi:10.1007/s00253-014-5819-z (2014).
- 154 Klechkovskaya, V. V. *et al.* Structure of cellulose *Acetobacter xylinum*. *Crystallogr Rep* **48**, 755-762, doi:Doi 10.1134/1.1612596 (2003).
- 155 Moharram, M. A. & Mahmoud, O. M. X-ray diffraction methods in the study of the effect of microwave heating on the transformation of cellulose I into cellulose II during mercerization. *J Appl Polym Sci* **105**, 2978-2983, doi:Doi 10.1002/App.26580 (2007).
- 156 Mansikkamäki, P., Lahtinen, M. & Rissanen, K. Structure changes of cellulose crystallites induced by mercerization in different solvent system; determined by powder X-ray diffraction method. *Cellulose* **12**, 233-242 (2005).

- 157 Anderson, J. M. & Langone, J. J. Issues and perspectives on the biocompatibility and immunotoxicity evaluation of implanted controlled release systems. *J Control Release* **57**, 107-113 (1999).
- 158 Anderson, J. M. & Shive, M. S. Biodegradation and biocompatibility of PLA and PLGA microspheres. *Adv Drug Deliv Rev* **28**, 5-24 (1997).
- 159 Anderson, J. M. Biological Responses to Materials. *Ann Rev Mater Res* **31**, 81-110, doi:doi:10.1146/annurev.matsci.31.1.81 (2001).
- 160 Robitaille, R. *et al.* Inflammatory response to peritoneal implantation of alginate-poly-L-lysine microcapsules. *Biomaterials* **26**, 4119-4127, doi:10.1016/j.biomaterials.2004.10.028 (2005).
- 161 Almeida, C. R. *et al.* Impact of 3-D printed PLA- and chitosan-based scaffolds on human monocyte/macrophage responses: unraveling the effect of 3-D structures on inflammation. *Acta Biomater* **10**, 613-622, doi:10.1016/j.actbio.2013.10.035 (2014).
- 162 Anderson, J. M. Mechanisms of inflammation and infection with implanted devices. *Cardiovasc Pathol* **2**, 33S-41S (1993).
- 163 Klemm, D., Heublein, B., Fink, H.-P. & Bohn, A. Cellulose: Fascinating Biopolymer and Sustainable Raw Material. *Angewandte Chemie International Edition* **44**, 3358-3393 (2005).
- 164 Petersen, N. & Gatenholm, P. Bacterial cellulose-based materials and medical devices: current state and perspectives. *Appl Microbiol Biot* **91**, 1277-1286, doi:10.1007/s00253-011-3432-y (2011).
- 165 Feldmann, E. M. *et al.* Description of a novel approach to engineer cartilage with porous bacterial nanocellulose for reconstruction of a human auricle. *J Biomater Appl* **28**, 626-640, doi:10.1177/0885328212472547 (2013).
- 166 Martínez Ávila, H. *et al.* Novel bilayer bacterial nanocellulose scaffold supports neocartilage formation in vitro and in vivo. *Biomaterials* **44**, 122-133, doi:10.1016/j.biomaterials.2014.12.025 (2015).
- 167 Chen, H.-L., Kao, H.-F., Wang, J.-Y. & Wei, G.-T. Cytotoxicity of Imidazole Ionic Liquids in Human Lung Carcinoma A549 Cell Line. *J Chin Chem Soc-Taip* **61**, 763-769, doi:10.1002/jccs.201300632 (2014).
- 168 Marijnissen, W. J., van Osch, G. J., Aigner, J., Verwoerd-Verhoef, H. L. & Verhaar, J. A. Tissue-engineered cartilage using serially passaged articular chondrocytes. Chondrocytes in alginate, combined in vivo with a synthetic (E210) or biologic biodegradable carrier (DBM). *Biomaterials* **21**, 571-580 (2000).
- 169 Marijnissen, W. J. *et al.* Alginate as a chondrocyte-delivery substance in combination with a non-woven scaffold for cartilage tissue engineering. *Biomaterials* **23**, 1511-1517 (2002).
- 170 Häuselmann, H. J. *et al.* Phenotypic stability of bovine articular chondrocytes after long-term culture in alginate beads. *J Cell Sci* **107 (Pt 1)**, 17-27 (1994).
- 171 Puelacher, W. C. *et al.* Tissue-engineered growth of cartilage: the effect of varying the concentration of chondrocytes seeded onto synthetic polymer matrices. *Int J Oral Maxillofac Surg* **23**, 49-53 (1994).
- 172 Lang, P., Noorbakhsh, F. & Yoshioka, H. MR Imaging of Articular Cartilage: Current State and Recent Developments. *Radiologic Clinics of North America* **43**, 629-639, doi:10.1016/j.rcl.2005.02.009 (2005).
- 173 Hua, K. *et al.* Translational study between structure and biological response of nanocellulose from wood and green algae. *RSC Advances* **4**, 2892, doi:10.1039/c3ra45553j (2014).
- 174 Bhattacharya, M. *et al.* Nanofibrillar cellulose hydrogel promotes three-dimensional liver cell culture. *Journal of Controlled Release* **164**, 291-298, doi:10.1016/j.jconrel.2012.06.039 (2012).
- 175 Fedorovich, N. E. *et al.* Evaluation of Photocrosslinked Lutrol Hydrogel for Tissue Printing Applications. *Biomacromolecules* **10**, 1689-1696, doi:10.1021/bm801463q (2009).

- 176 Dreier, R., Wallace, S., Fuchs, S., Bruckner, P. & Grassel, S. Paracrine interactions of chondrocytes and macrophages in cartilage degradation: articular chondrocytes provide factors that activate macrophage-derived pro-gelatinase B (pro-MMP-9). *J Cell Sci* **114**, 3813-3822 (2001).
- 177 Galasso, O., Familiari, F., De Gori, M. & Gasparini, G. Recent Findings on the Role of Gelatinases (Matrix Metalloproteinase-2 and -9) in Osteoarthritis. *Advances in Orthopedics* **2012**, 1-7, doi:10.1155/2012/834208 (2012).
- 178 Polacek, M., Bruun, J.-A., Elvenes, J., Figenschau, Y. & Martinez, I. The Secretory Profiles of Cultured Human Articular Chondrocytes and Mesenchymal Stem Cells: Implications for Autologous Cell Transplantation Strategies. *Cell Transplantation* **20**, 1381-1393, doi:10.3727/096368910x550215 (2011).
- 179 Nuernberger, S. *et al.* The influence of scaffold architecture on chondrocyte distribution and behavior in matrix-associated chondrocyte transplantation grafts. *Biomaterials* **32**, 1032-1040, doi:10.1016/j.biomaterials.2010.08.100 (2011).
- 180 Schuh, E. *et al.* Chondrocyte redifferentiation in 3D: The effect of adhesion site density and substrate elasticity. *Journal of Biomedical Materials Research Part A* **100A**, 38-47, doi:10.1002/jbm.a.33226 (2012).
- 181 Schwarz, S. *et al.* Processed xenogenic cartilage as innovative biomatrix for cartilage tissue engineering: effects on chondrocyte differentiation and function. *J Tissue Eng Regen Med*, doi:10.1002/term.1650 (2012).
- 182 Zaucke, F., Dinser, R., Maurer, P. & Paulsson, M. Cartilage oligomeric matrix protein (COMP) and collagen IX are sensitive markers for the differentiation state of articular primary chondrocytes. *Biochem J* **358**, 17-24 (2001).
- 183 Kaps, C. *et al.* Gene expression profiling of human articular cartilage grafts generated by tissue engineering. *Biomaterials*, doi:10.1016/j.biomaterials.2006.02.017 (2006).
- 184 Yang, X. *et al.* Matrilin-3 Inhibits Chondrocyte Hypertrophy as a Bone Morphogenetic Protein-2 Antagonist. *Journal of Biological Chemistry* **289**, 34768-34779, doi:10.1074/jbc.M114.583104 (2014).
- 185 Kanbe, K., Yang, X., Wei, L., Sun, C. & Chen, Q. Pericellular Matrilins Regulate Activation of Chondrocytes by Cyclic Load-Induced Matrix Deformation. *Journal of Bone and Mineral Research* **22**, 318-328, doi:10.1359/jbmr.061104 (2006).
- 186 Nicolae, C. *et al.* Abnormal Collagen Fibrils in Cartilage of Matrilin-1/Matrilin-3-deficient Mice. *Journal of Biological Chemistry* **282**, 22163-22175, doi:10.1074/jbc.M610994200 (2007).
- 187 Abraham, T., Fong, G. & Scott, A. Second harmonic generation analysis of early Achilles tendinosis in response to in vivo mechanical loading. *BMC Musculoskelet Disord* **12**, 26, doi:10.1186/1471-2474-12-26 (2011).
- 188 Filova, E. *et al.* Analysis and three-dimensional visualization of collagen in artificial scaffolds using nonlinear microscopy techniques. *Journal of Biomedical Optics* **15**, 066011, doi:10.1117/1.3509112 (2010).
- 189 Caves, J. M. *et al.* Fibrillogenesis in Continuously Spun Synthetic Collagen Fiber. *Journal of Biomedical Materials Research Part B-Applied Biomaterials* **93B**, 24-38, doi:Doi 10.1002/Jbm.B.31555 (2010).
- 190 Zeugolis, D. I. *et al.* Electro-spinning of pure collagen nano-fibres - Just an expensive way to make gelatin? *Biomaterials* **29**, 2293-2305, doi:DOI 10.1016/j.biomaterials.2008.02.009 (2008).
- 191 Upton, M. L., Gilchrist, C. L., Guilak, F. & Setton, L. A. Transfer of Macroscale Tissue Strain to Microscale Cell Regions in the Deformed Meniscus. *Biophysical Journal* **95**, 2116-2124 (2008).
- 192 van der Meulen, M. C. & Huijkes, R. Why mechanobiology? A survey article. *Journal of Biomechanics* **35**, 401-414 (2002).